TECHNICKÁ UNIVERZITA V LIBERCI

Nové možnosti rozvoje vzdělávání na Technické univerzitě v Liberci

Specifický cíl A2: Rozvoj v oblasti distanční výuky, online výuky a blended learning

NPO_TUL_MSMT-16598/2022

Smart oděvy

Financováno Evropskou unií
NextGenerationEU

Národní plán obnovy

MINISTERSTVO ŠKOLSTVÍ, MLÁDEŽE A TĚLOVÝCHOVY

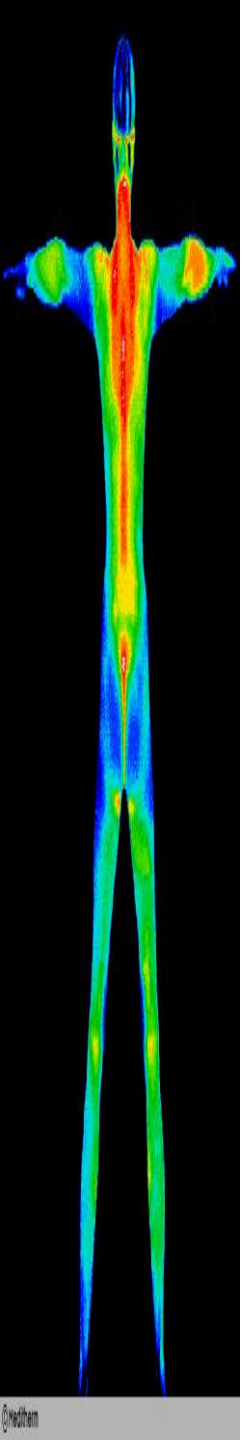

SOD

Smart oděvy

e-textilie - senzory

Senzory

Financováno Evropskou unií NextGenerationEU
Národní plán obnovy
MINISTERSTVO ŠKOLSTVÍ, MLÁDEŽE A TĚLOVÝCHOVY
NPO_TUL_MSMT-16598/2022

Senzory

- *Měření tlaku, teploty, vlhkosti*
- *Senzory plynů*
  - *výbušné – metan, propan, butan, páry hořlavých látek,..*
  - *Produkty hoření – oxidy dusíku, síry, uhlíku, produkty hoření plastů*
  - *Smog*
  - *Mění se elektrické, optické či jiné vlastnosti senzoru, to lze snímat a vyhodnotit*
- *Lze je integrovat do textilu*

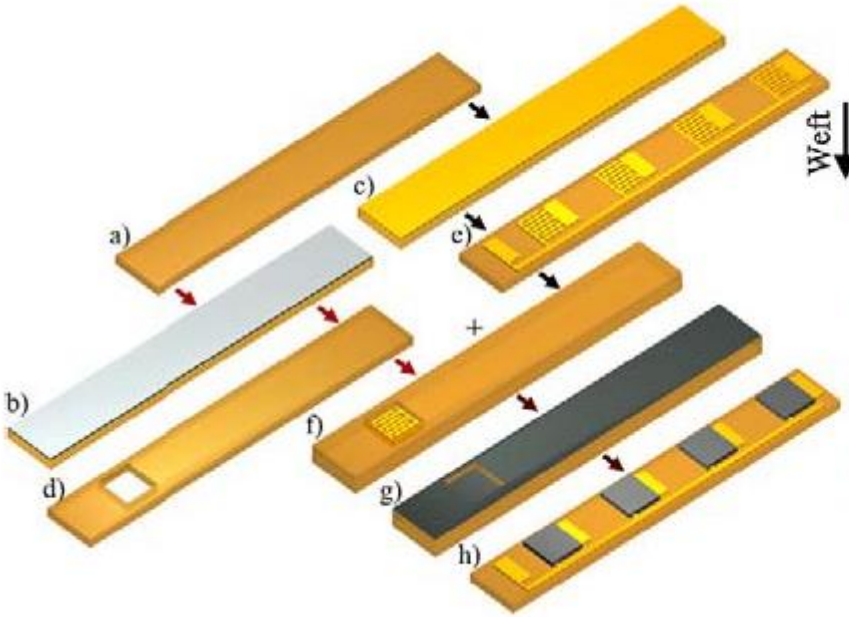

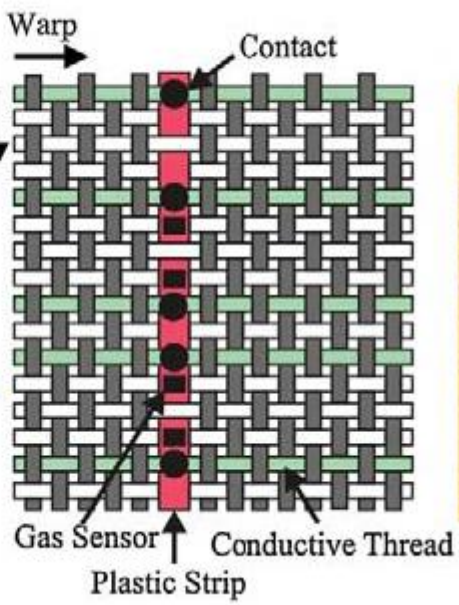

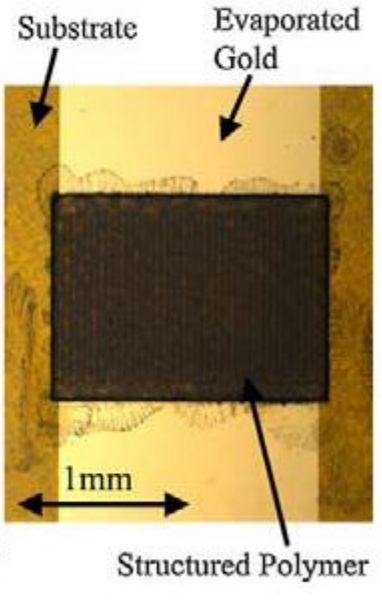

Senzory

- *Oděvy pro hasiče, polici, záchranáře, armádu, atd.*
- *Integrace do oděvu, uniformy*
- *Monitorování životních funkcí*

Senzory

- *Monitorování životních funkcí*
- *EKG (např. vyšívané elektrody)*
- *Tepová frekvence*
- *Frekvence dýchání*
- *Tlak krve*
- *Teplota, vlhkost*
- *Poloha těla*

Senzory

An overview of the most common sensors used in smart clothing:

Breathing (respiration) - sensor for monitoring breathing frequency. It is based on changes in elasticity and conductivity of the material.

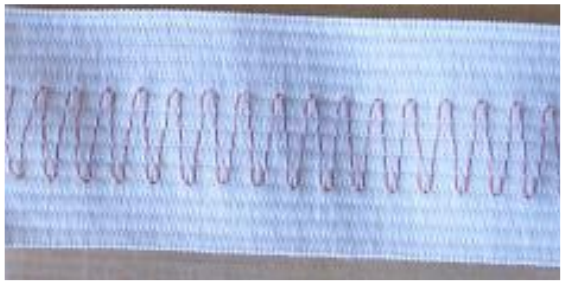

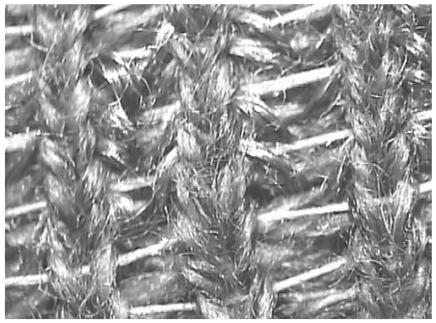

Senzory

Puls

the sensor for monitoring pulse.

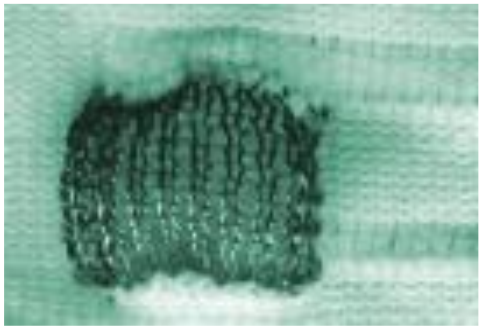

- **Pressure**

– the sensor for measuring pressure, max. Field size is 500 x 400 mm. The maximum pressure range is 7-350 kPa, the substrate material is - elastomer Lycra (Dupont).

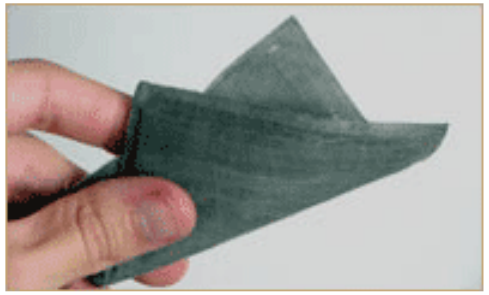

Senzory

Thermal field

sensor for measuring the **thermal field** using copper wire network.

Measurement consists in the use of constant current and recording the temperature change that is converted into an electrical resistance.

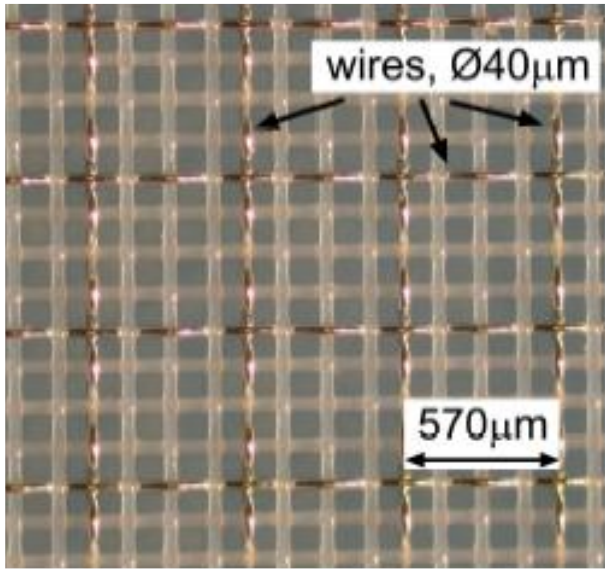

Senzory

Textile electrode - multi-layer knitted fabric that contains as an active layer, and a protective inactive.

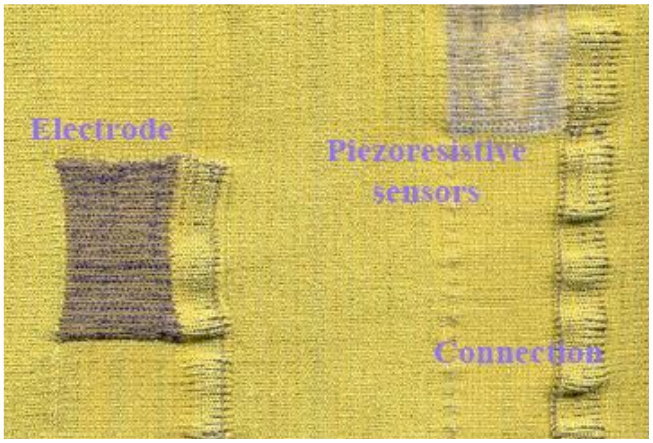

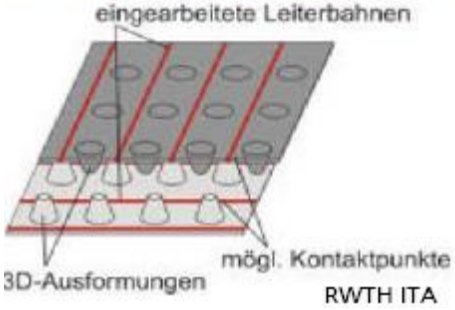

Senzory

Textrody – ECG T-shirt

It measures the cardiovascular system of the wearer, is used as a substitute for conventional gel electrodes. The use of electrolytic properties of sweat, direct contact with the skin (without the use of electrical stimulation gel).

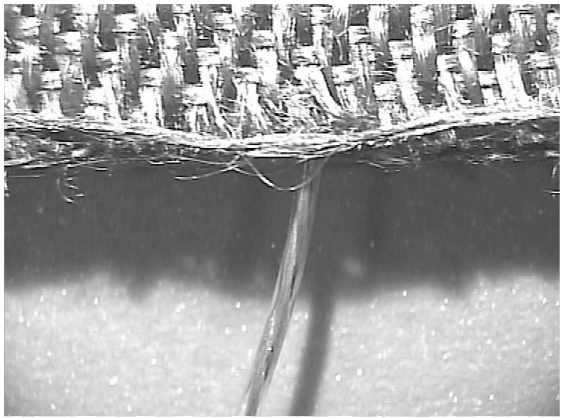

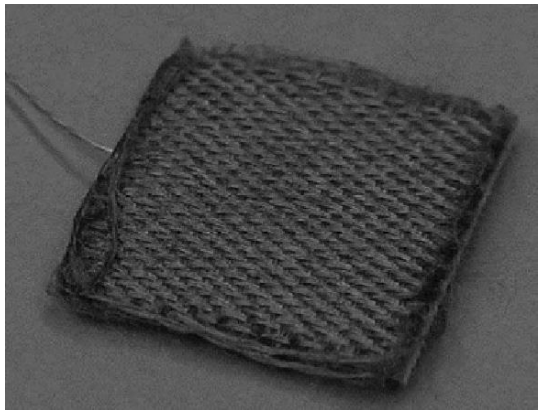

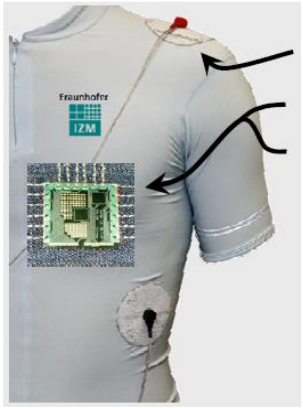

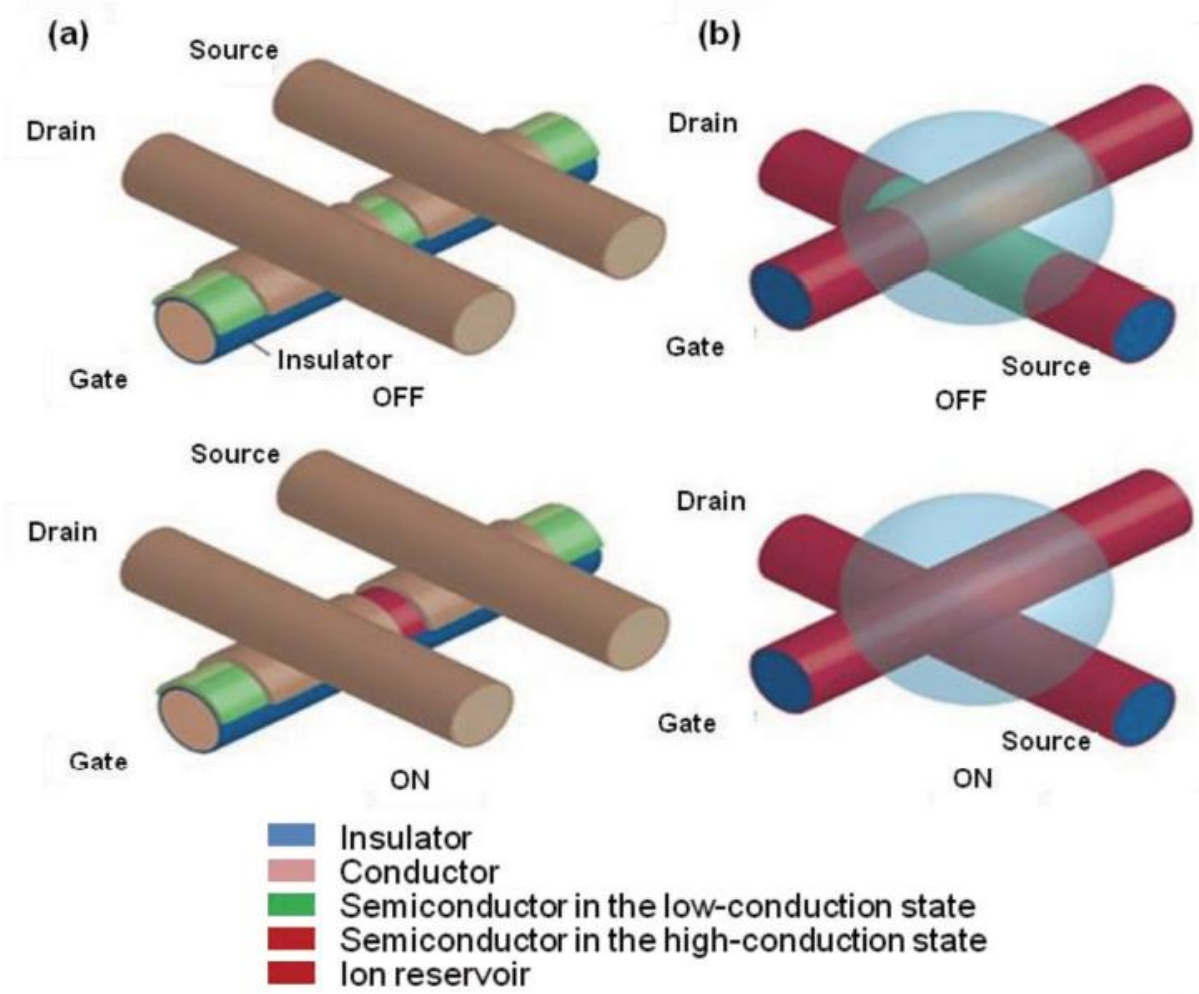

Figure 3. Fiber transistors: (a) fiber organic field-effect transistors (OFETs), (b) wire electrochemical transistors (WECT). Reproduced with permission.[78a] Copyright 2007, Nature Publishing Group.

Anténa

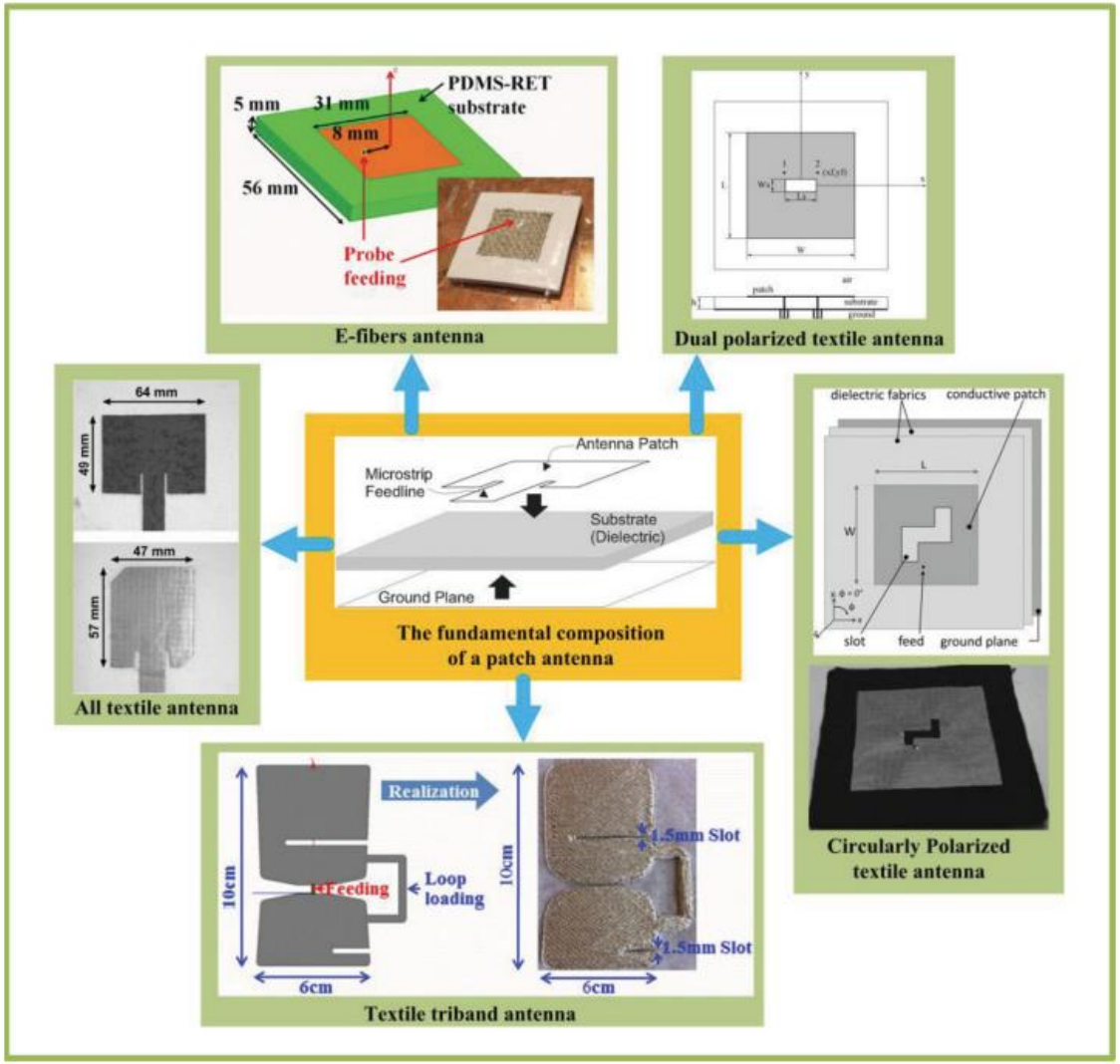

Figure 4. Fabric antennas based on the fundamental composition of a patch antenna: E-fiber antenna,[87] textile triband antenna,[89] dual polarized textile antennas,[90] all textile antenna,[85] and circularly polarized antenna.[91] Reproduced with permission. Copyright, respectively, 2012, 2012, 2011, 2006, 2011, IEEE.

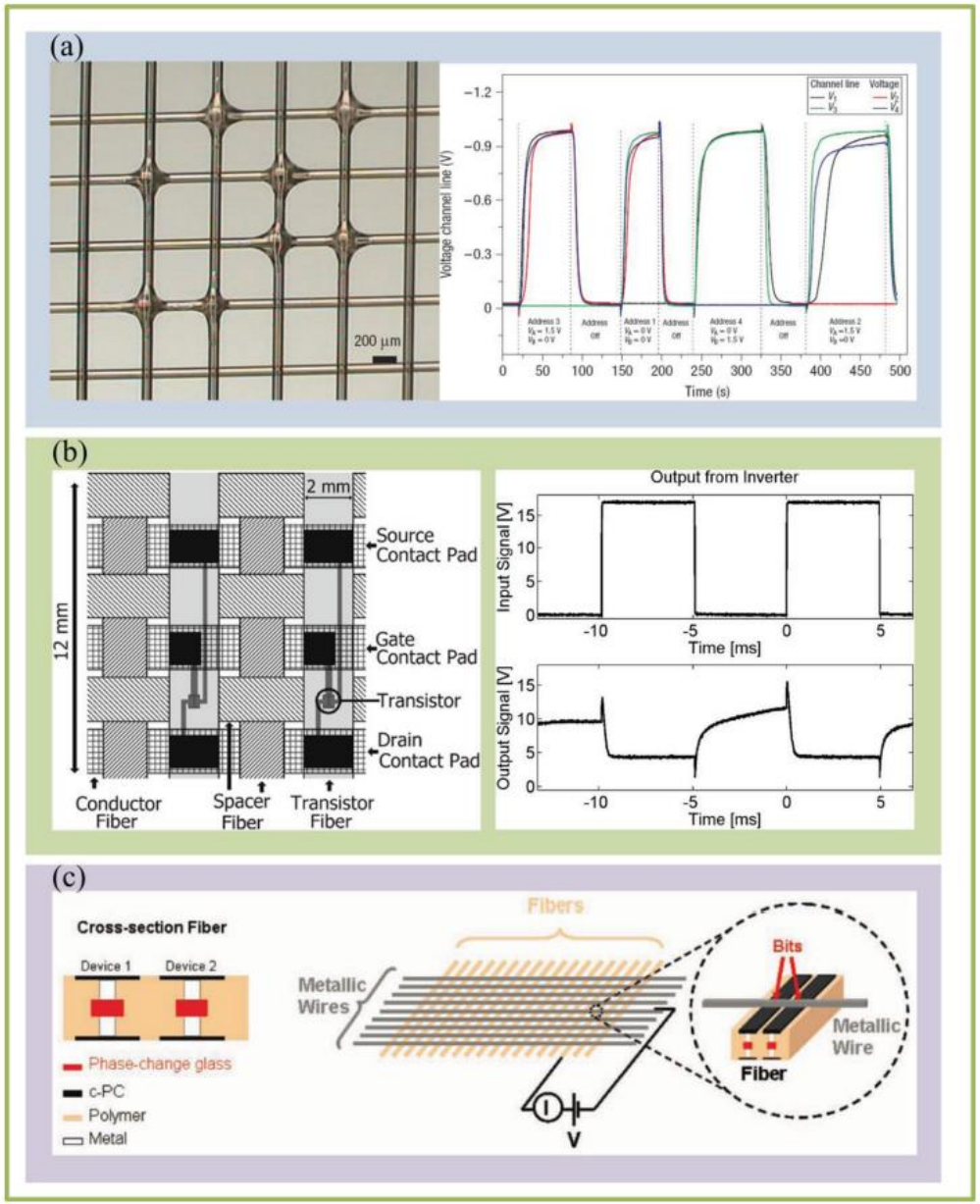

Figure 7. Fiber circuitry: (a) A binary tree multiplexer constructed from WECTs and their dynamic electrical characteristics, Reproduced with permission.[52] Copyright 2007, Nature Publishing Group. (b) A woven inverter circuit and its dynamic electrical characteristics, Reproduced with permission.[135] Copyright 2004, IEEE. (c) Fiber-based fabric-array memory device. Reproduced with permission.[136] Copyright 2011, WILEY-VCH Verlag GmbH & Co. KGaA, Weinheim.

Figure 8. Fiber-based sensors: (a) Fabric bio-potential electrode and its SEM photo, Reproduced with permission.[144] Copyright 2010, IEEE. (b) Pulse-driven fiber nanogenerator by ZnO thin films grown around a carbon fiber as a strain sensor, Reproduced with permission.[6a] Copyright 2011, WILEY-VCHVerlag GmbH & Co. KGaA, Weinheim. (c)Vibration sensor arrays of piezoelectric fibers in gloves for detection and suppression of Parkinson's tremor in the hand, Reproduced with permission.[145] Copyright 2009, Textile Bioengineering and Informatics Society. (d) Carbon loaded elastomer sensorized garment for kinesthetic monitoring, Reproduced with permission.[146] Copyright 2011, Cambridge University Press. (e) Strain-gauge sensor based on the reversible interlocking of Pt-coated polymer nanofibres, Reproduced with permission.[140k] Copyright 2012, Nature Publishing Group. (f) Carbon nanotube strain sensor for human motion detection, Reproduced with permission.[20c] Copyright 2011, Nature Publishing Group. (g)Woven electronic fibers with sensing and display functions, Reproduced with permission.[5b] Copyright 2010, WILEY-VCH Verlag GmbH & Co. KGaA, Weinheim. (h) In-shoe plantar pressure monitoring in daily activities by fabric pressure sensors. Reproduced with permission.[140i] Copyright 2010, IEEE.

Zdroje napájení?

Financováno Evropskou unií NextGenerationEU
Národní plán obnovy
MINISTERSTVO ŠKOLSTVÍ, MLÁDEŽE A TĚLOVÝCHOVY
NPO_TUL_MSMT-16598/2022

Dá se energie získat?

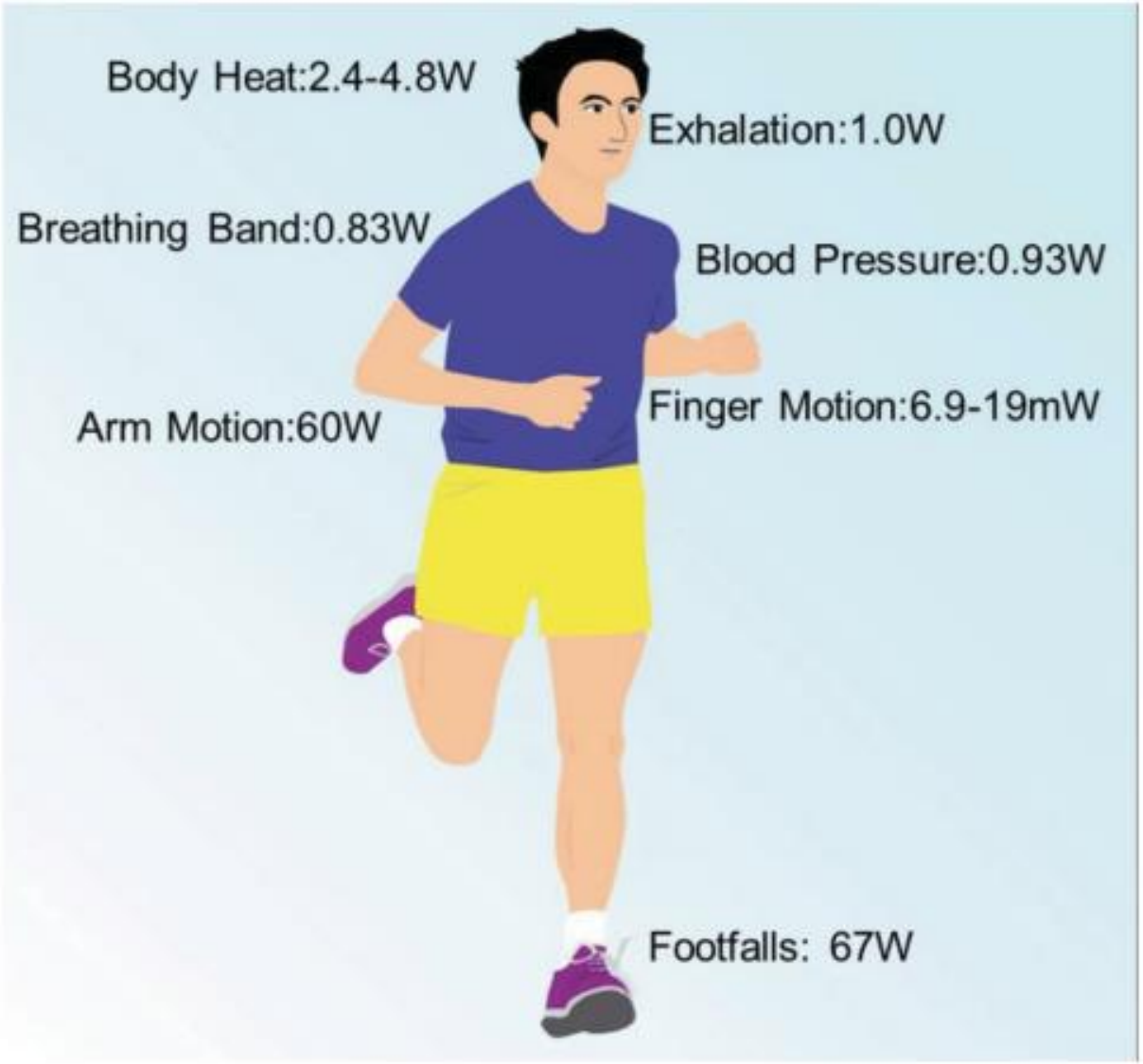

Figure 10. Available power for everyday bodily activities of human being.[153]

Tlak

Sensor tlaku

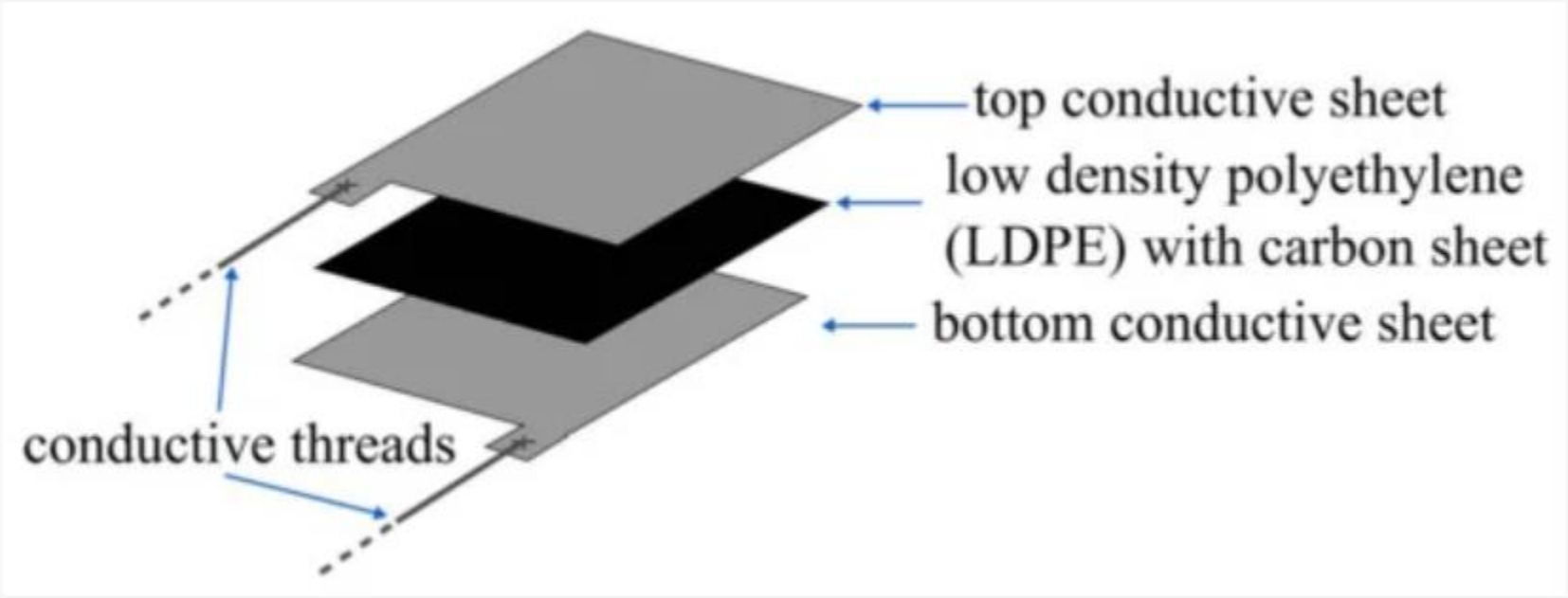

Sensors **2018**, *18*(4), 1190; https://doi.org/10.3390/s18041190

Sensor tlaku

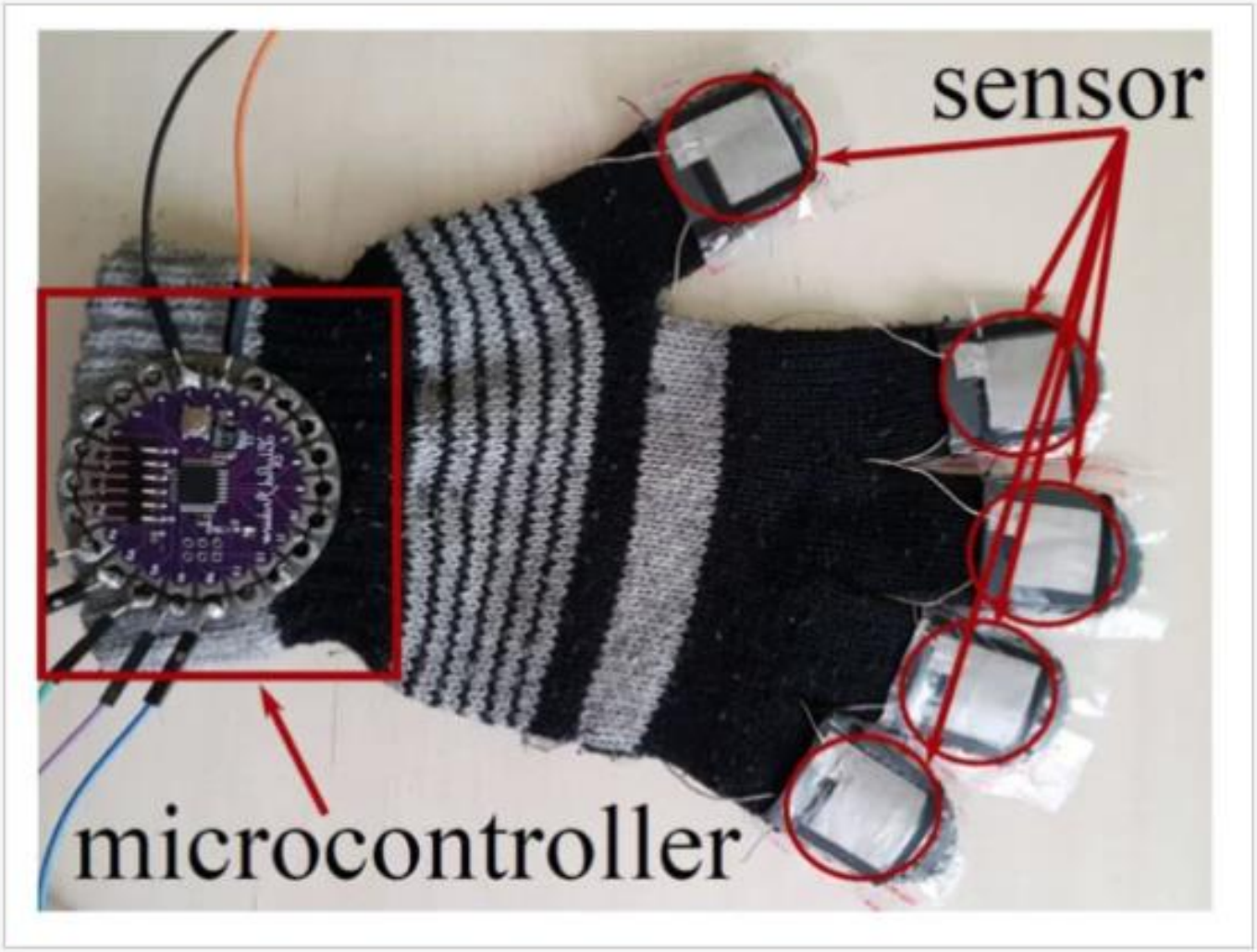

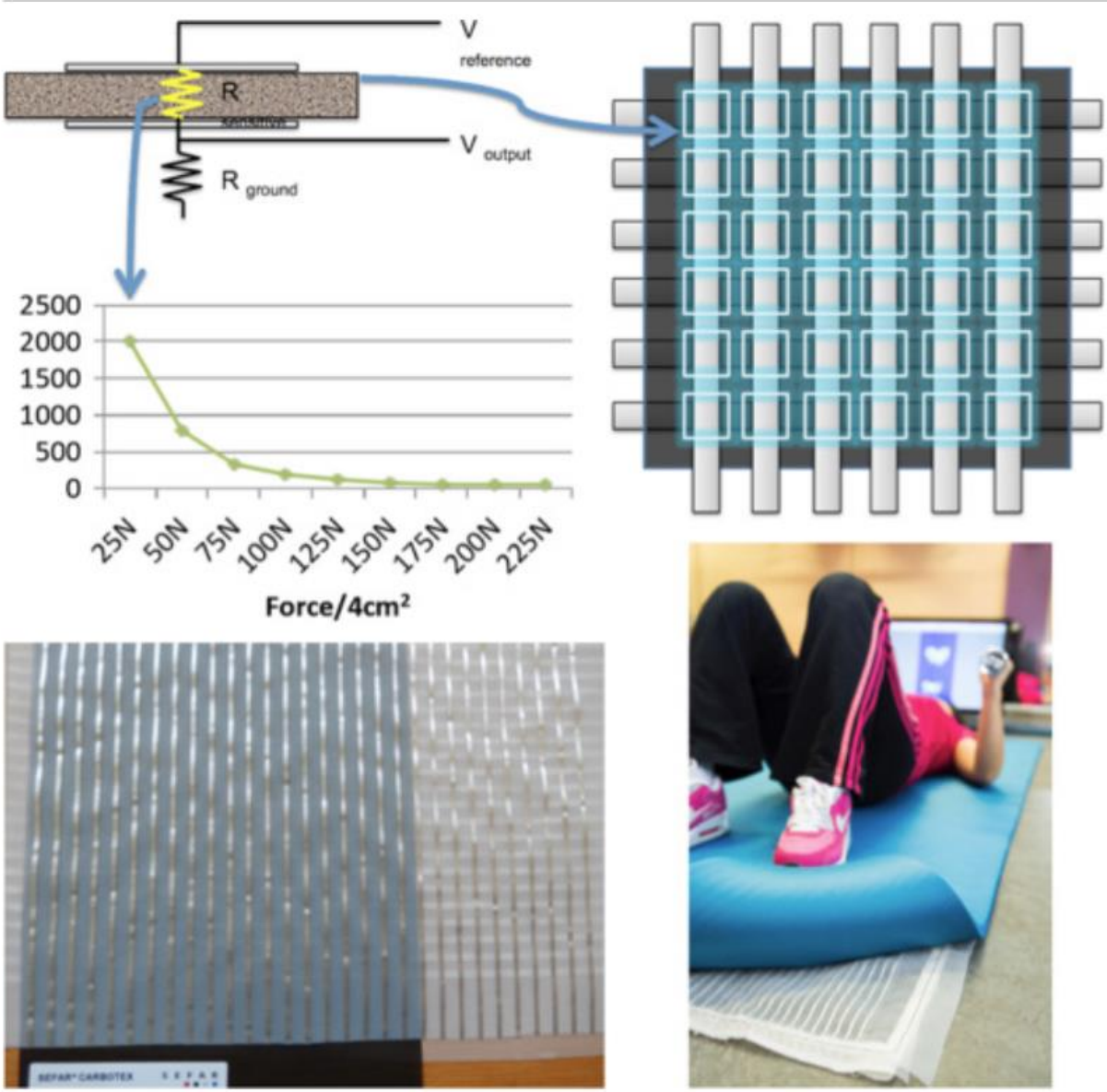

Smart-surface: Large scale textile pressure sensors arrays for activity recognition

JingyuanChengMathiasSundholmBoZhouMarcoHirschPaulLukowicz

Smart-surface: Large scale textile pressure sensors arrays for activity recognition - ScienceDirect

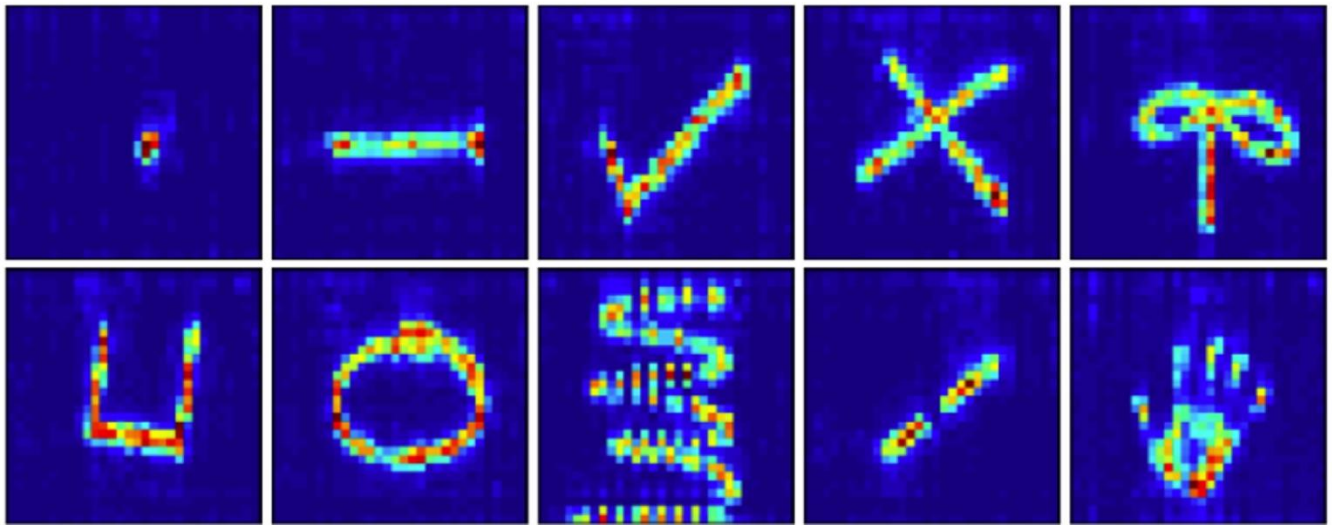

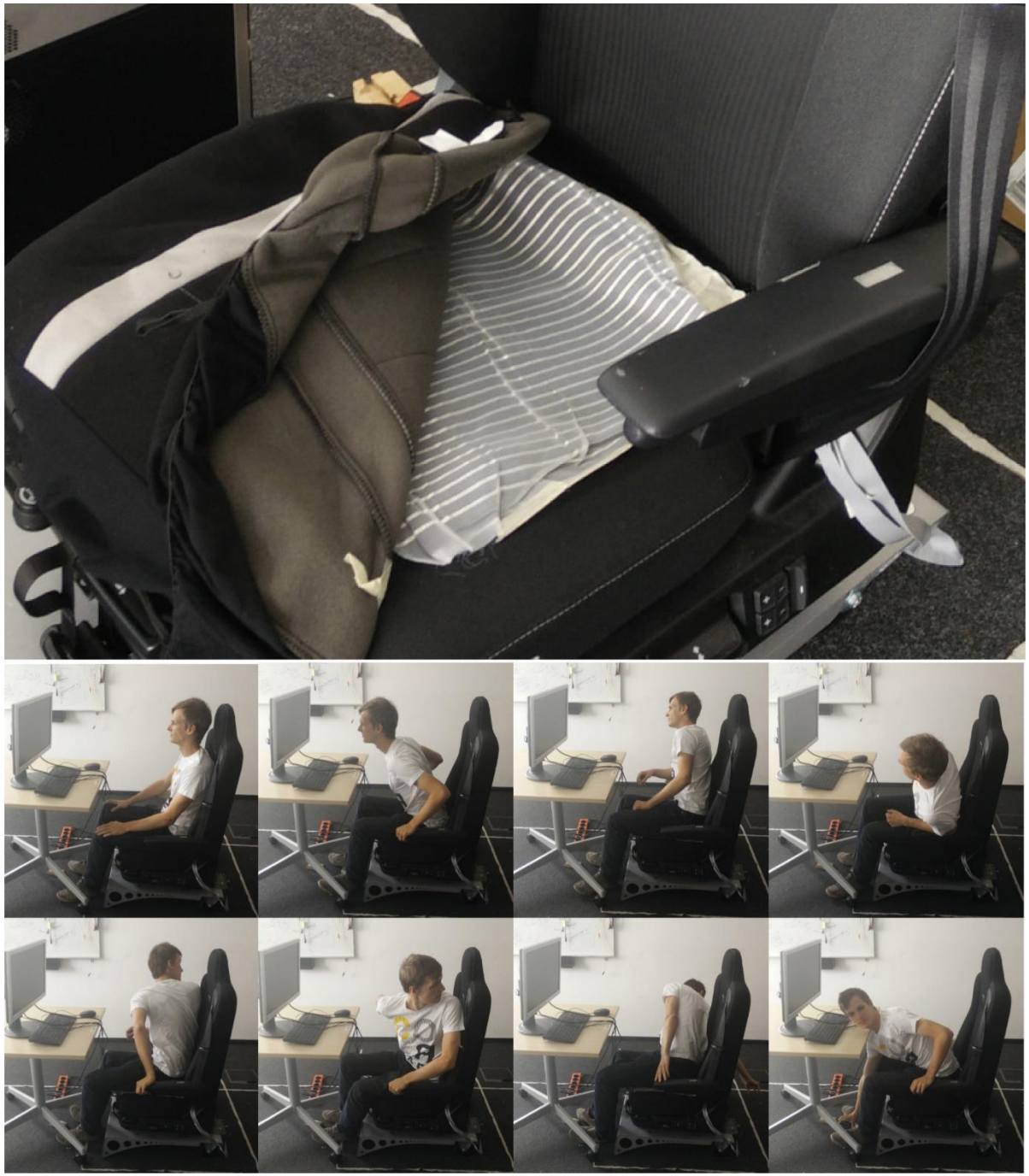

Monitorování tlakového pole

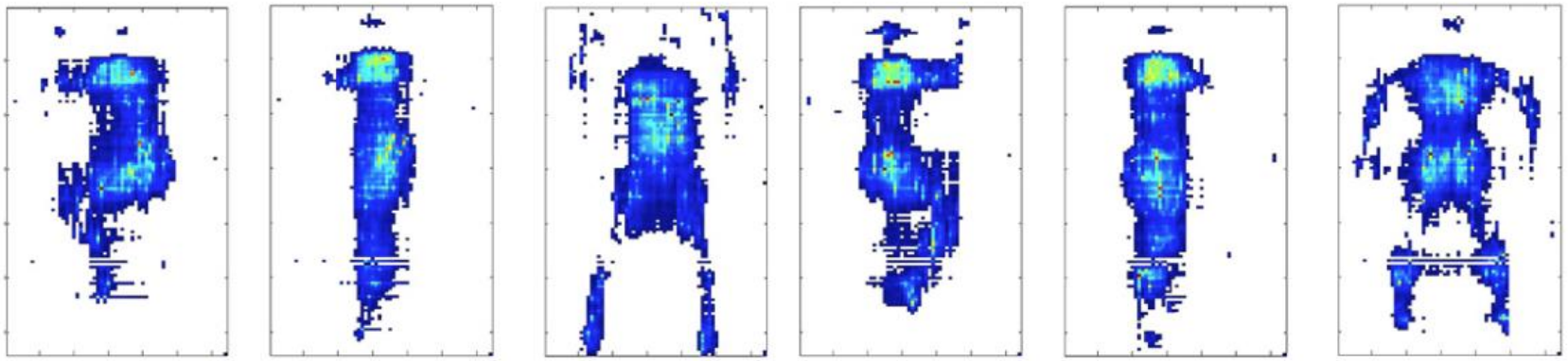

Fig. 1. Human body pressure image samples.

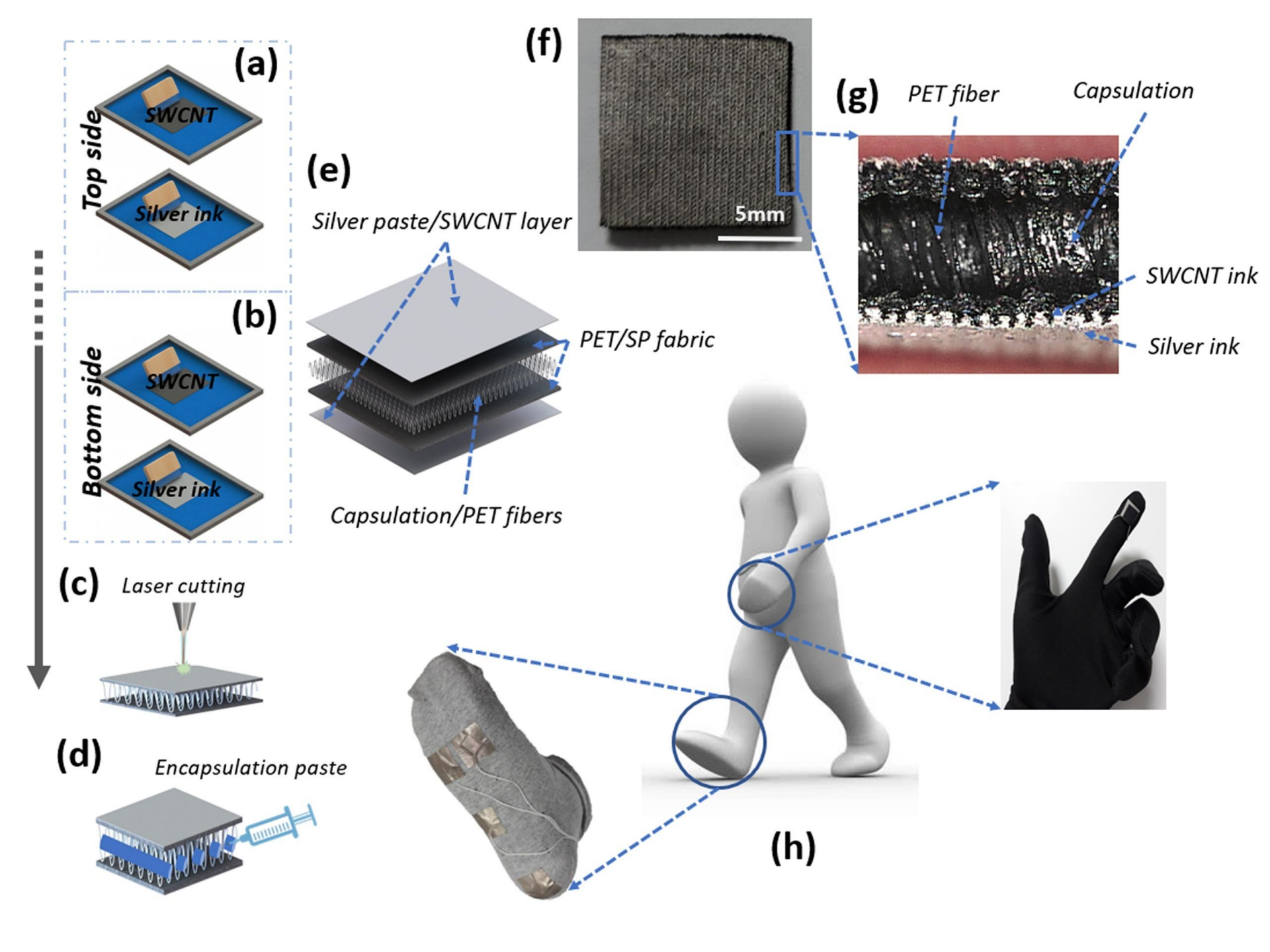
(a)
SWCNT
Top side
Silver ink
(b)
SWCNT
Bottom side
Silver ink
(c)
Laser cutting
(d)
Encapsulation paste
(e)
Silver paste/SWCNT layer
PET/SP fabric
Capsulation/PET fibers
(f)
5mm
(g)
PET fiber
Capsulation
SWCNT ink
Silver ink
(h)

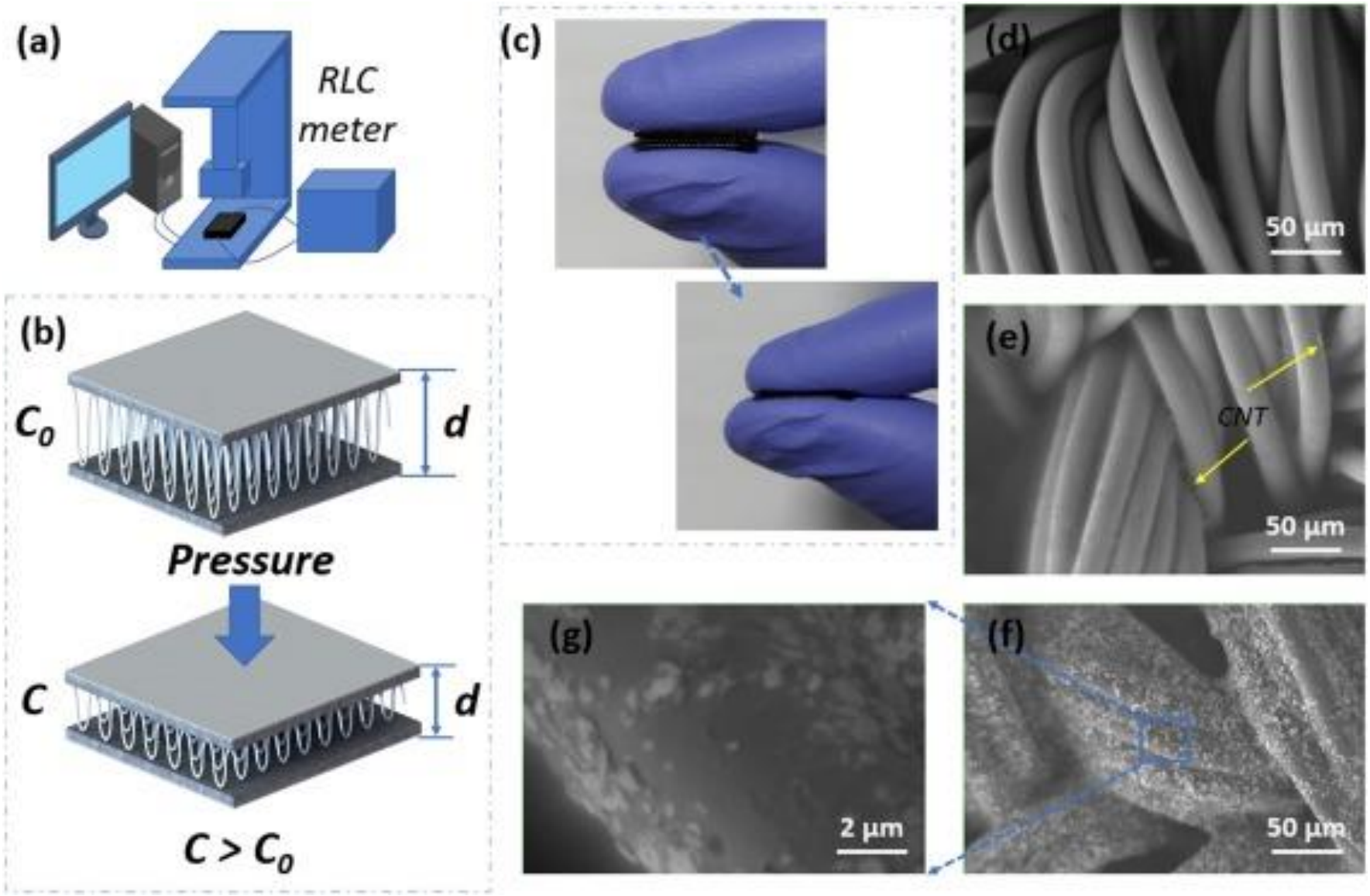

Highly elastic capacitive pressure sensor based on smart textiles for full-range human motion monitoring - ScienceDirect

The sock and anklet work together to provide runners with valuable data.
© Sensoria

Each smart sock is infused with three thin, soft textile pressure sensors.

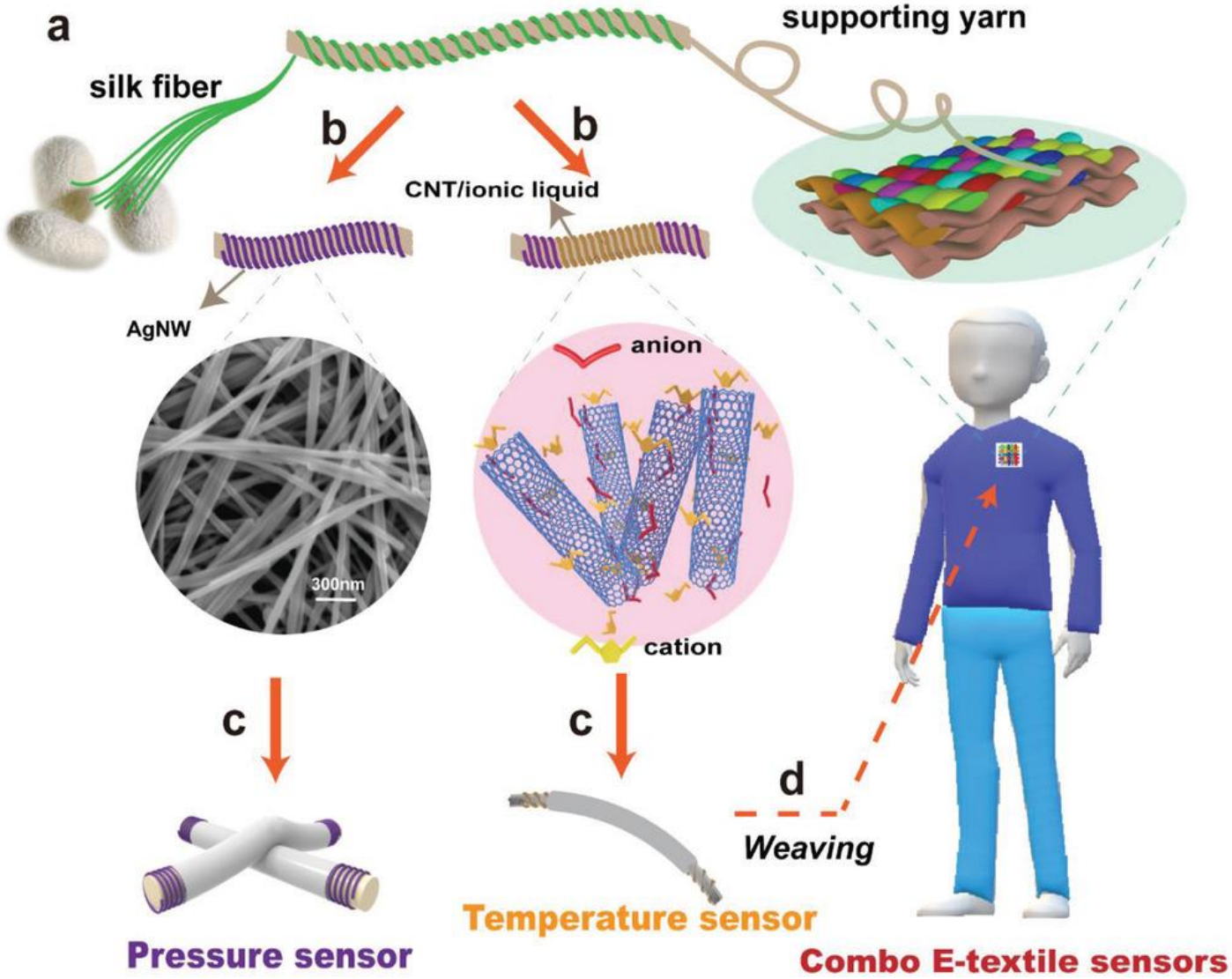

https://doi.org/10.1002/smll.201901558
Silk Composite Electronic Textile Sensor for High Space Precision 2D Combo Temperature-Pressure Sensing - Wu - 2019 - Small - Wiley Online Library

Schema of the strategy of fabrication of silk fibers-wrapped combo temperature–pressure sensors:

a) Coiling supporting yarns by silkworm silk fibers;
b) coating the silk fibers coiled yarns with temperature or pressure sensing materials (the mixture of CNT and a ionic liquid for temperature sensing; and Ag NWs for pressure sensing);
c) coating the protection or dielectric layers on the functional yarns/fibrous sensors;
d) weaving the fibrous sensors into a combo two-layer multimode sensors textile.

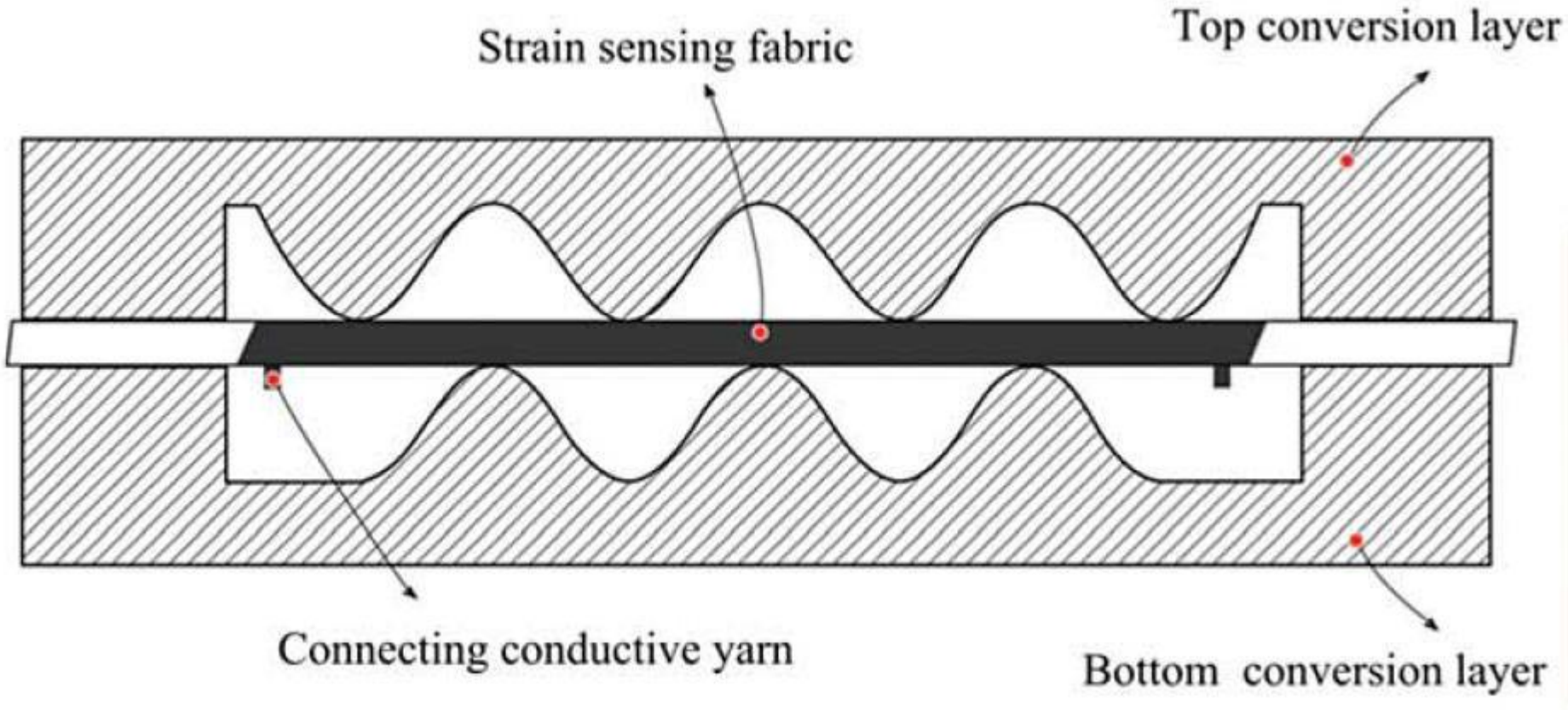

In HK, Fashion Can Be Intelligent | Fashion in HK (wordpress.com)

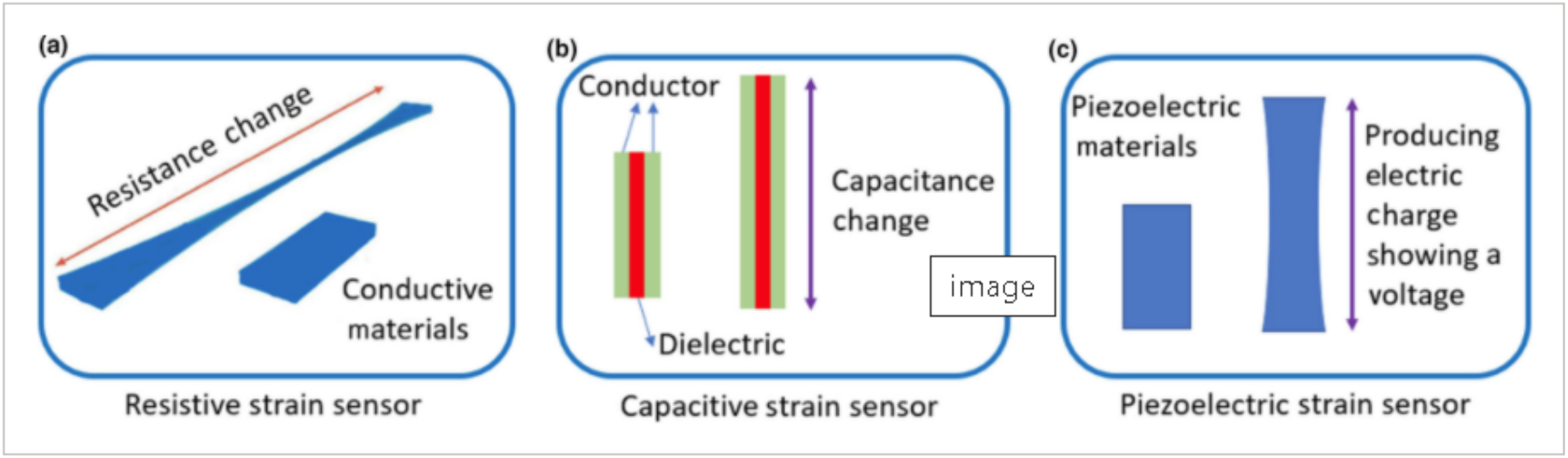
(a)
Resistance change
Conductive materials
Resistive strain sensor
(b)
Conductor
Capacitance change
Dielectric
Capacitive strain sensor
(c)
Piezoelectric materials
Producing electric charge showing a voltage
Piezoelectric strain sensor

image

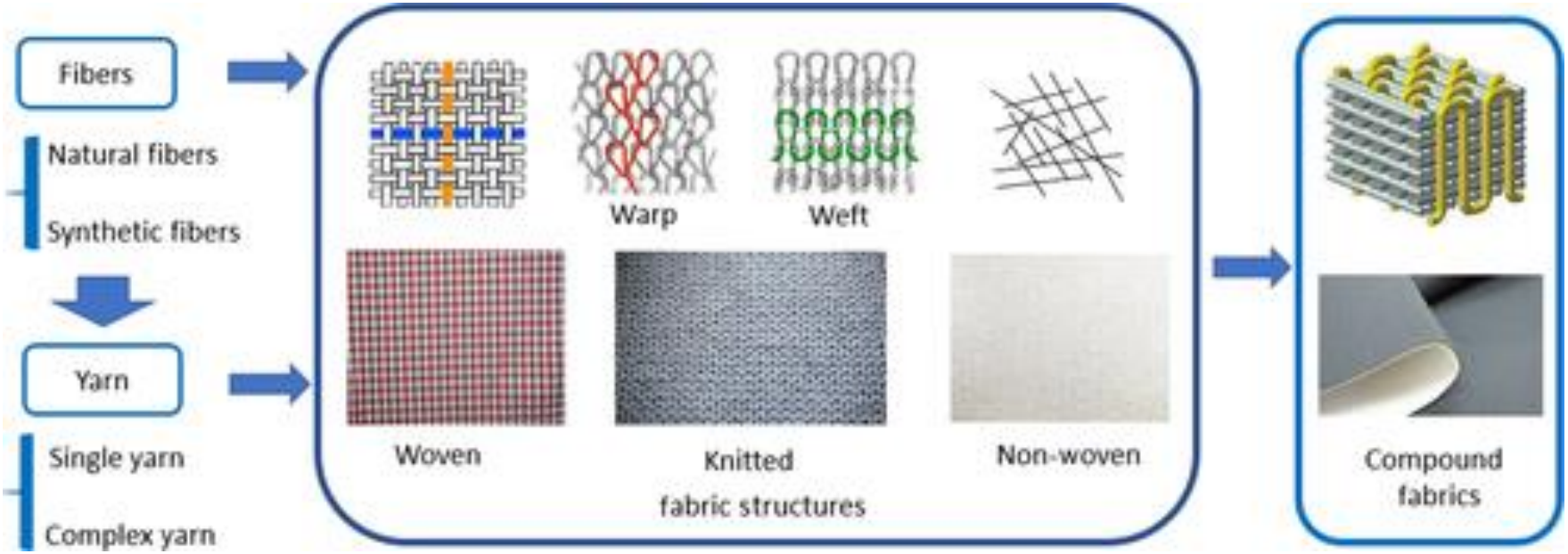
Fibers
Natural fibers
Synthetic fibers
Yarn
Single yarn
Complex yarn
Warp
Weft
Woven
Knitted
Non-woven
fabric structures
Compound fabrics

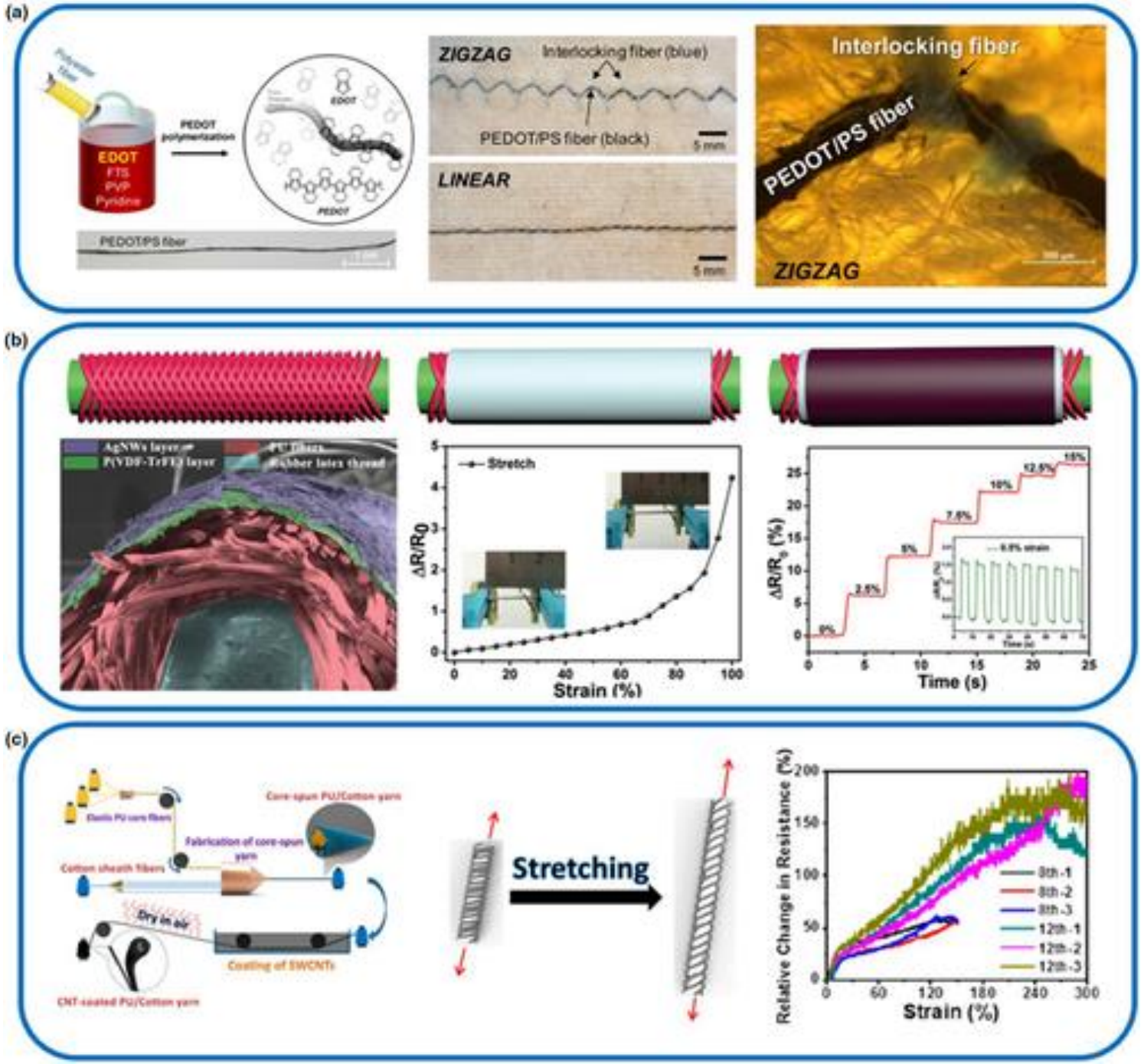
(a)
EDOT
FTS
PVP
Pyridine
PEDOT polymerization
EDOT
PEDOT
PEDOT:PS fiber
ZIGZAG
Interlocking fiber (blue)
PEDOT:PS fiber (black)
5 mm
LINEAR
5 mm
Interlocking fiber
PEDOT:PS fiber
ZIGZAG
(b)
AgNWs layer
P(VDF-TrFE) layer
PET fabric
Rubber latex thread
Stretch
ΔR/R0
Strain (%)
ΔR/R0 (%)
0%
2.5%
5%
7.5%
10%
12.5%
15%
Time (s)
(c)
Elastic PU core fibers
Core-spun PU/Cotton yarn
Fabrication of core-spun yarn
Cotton sheath fibers
Dry in air
Coating of SWCNTs
CNT-coated PU/Cotton yarn
Stretching
Relative Change in Resistance (%)
Strain (%)
8th-1
8th-2
8th-3
12th-1
12th-2
12th-3

- a) Left: Schematic illustration of polymerization of PEDOT on a polyester (PS) fiber. Middle: optical images of linear- and zigzag-type textile strain sensor-embedded fabrics. Right: optical microscope images of PEDOT/PS textile strain sensors showing the immobilized PEDOT/PS fibers after interlocking with the PS fibers. Reprinted with permission from Ref.78 Copyright 2017 American Chemical Society. b) Schematic structure and SEM image of (Top left) the elastic thread surface, (Top middle) the P(VDF-TrFE) layer around the thread fiber surface after electrospinning, and (Top right) the Ag nanowires layer after five dip-coating times. Bottom left: SEM image of the cross section of AgNW coated core-spun yarn. Bottom middle: elative resistance variation in P(VDF-TrFE)-based fibers when being stretched up to 100% strain. Bottom right: resistance variation under gradually ascending step strain from 0% to 15% strain. The inset shows the cyclic response curve at consecutive input step strain of 0.5%. Reprinted with permission from Ref.68 Copyright 2016 John Wiley & Sons, Inc. c) Left: schematics illustration of the self-developed fabrication process of the PU/cotton/CNT yarn. Middle: schematics illustration showing the stretchability and the morphological comparison before and after stretching. Right: relative change in resistance of the eighth and 12th immersed yarns vs strain (%) (relative change in resistance defined as: $\Delta R/R_0$). Reprinted with permission from Ref.84 Copyright 2016 American Chemical Society.

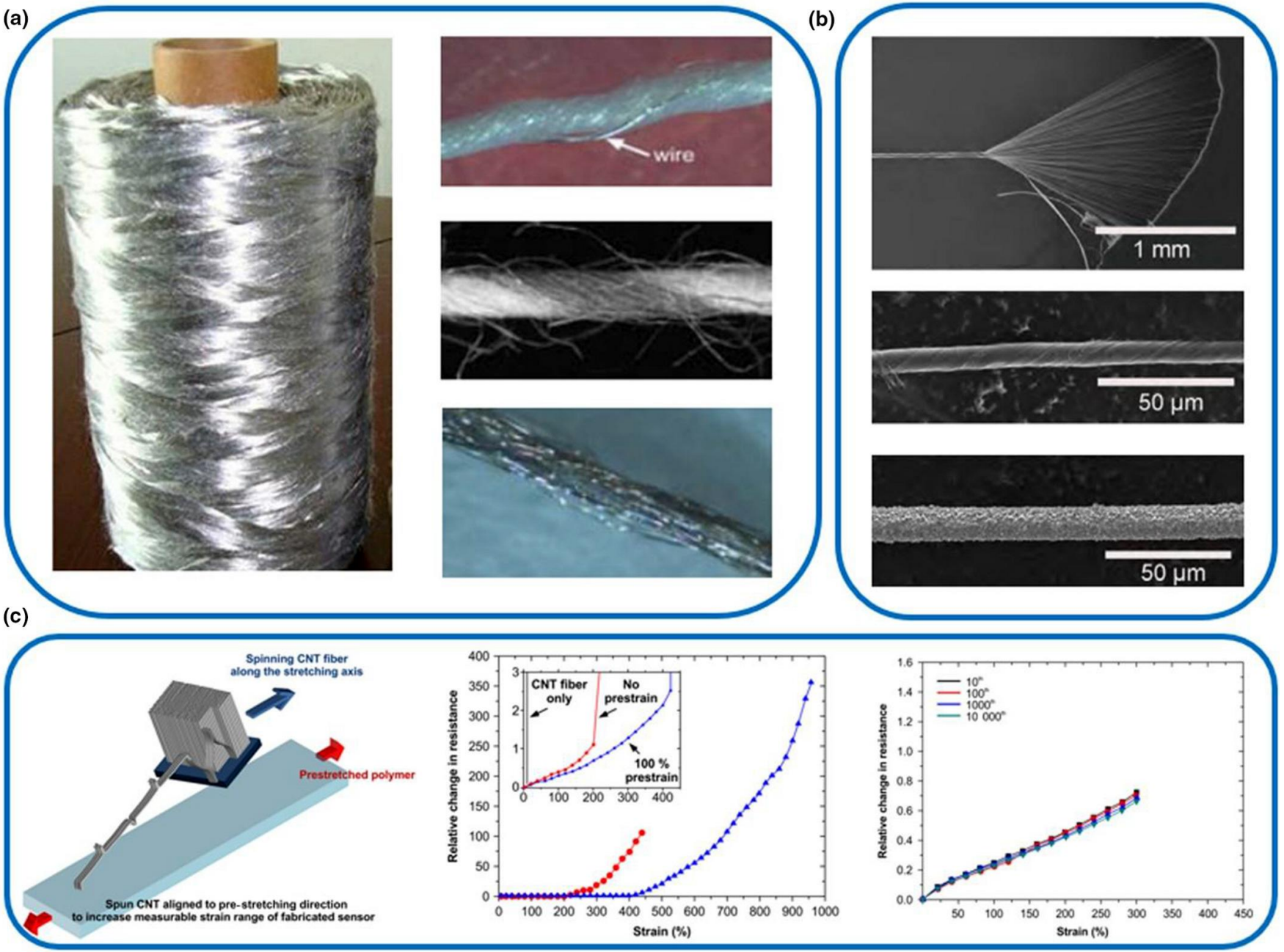
(a)
wire
(b)
1 mm
50 μm
50 μm
(c)
Spinning CNT fiber
along the stretching axis
Prestretched polymer
Spun CNT aligned to pre-stretching direction
to increase measurable strain range of fabricated sensor
CNT fiber
only
No
prestrain
100 %
prestrain
Relative change in resistance
Strain (%)
10"
100"
1000"
10 000"
Relative change in resistance
Strain (%)

- a) Left: aluminum fiber; Right top: twisted metal wire; Right middle: metal filaments yarn; Right bottom: metal-coated yarn. b) Top: SEM of directly spun CNT yarns from the as-grown CNT array. Middle: low magnification SEM of an as-spun yarn. Bottom: low magnification SEM of a yarn end coated with Al. Reprinted with permission from Ref.90 Copyright 2010 IOP Publishing Ltd. c) Left: illustration of the fabrication process. The dry-spun CNT fibers attach directly to the elastic Ecoflex substrate. Middle: relative change in resistance versus strain for unsupported CNT fibers (black), CNT fibers on an unstrained Ecoflex substrate (red), and CNT fibers on an Ecoflex substrate prestrained by 100% (blue); the strain ranged from 0% to 450% strain (inset). Right: relative change in resistance versus strain for 10 (black), 1 000 (red), 1 000 (blue), and 10 000 cycles (green) for increases in the strain from 0% to 300%. Reprinted with permission from Ref.93 Copyright 2015 American Chemical Society.

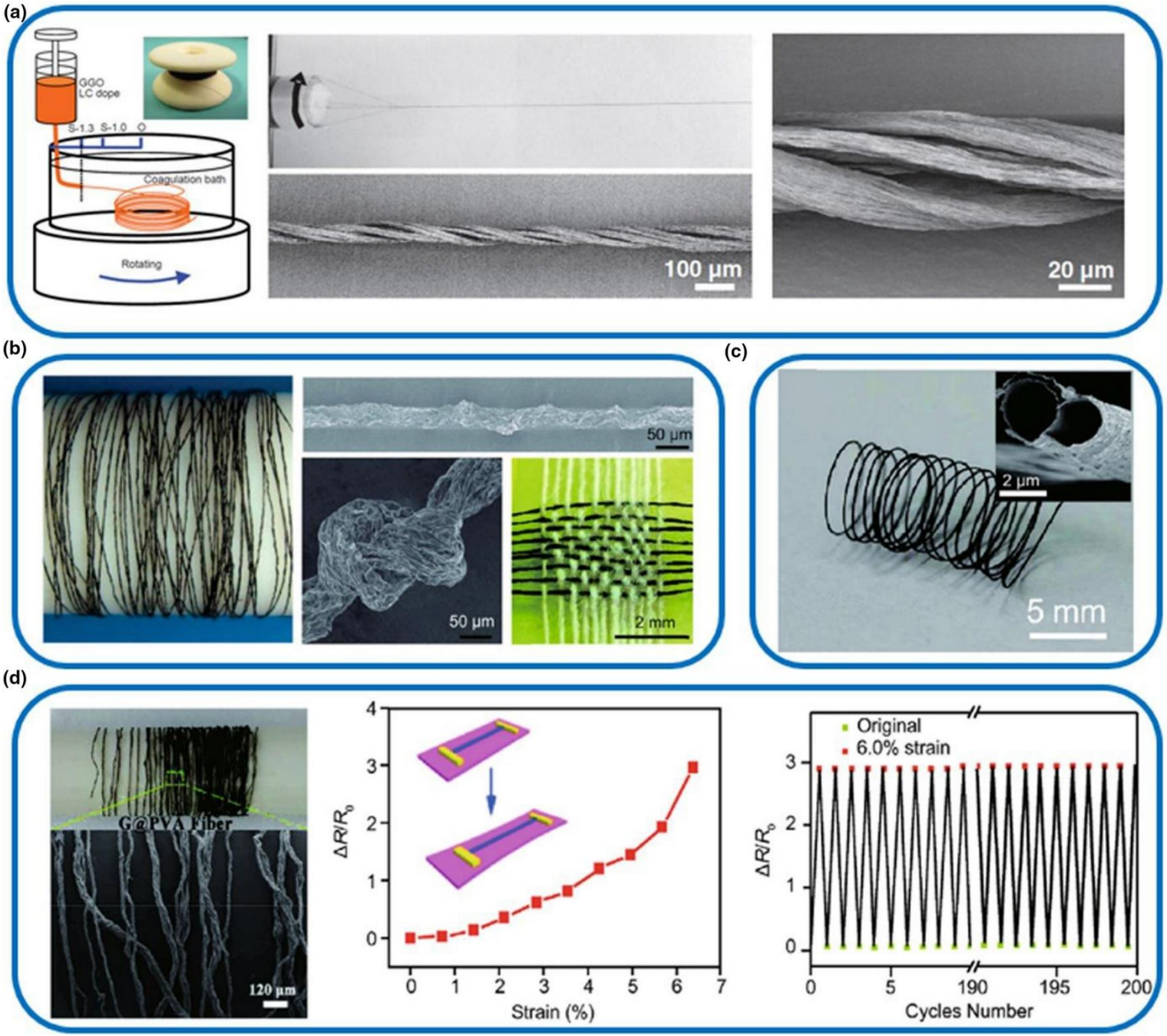
(a)
GGO
LC dope
S-1.3 S-1.0 Q
Coagulation bath
Rotating
100 μm
20 μm
(b)
50 μm
50 μm
2 mm
(c)
2 μm
5 mm
(d)
G@PVA Fiber
120 μm
ΔR/R0
Strain (%)
Original
6.0% strain
ΔR/R0
Cycles Number

- a) Left: schematic diagram showing the process to prepare GO fibers by wet-spinning methods and an image showing the continuous GO fibers wound around a ceramic reel; Right: photograph of the process to twist graphene fibers to yarns, and SEM images of the twisted yarn at different magnitudes. Reprinted with permission from Ref.96 Copyright 2013, Wiley-VCH. b) Left: 4-m-long GO fiber wound on a Teflon drum (diameter, 2 cm); Right: SEM image of the fiber, and the surface winkled morphology of the tighten knot of graphene fiber, and A mat of graphene fibers (horizontal) woven together with cotton threads (vertical). Reprinted with permission from Ref.95 Copyright 2011, Nature Publishing Group. c) Photograph and SEM images of graphene microtubings obtained by a confined hydrothermal technique. Reprinted with permission from Ref.98 Copyright 2012, the American Chemical Society. d) Graphene fibers prepared by CVD combined with PVA for strain sensors. Reprinted with permission from Ref.99 Copyright 2015, American Chemical Society.

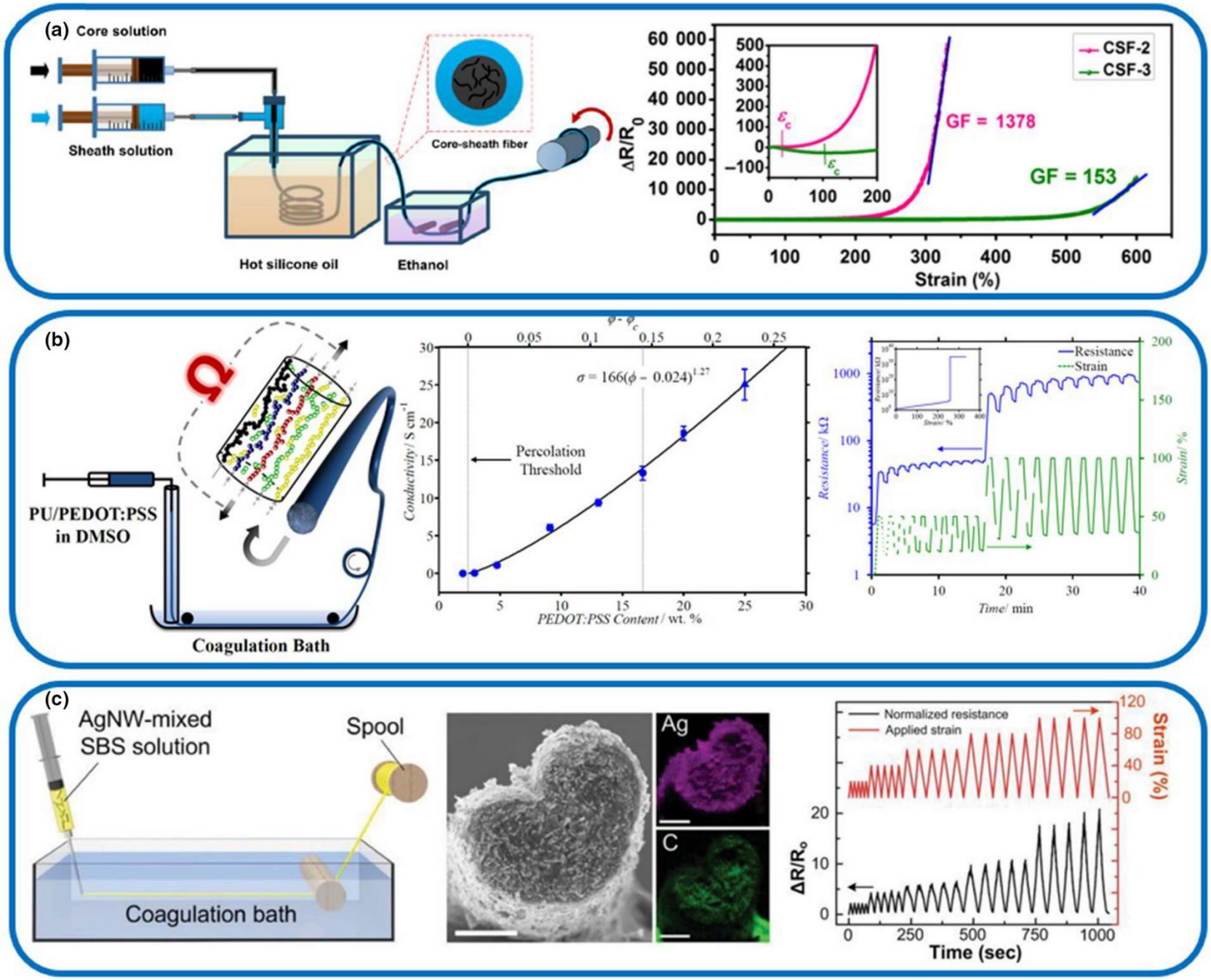
(a)
Core solution
Sheath solution
Core-sheath fiber
Hot silicone oil
Ethanol
ΔR/R0
Strain (%)
CSF-2
CSF-3
GF = 1378
GF = 153
(b)
PU/PEDOT:PSS
in DMSO
Coagulation Bath
Conductivity/ S cm-1
PEDOT:PSS Content / wt. %
Percolation
Threshold
Resistance/ kΩ
Strain/ %
Time/ min
Resistance
Strain
(c)
AgNW-mixed
SBS solution
Spool
Coagulation bath
Ag
C
Normalized resistance
Applied strain
Strain (%)
ΔR/R0
Time (sec)

- a) Left: schematic illustration of the coaxial spinning process for the highly stretchable fibers. Right: resistance change ($\Delta R/R_0$) as a function of the applied strain with different CNT contents, that is, 2 and 3 wt%. Reprinted with permission from Ref. 103 Copyright 2018 American Chemical Society. b) Left: schematic illustration of conducting elastomeric fibers based on composite of polyurethane (PU) and PEDOT:PSS produced by wet-spinning method. Middle: conductivity of PU/PEDOT:PSS fibers at different PEDOT:PSS contents (● PU 50 mg mL^{-1}, ■ PU 40 mg mL^{-1}, and ▲ PU 30 mg mL^{-1}). The curve indicates the best fit obtained using percolation theory. Right: resistance change by strain for PU/PEDOT:PSS fiber with 13.0 wt% PEDOT:PSS (No.6) in a cyclic electromechanical test at 50% and 100% strains for 10 cycles (inset shows the electromechanical tensile test for the same fiber). Reprinted with permission from Ref. 109 Copyright 2014 John Wiley & Sons, Inc. c) Left: schematic illustration of the fabrication process for the highly stretchable conductive fiber. Middle: cross-sectional SEM image and EDS mapping images of Ag, and C obtained from the 0.56 wt% AgNW–AgNP embedded composite fiber. Scale bar: 100 μm. Right: the normalized resistance changes varying the applied strains at 0%, 20%, 40%, 60%, 80%, and 100%. Reprinted with permission from Ref. 110 Copyright 2015 John Wiley & Sons, Inc.

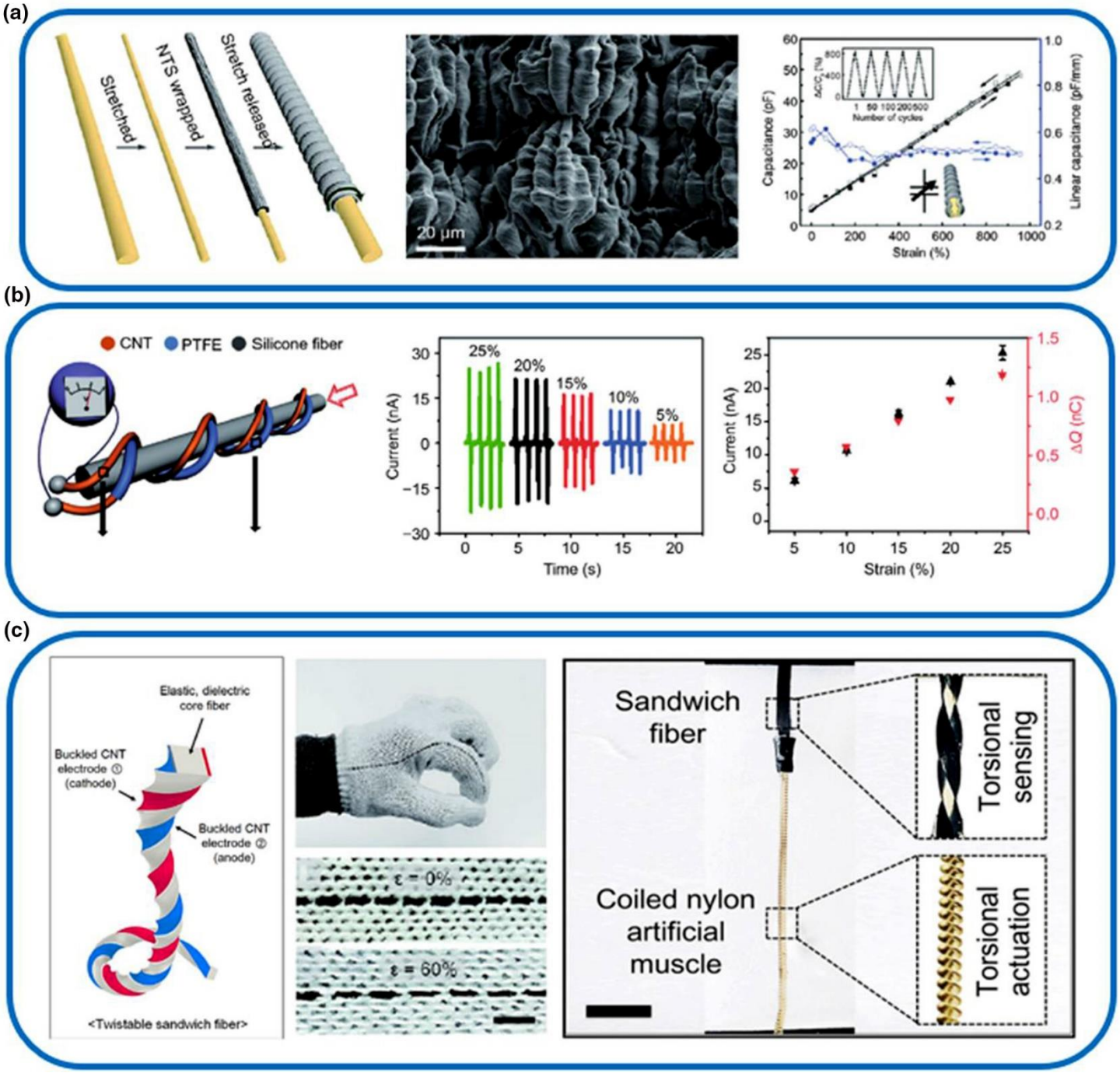
(a)
Stretched
NTS wrapped
Stretch released
20 μm
Capacitance (pF)
Linear capacitance (pF/mm)
Strain (%)
Number of cycles
(b)
CNT
PTFE
Silicone fiber
25%
20%
15%
10%
5%
Current (nA)
Time (s)
ΔQ (nC)
Strain (%)
(c)
Elastic, dielectric core fiber
Buckled CNT electrode ① (cathode)
Buckled CNT electrode ② (anode)
<Twistable sandwich fiber>
ε = 0%
ε = 60%
Sandwich fiber
Coiled nylon artificial muscle
Torsional sensing
Torsional actuation

- a) Left: schematic illustration showing the fabrication process of a sheath-core fiber; Middle: the hierarchical buckling shown in the SEM image; Right: sheath-core CNT fibers for strain sensors. Reprinted with permission from Ref.54 Copyright 2015, the American Association for the Advancement of Science. b) Left: schematic illustration showing the fabrication process of a self-powered strain sensor made of an elastic fiber and two cotton threads coated with CNTs and PTFE/CNTs, respectively; Middle: output current–time curves; Right: the peak value of the output currents and integral transferred charges of an AFSS varied with stimulated strains of 5%, 10%, 15%, 20%, and 25%. Reprinted with permission from Ref.126 Copyright 2015, Wiley-VCH. c) Left: schematic illustration of a twist-inserted rectangular sandwich fiber, which comprises an Ecoflex rubber core and two symmetric, buckled CNT electrodes; Middle: photographs of 20 cm long sandwich fiber woven into a commercial glove and magnified images thereof before and after application of 60% tensile strain (scale bar: 8 mm); Right: photograph image showing an 8 cm long coiled nylon torsional artificial muscle and attached sandwich sensor (scale bar = 2 cm). Inset images show the magnified muscle and sensor when heated by a heat gun. Reprinted with permission from Ref.55 Copyright 2016, the American Chemical Society.

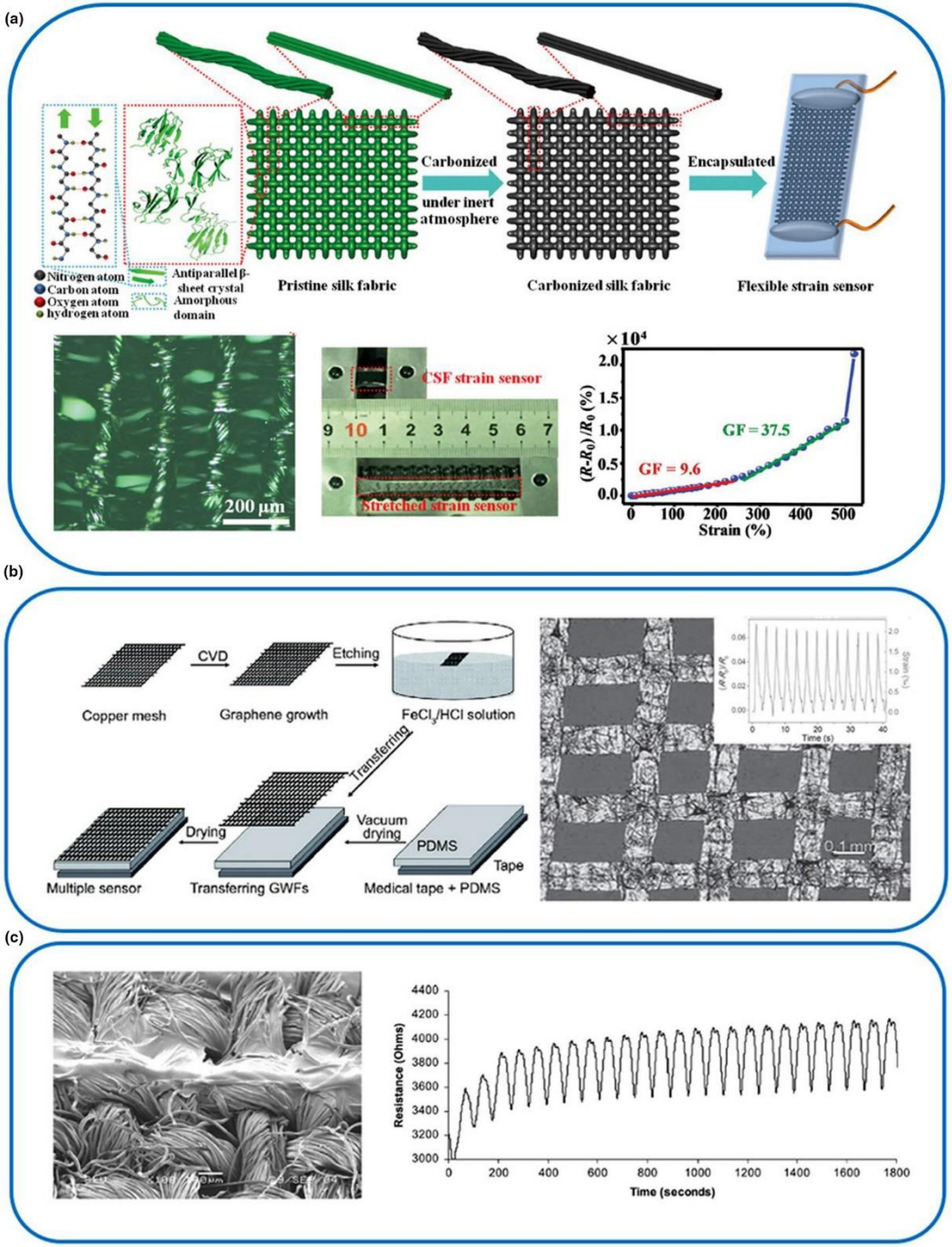
(a)
Carbonized
under inert
atmosphere
Encapsulated
Nitrogen atom
Carbon atom
Oxygen atom
hydrogen atom
Antiparallel β-sheet crystal
Amorphous domain
Pristine silk fabric
Carbonized silk fabric
Flexible strain sensor
200 μm
CSF strain sensor
Stretched strain sensor
×10⁴
GF = 37.5
GF = 9.6
(R-R0)/R0 (%)
Strain (%)
(b)
CVD
Etching
Copper mesh
Graphene growth
FeCl3/HCl solution
Transferring
Drying
Vacuum drying
PDMS
Tape
Multiple sensor
Transferring GWFs
Medical tape + PDMS
0.1 mm
Time (s)
Strain (%)
(c)
Resistance (Ohms)
Time (seconds)

- a) Top: illustration showing the hierarchical structures and the fabrication of CSF strain sensors. A plain weave structure is used as an example; Bottom: enlarged optical images of a carbonized plain weave silk fabric, and a photograph of the pristine and stretched CSF strain sensor, showing its ultraelasticity, and relative change in resistance of the strain sensor versus the applied strain in the y-direction (strain rate 30% min^{-1}). Reprinted with permission from Ref. 132 Copyright 2016, Wiley-VCH. b) Left: schematic illustrations of fabrication procedure of a human motion sensor based on graphene woven fabrics (GWFs)-PDMS-medical tape film; Right: a magnification of the optical microscope image and the inset is the relative change in resistance between 0% and 0.2% strain. Reprinted with permission from Ref. 133 Copyright 2014, Wiley-VCH. c) PEDOT-printed woven cotton fabric and resistance of PEDOT-PSS sensor with 25 repeated cycles of strain to 5% and relaxation. Reprinted with permission from Ref. 134 Copyright 2008 Taylor and Francis.

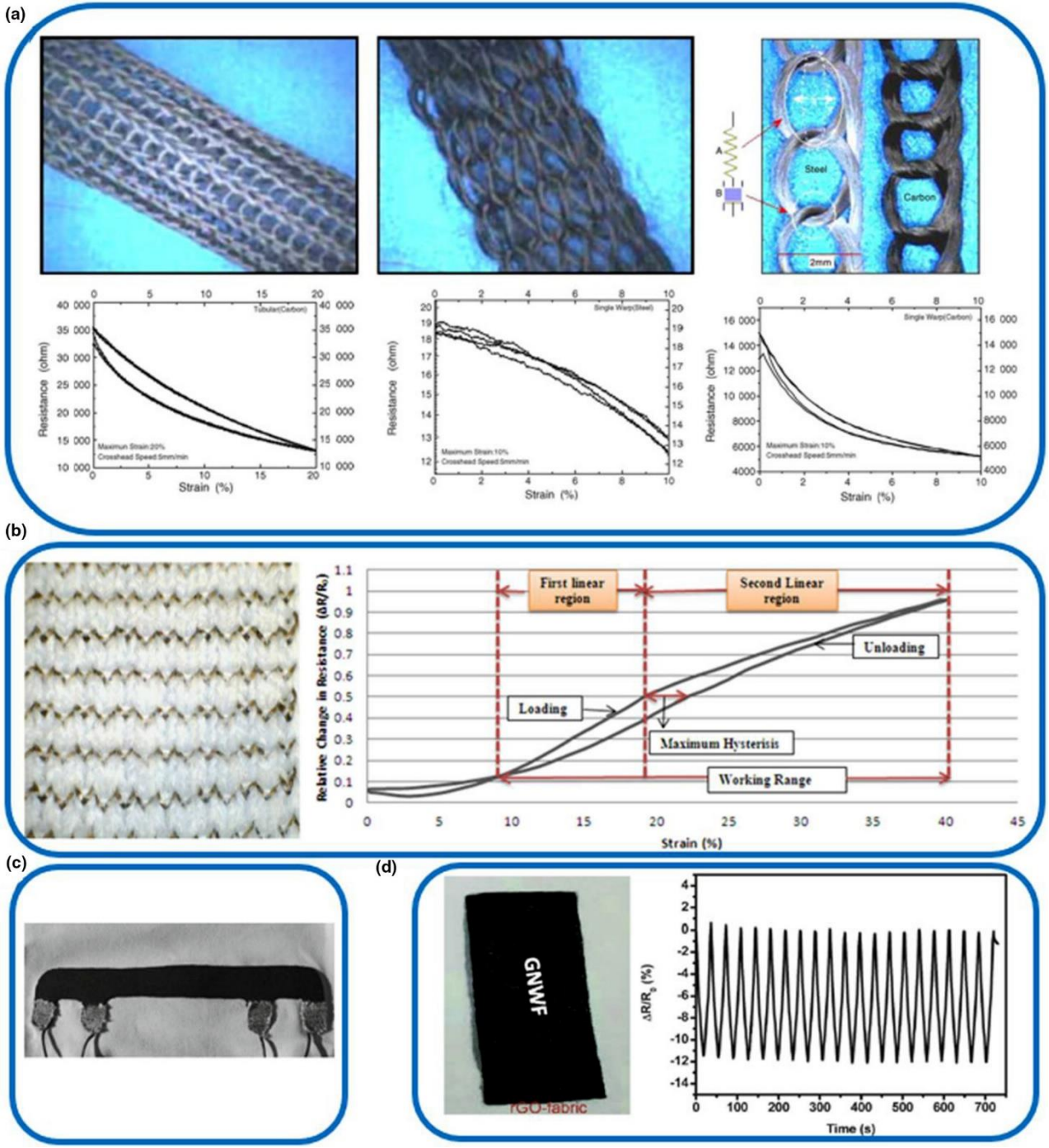
(a)
A
B
Steel
Carbon
2mm
Resistance (ohm)
Strain (%)
Tubular(Carbon)
Maximun Strain:20%
Crosshead Speed:5mm/min
Single Warp(Steel)
Maximum Strain:10%
Crosshead Speed:5mm/min
Single Warp(Carbon)
Maximum Strain:10%
Crosshead Speed:5mm/min
(b)
Relative Change in Resistance (ΔR/R0)
First linear region
Second Linear region
Unloading
Loading
Maximum Hysterisis
Working Range
Strain (%)
(c)
(d)
GNWF
rGO-fabric
ΔR/R0 (%)
Time (s)

- a) Tubular steel (Top left) and carbon (Top middle) knitted fabric; Top right: single warp steel (left) and carbon (right) knitted fabric, resistance–strain relationships of samples: tubular carbon knitted fabric (Bottom left), single warp steel (Bottom middle) and carbon (Bottom right) knitted fabric. Reprinted with permission from Ref.139 Copyright 2005 Elsevier B.V. b) Technical face of knitted sample shows conductive loops in the structure and relative change in resistance–strain graphs. Reprinted with permission from Ref.141 Copyright 2013 MDPI. c) Single-layer knitted piezoresistive fabrics (KPF) sample attached to a Lycra® substrate. Reprinted with permission from Ref.142 Copyright 2017 Springer International Publishing AG. d) Optical images of the graphene non-woven fabric (GNWF) (reduced GO (rGO) loading 2.3%) and normalized resistance change during a cyclic bending test. Reprinted with permission from Ref.143 Copyright 2016 the Royal Society of Chemistry.

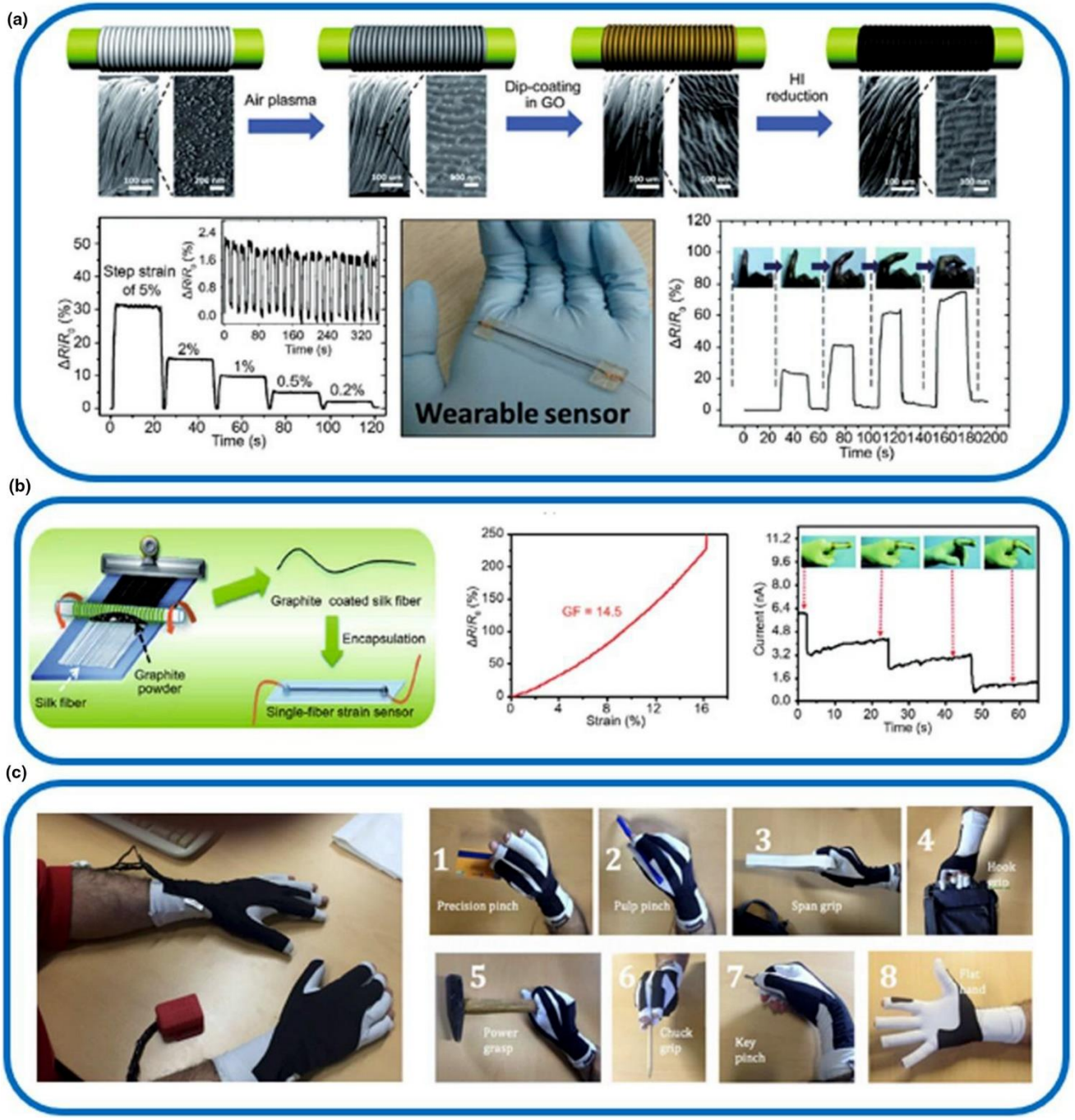
(a)
Air plasma
Dip-coating in GO
HI reduction
Step strain of 5%
2%
1%
0.5%
0.2%
Time (s)
Wearable sensor
(b)
Graphite coated silk fiber
Encapsulation
Graphite powder
Silk fiber
Single-fiber strain sensor
GF = 14.5
Strain (%)
Current (nA)
(c)
1 Precision pinch
2 Pulp pinch
3 Span grip
4 Hook grip
5 Power grasp
6 Chuck grip
7 Key pinch
8 Flat hand

- a) Top: schematic illustration of the fabrication process and the characterization of the graphene-based fiber; Bottom left: resistance variation under gradually diminishing step strain from 5% to 0.2% strain. The inset shows the response signal at 20 consecutive input step strain of 0.2%. Bottom middle: photograph of the wearable sensor. Bottom right: response signal of wearable sensor in monitoring finger bending. Inset: photographs of finger bending to the corresponding positions. Reprinted with permission from Ref.100 Copyright 2015 Wiley-VCH. b) Left: fabrication of sheath-core structured graphite/silk strain sensors through a dry-Meyer-rod-coating process; Middle: relative change in resistance versus strain of a graphite/silk fiber (GSF) strain sensor when being stretched until broken; Right: response of the wearable sensor to stepwise bending of an index finger (insets show photographs of a strain sensor attached along a finger, using adhesive tape). Reprinted with permission from Ref.86 Copyright 2016, the American Chemical Society. c) Kinesthetic and kinetic glove pair and functional hand grips to be classified. Reprinted with permission from Ref.144 Copyright 2016 Lorussi, Carbonaro, De Rossi, Paradiso, Veltink, and Tognetti

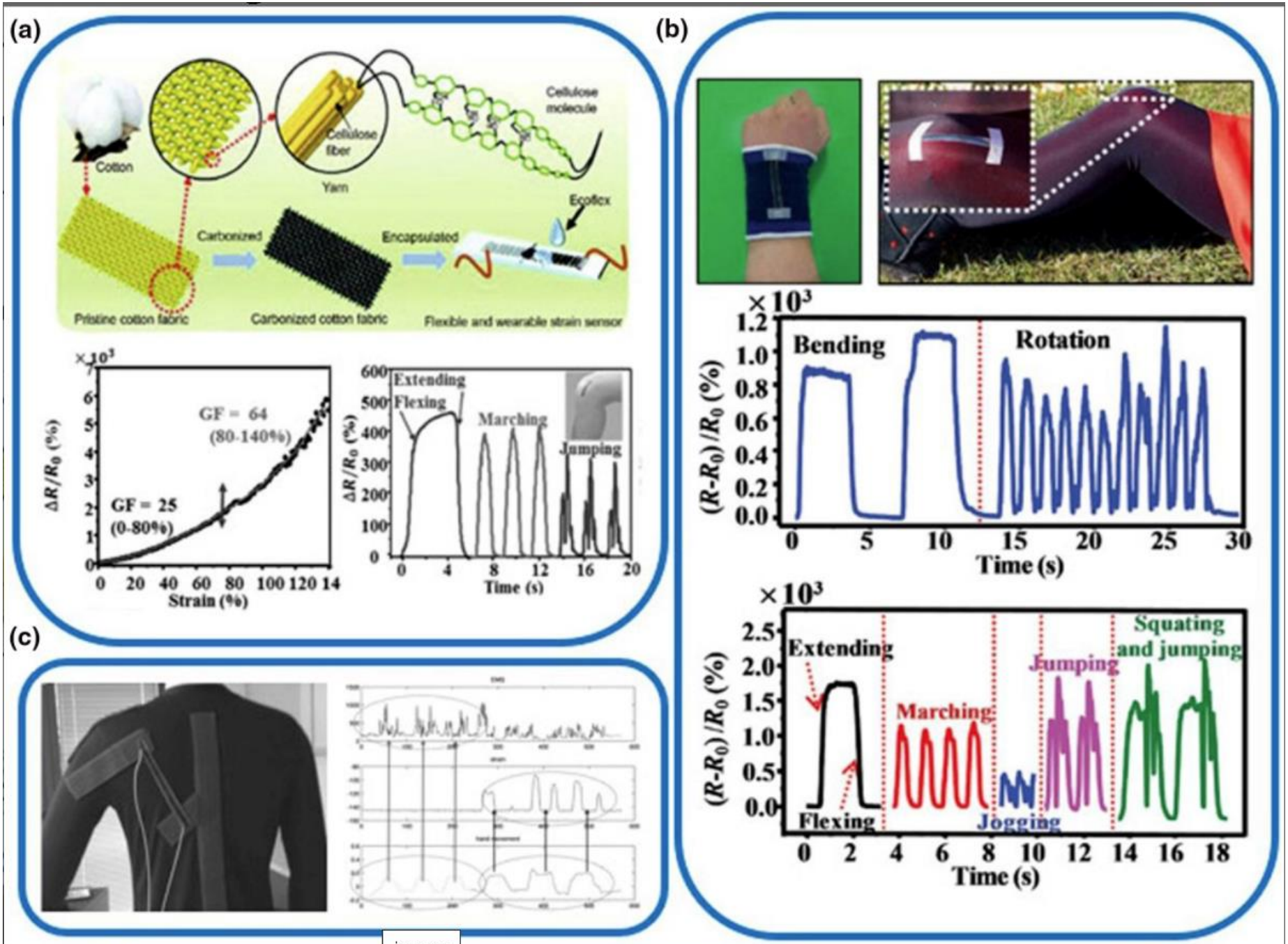
(a)
Cotton
Cellulose fiber
Yarn
Cellulose molecule
Ecoflex
Carbonized
Encapsulated
Pristine cotton fabric
Carbonized cotton fabric
Flexible and wearable strain sensor
×10³
ΔR/R₀ (%)
GF = 64
(80-140%)
GF = 25
(0-80%)
Strain (%)
Extending
Flexing
Marching
Jumping
Time (s)
(b)
×10³
(R-R₀)/R₀ (%)
Bending
Rotation
Time (s)
Extending
Flexing
Marching
Jogging
Jumping
Squating and jumping
(c)

image

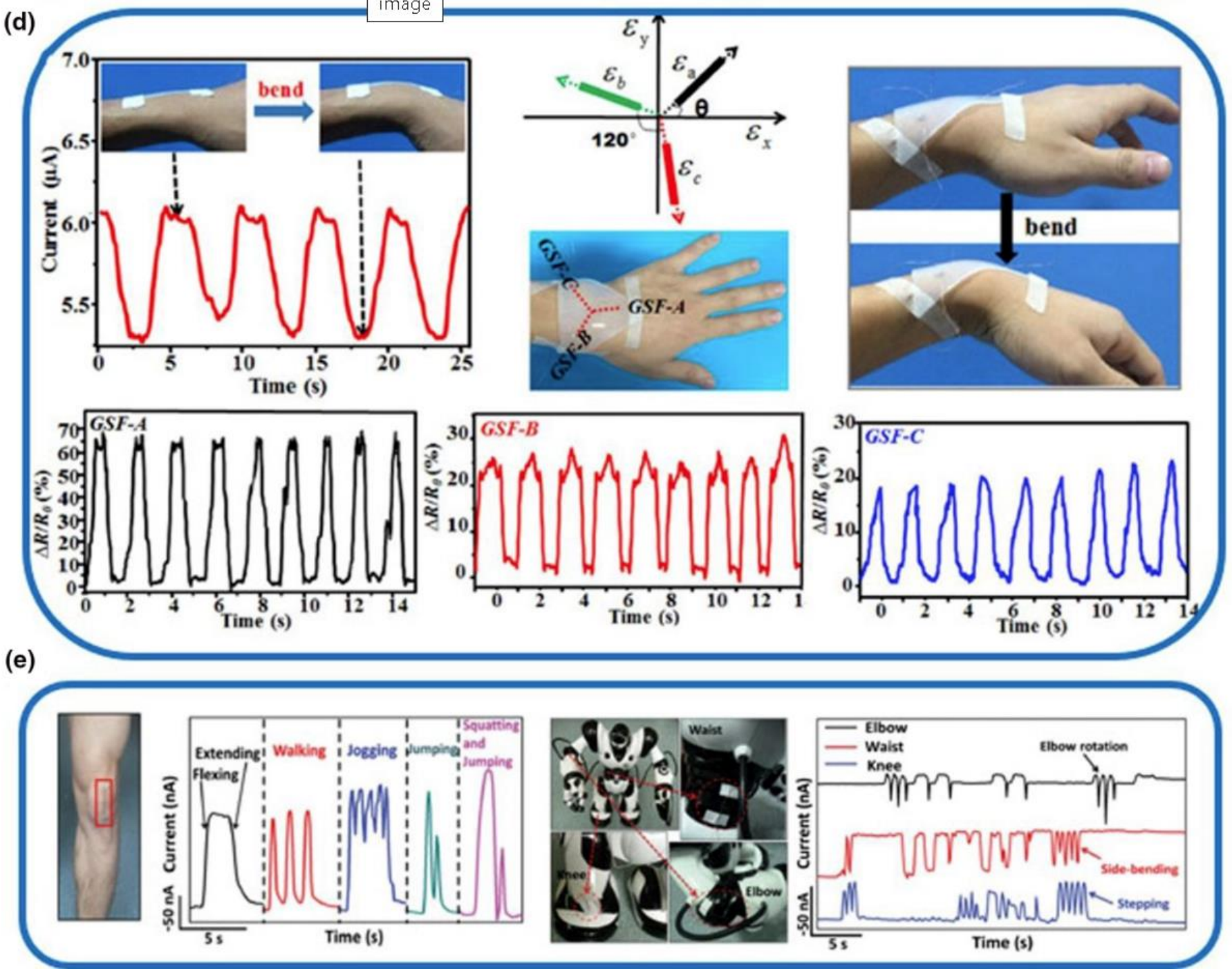
(d)
bend
Current (μA)
Time (s)
ε_y
ε_a
ε_b
θ
120°
ε_x
ε_c
GSF-C
GSF-A
GSF-B
bend
GSF-A
GSF-B
GSF-C
$\Delta R/R_0$ (%)
Time (s)
(e)
Extending
Flexing
Walking
Jogging
Jumping
Squatting and Jumping
Current (nA)
-50 nA
5 s
Time (s)
Waist
Knee
Elbow
Elbow
Waist
Knee
Elbow rotation
Side-bending
Stepping
Current (nA)
-50 nA
5 s
Time (s)

- a) Top: illustration showing the structure of the pristine cotton fabric and the fabrication process of the carbonized plain weave cotton fabric (CPCF) strain sensor; Bottom: relative resistance change as a function of tensile strain, and monitoring of human motion using the CPCF strain sensors and the response to motions of knee joint, the insert is the photograph of the strain sensor. Reprinted with permission from Ref.135 Copyright 2016, Wiley-VCH. b) Top: a wrist guard and a stocking. Middle: the corresponding signals of the bending and rotation of a wrist; Bottom: the corresponding signals of flexing/extending, marching, jogging, jumping, and squatting-jumping of a knee joint. Reprinted with permission from Ref.132 Copyright 2016, Wiley-VCH. c) Single-layer strain sensor is positioned in the scapular area in order to detect scapular elevations and abductions, and IMU (bottom), strain sensor (middle), and EMG (top) outputs during reaching activity. Left plot data acquired during a correct reaching movement. Right plot data derived from a compensatory movement are plotted. Reprinted with permission from Ref.144 Copyright 2016 Lorussi, Carbonaro, De Rossi, Paradiso, Veltink, and Tognetti. d) Top left: response of the wearable sensor to cyclic motion of a wrist (insets show photographs of a strain sensor attached on a wrist) and integrated rosette-shaped GSF strain senor for multidirectional motion detection. Top middle: illustration of the configuration of the strain sensor composed of three individual fiber strain sensors (GSF-A, GSF-B, and GSF-C); Top right: photographs of the strain sensor attached on a wrist. Bottom: responsive signals of GSF-A (left), GSF-B (middle), and GSF-C (right) during cyclic bending − unbending motion of the wrist. Reprinted with permission from Ref.86 Copyright 2016, the American Chemical Society. e) Left: wearable sensor attached to the knee, marked in the red box, and responsive curves of wearable sensor on the knee under motions of flexing/extending, walking, jogging, jumping, and squatting-jumping; Right: wearable sensor attached to the wrist, marked in the red box, and responsive curves of wearable sensor on the wrist before wearing (no load), and under normal/exercise conditions. Reprinted with permission from Ref.100 Copyright 2015 Wiley-VCH.

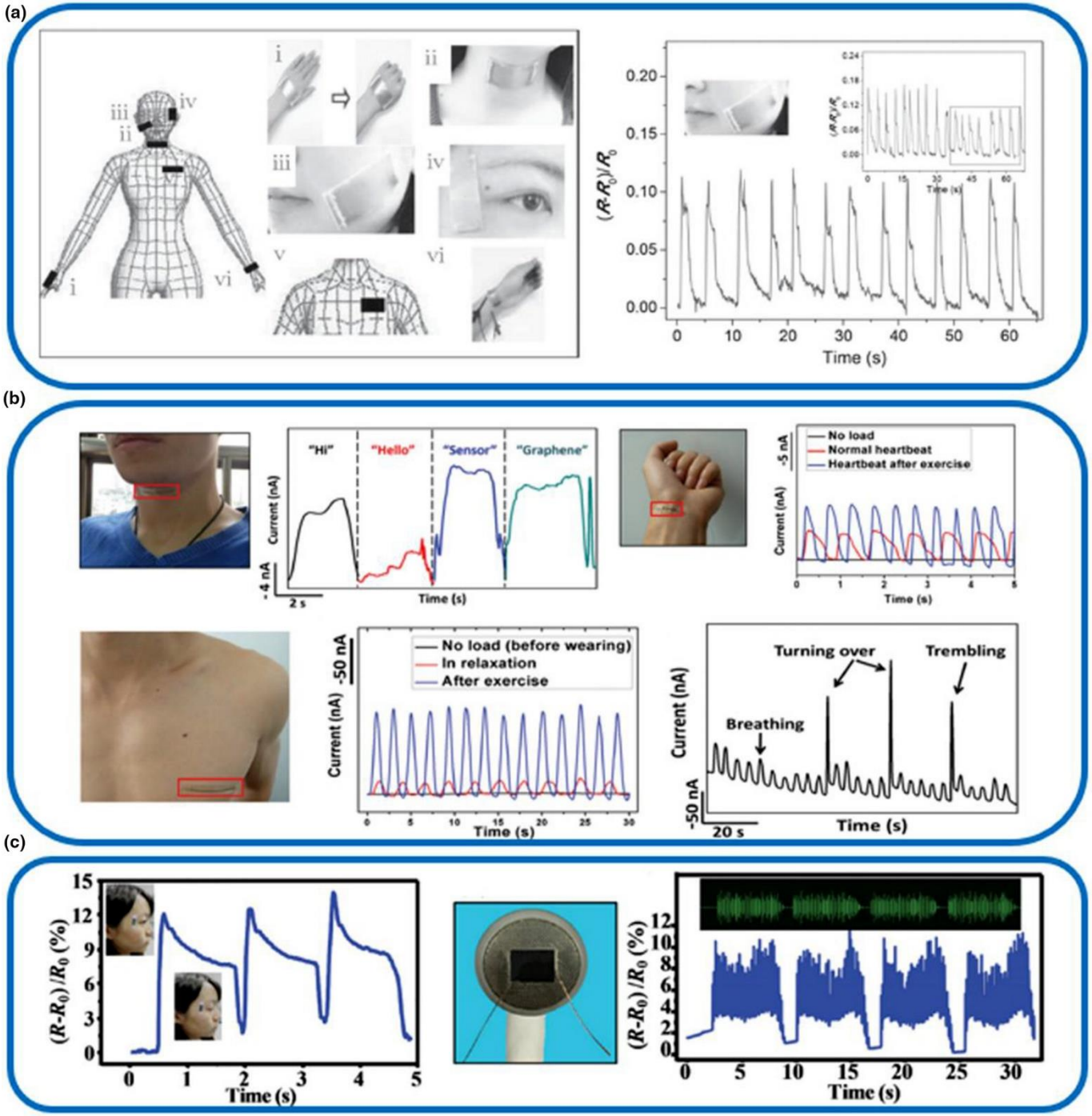
(a)
i
ii
iii
iv
v
vi
$(R-R_0)/R_0$
Time (s)
(b)
"Hi"
"Hello"
"Sensor"
"Graphene"
Current (nA)
-4 nA
2 s
Time (s)
No load
Normal heartbeat
Heartbeat after exercise
-5 nA
No load (before wearing)
In relaxation
After exercise
-50 nA
Turning over
Trembling
Breathing
20 s
(c)
$(R-R_0)/R_0$ (%)
Time (s)

- a) Photograph images of GWFs-PDMS-tape at various positions of, and relative change in resistance in muscle motions of expression changes. Reprinted with permission from Ref.133 Copyright 2014, Wiley-VCH. b) Top left: wearable sensor attached to the throat, marked in the red box, and responsive curves when wearer spoke “Hi,” “Hello,” “Sensor,” and “Graphene”; Top right: wearable sensor attached to the wrist, marked in the red box, and responsive curves of wearable sensor on the wrist before wearing (no load), and under normal/exercise conditions; Bottom left: wearable sensor attached to the chest; Bottom middle: responsive curves of wearable sensor on the chest before wearing, in relaxation, and after exercise; Bottom right: responsive curves of wearable sensor on the chest. The wearer simulates deep sleep (keeping still) and light sleep (turning over and trembling frequently). Reprinted with permission from Ref.100 Copyright 2015 Wiley-VCH. c) Signals showing the tiny muscle movement caused by blinking. Insets: photographs of eye-opening, eye-closing, and photograph showing a sensor attached on an earphone, and signals of the sensor corresponding to a warble audio. Inset: the sound wave profile. Reprinted with permission from Ref.132 Copyright 2016, Wiley-VCH.

Taktilní sensory

Financováno Evropskou unií NextGenerationEU
Národní plán obnovy
MINISTERSTVO ŠKOLSTVÍ, MLÁDEŽE A TĚLOVÝCHOVY
NPO_TUL_MSMT-16598/2022

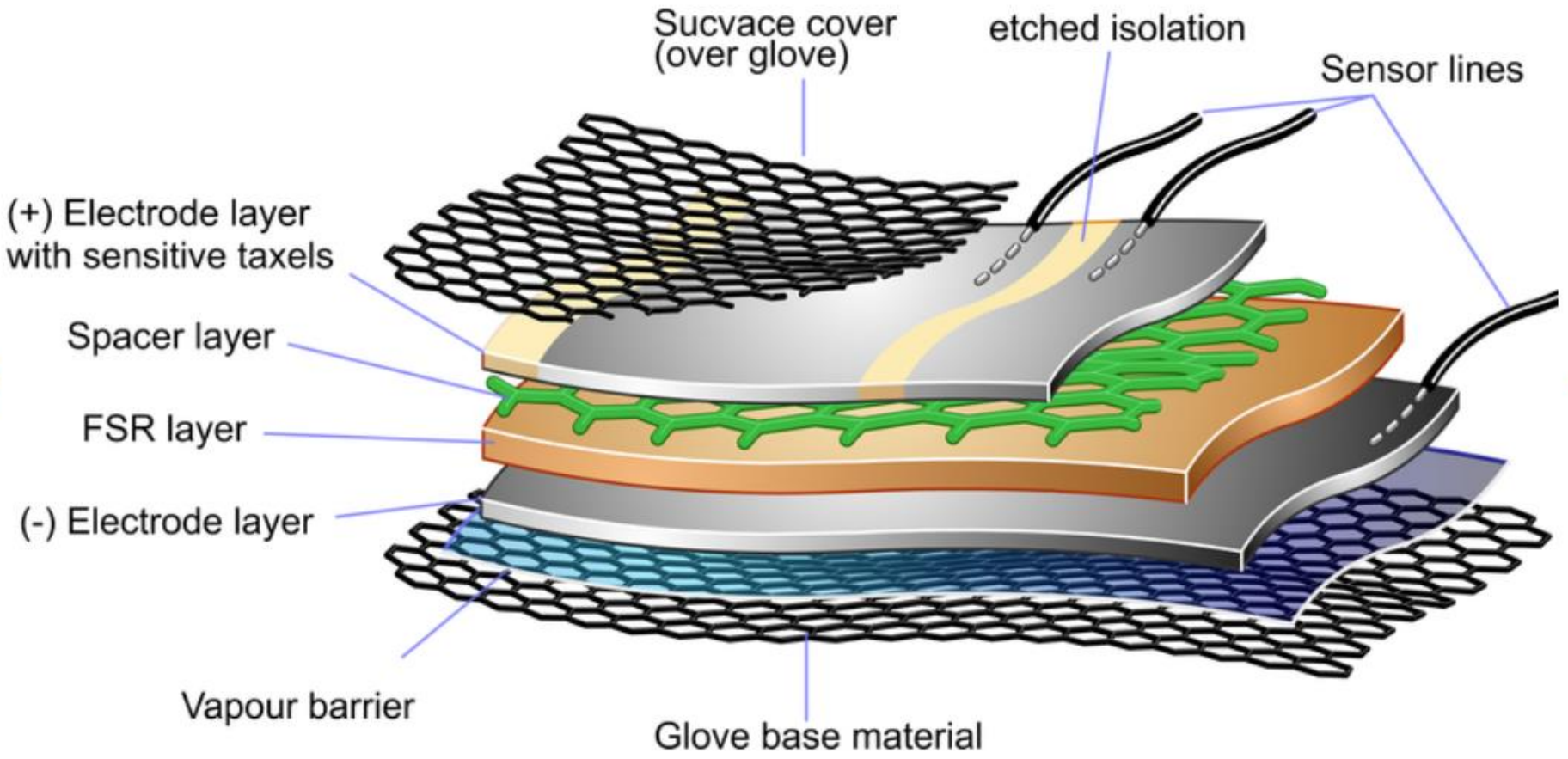

The flexible tactile sensing glove is manufactured from several layers of conductive and piezo-resistive fabrics.

- The flexible tactile sensing glove is manufactured from several layers... | Download Scientific Diagram (researchgate.net)

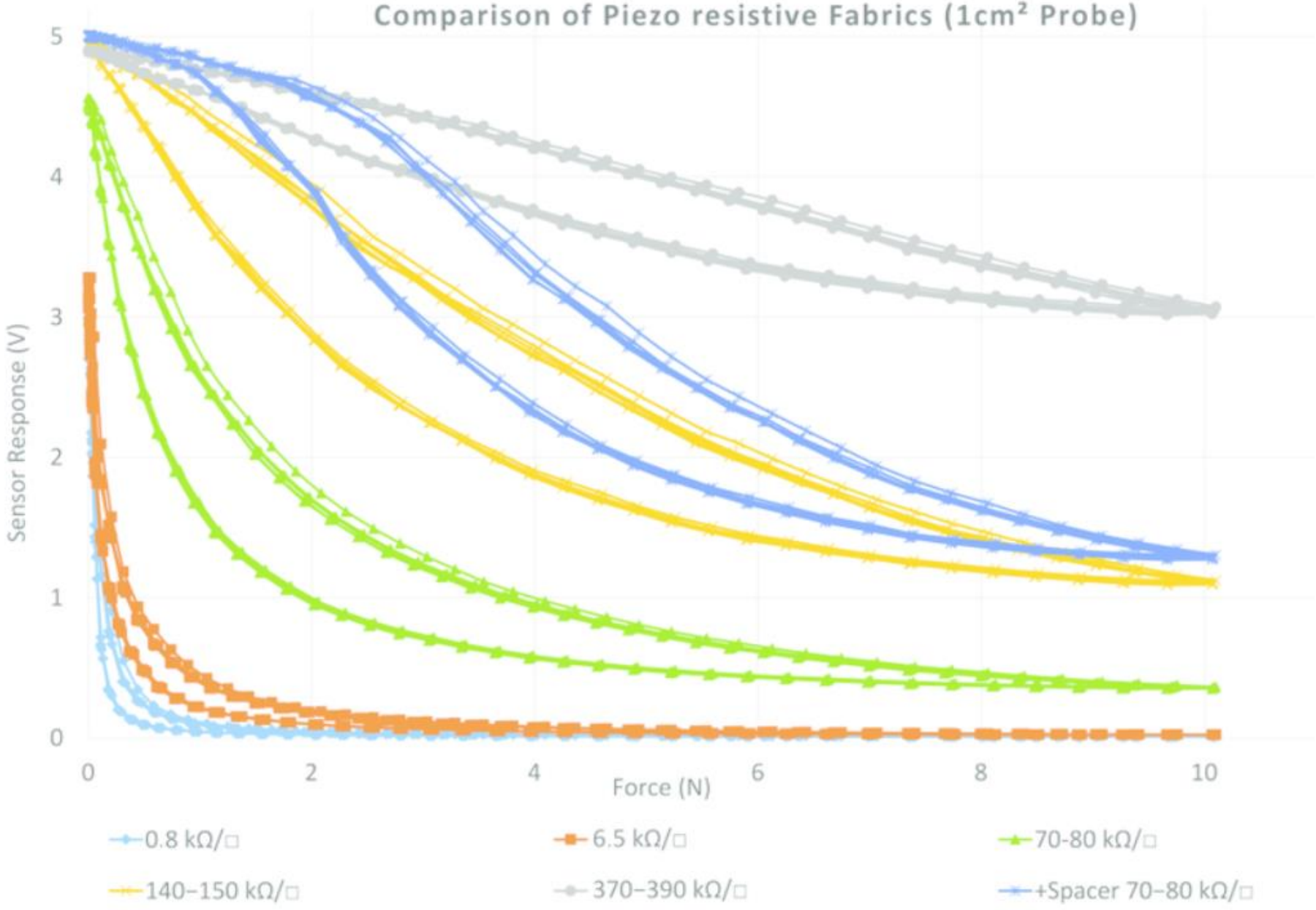
Comparison of Piezo resistive Fabrics (1cm² Probe)
Sensor Response (V)
0
1
2
3
4
5
0
2
4
6
8
10
Force (N)
0.8 kΩ/□
6.5 kΩ/□
70-80 kΩ/□
140–150 kΩ/□
370–390 kΩ/□
+Spacer 70–80 kΩ/□

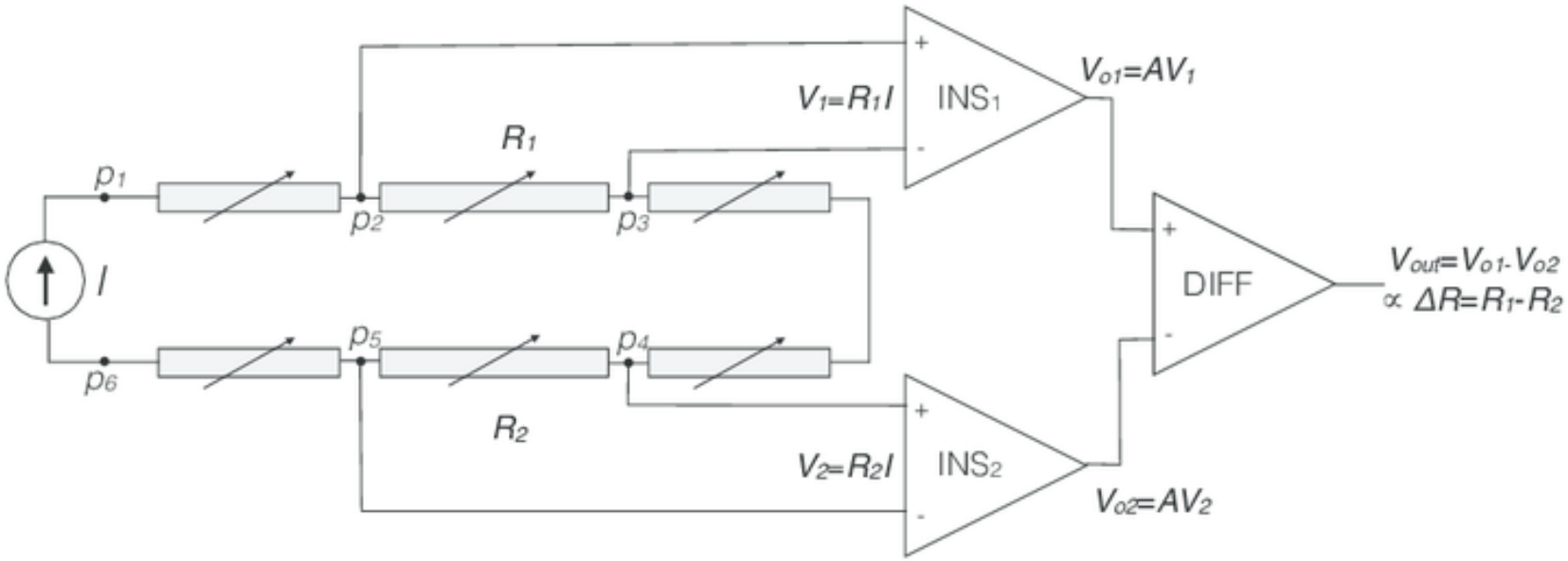
p1
p2
p3
p4
p5
p6
I
R1
R2
V1=R1I
V2=R2I
INS1
INS2
Vo1=AV1
Vo2=AV2
DIFF
Vout=Vo1-Vo2
∝ ΔR=R1-R2

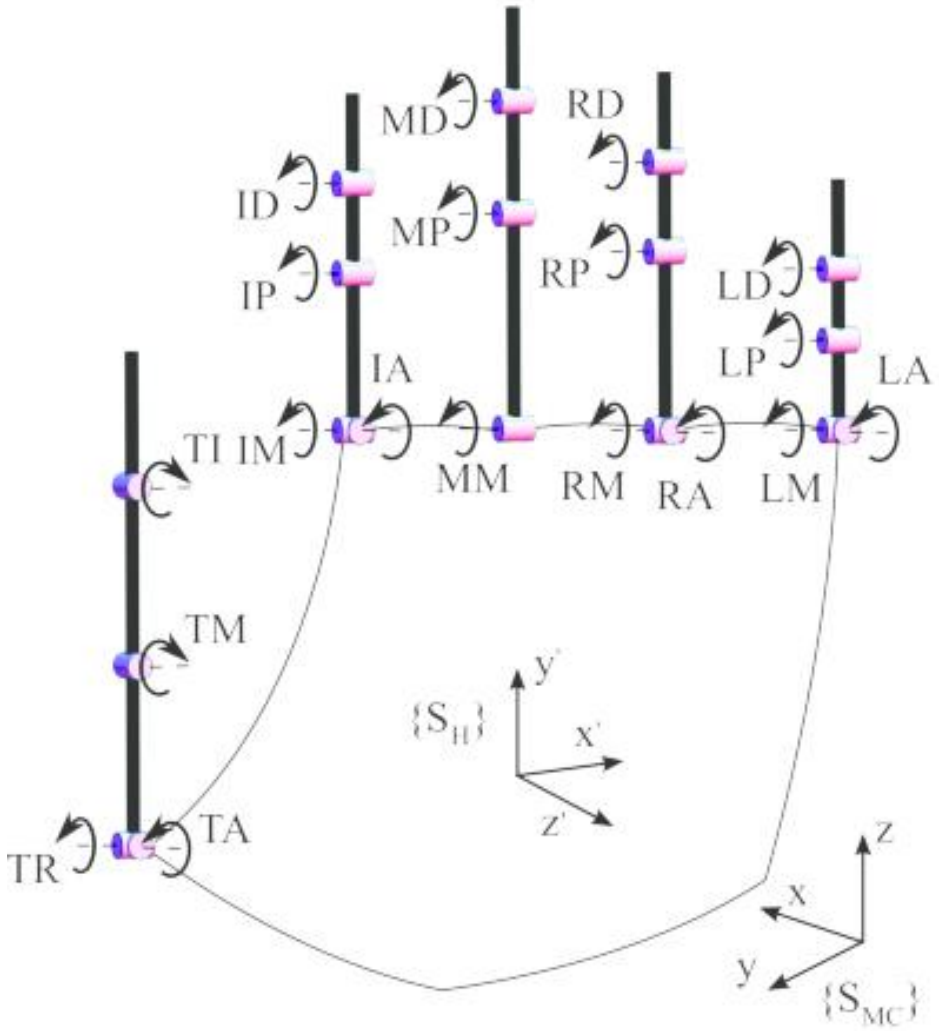

DoFs	Description
TA	Thumb Abduction
TR	Thumb Rotation
TM	Thumb Metacarpal
TI	Thumb Interphalangeal
IA	Index Abduction
IM	Index Metacarpal
IP	Index Proximal
ID	Index Distal
MM	Middle Metacarpal
MP	Middle Proximal
MD	Middle Distal
RA	Ring Abduction
RM	Ring Metacarpal
RP	Ring Proximal
RD	Ring Distal
LA	Little Abduction
LM	Little Metacarpal
LP	Little Proximal
LD	Little Distal

Joint	Sensor Lenght (mm)
TA	82
MM	72
RP	62
LM	60
LA	74

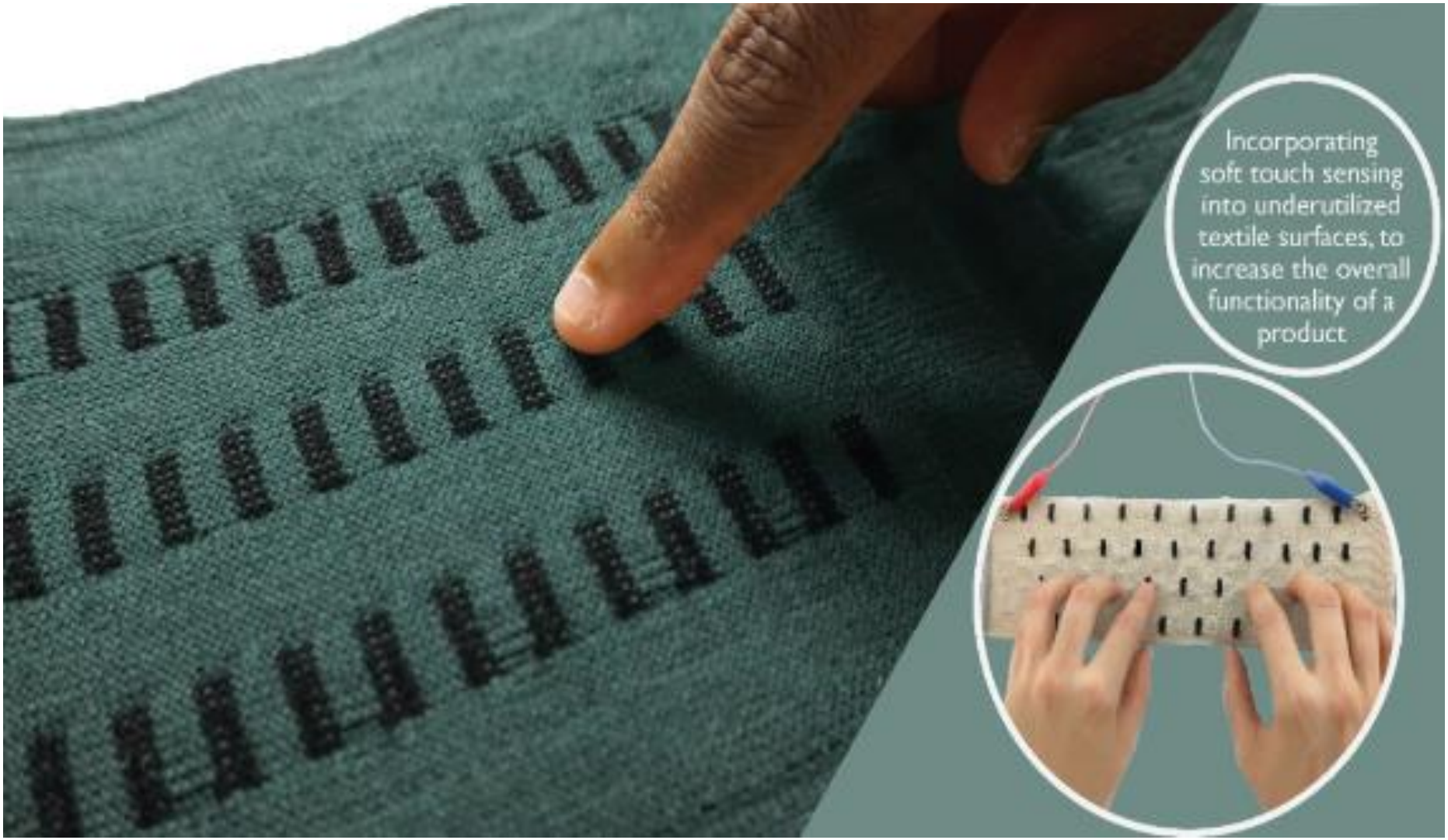
Incorporating soft touch sensing into underutilized textile surfaces, to increase the overall functionality of a product

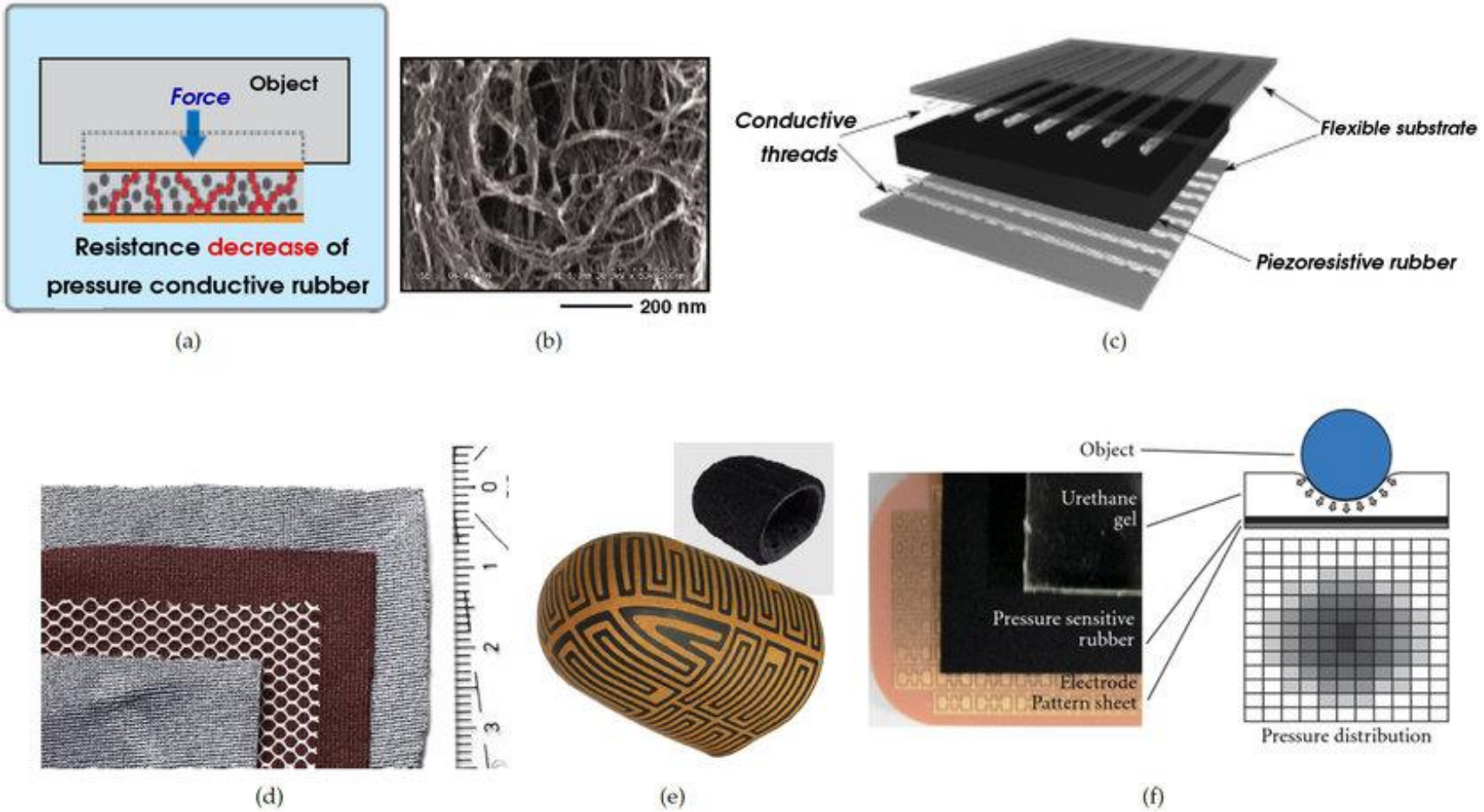

(a) (b) (c)

(d) (e) (f)

- Piezoresistive Tactile Sensor Arrays: (a) illustration of resistance changes in conductive rubber [47],(b) nano-scale image of conductive rubber [48], (c) structure of piezoresistive tactile array [49], (d) piezoresistive fabric tactile sensor [50], (e) schematic of electrode layer of the 3D-shaped tactile sensor [34], (f) tactile image of a piezo-resistive pressure sensor array [35].

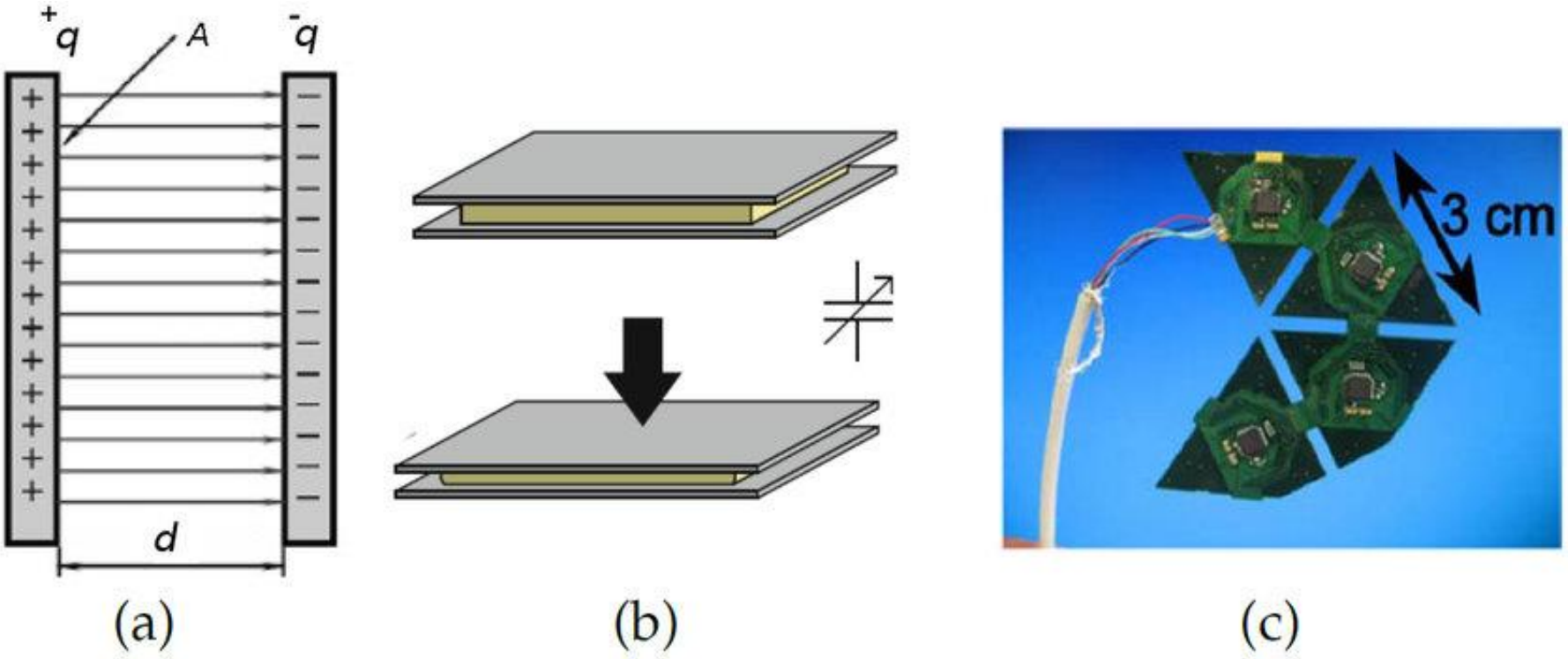

- Capacitive Tactile Sensing Technology: (a) capacitance of a parallel plate capacitor depends on distance between plates d and area of the plates A (q is the stored charge) [45]; (b) two conductive plates are separated by an elastic dielectric-as force is applied, the distance between the plates reduces, changing the capacitance [9]; (c) mesh of triangle shape capacitive sensors for the palm of the iCub humanoid robot [44].

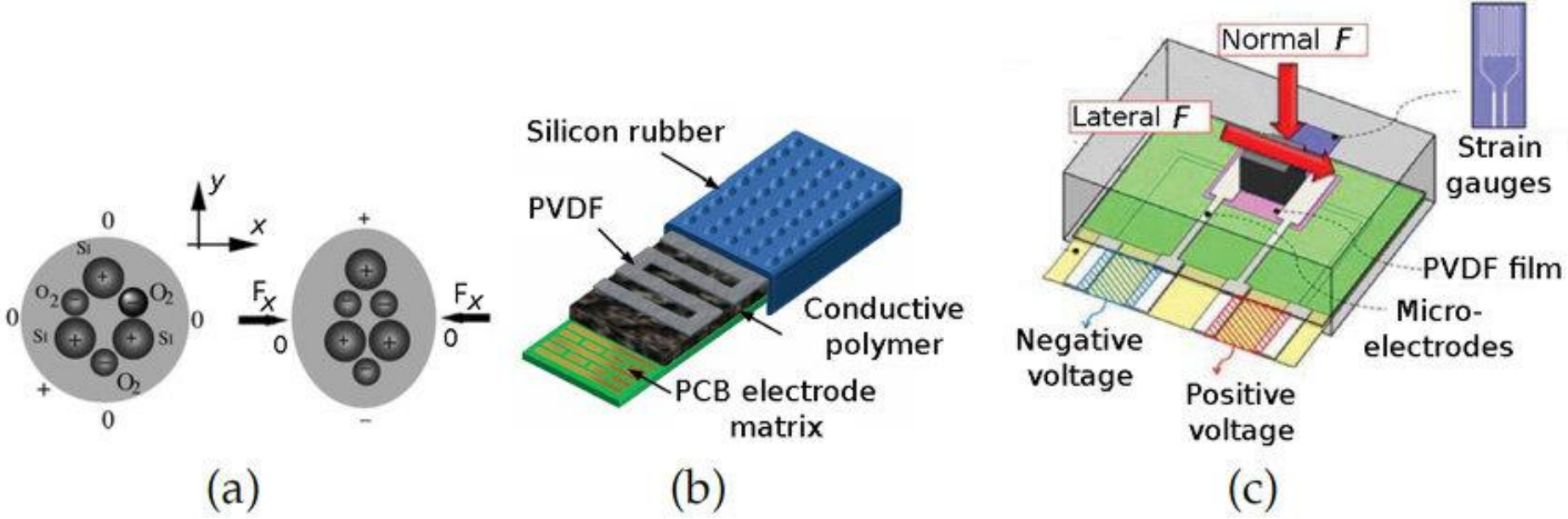

- Piezoelectric Tactile Sensing: (a) the piezoelectric effectan applied force causes rearrangement of positive Si and negative O 2 particles leading to an increase of potential [45]; (b) a tactile sensing array based on the piezoelectric effect with electrodes on the bottom layer, piezolectric material in the middle and rubber on the top [24], (c) schematic model of a piezoelectric sensing tactel [71]

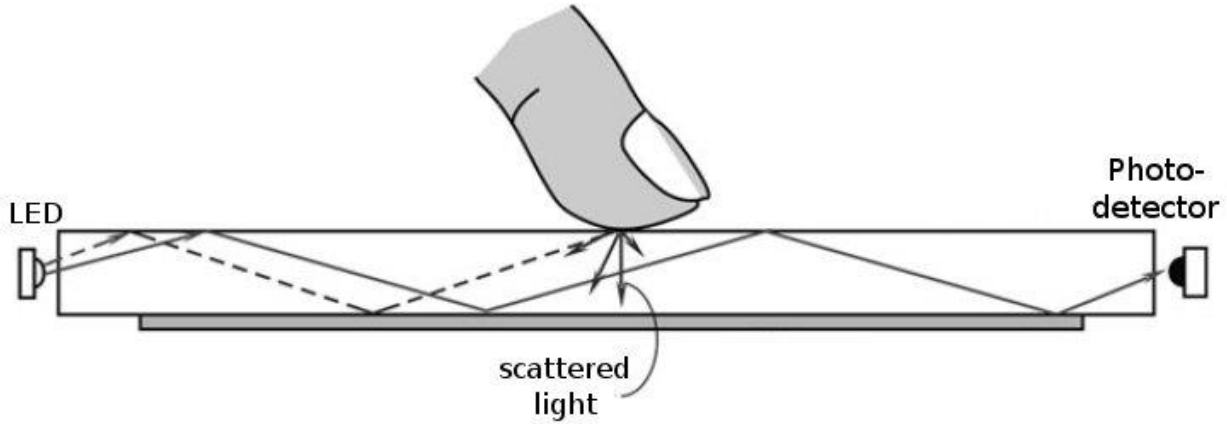
LED
Photo-
detector
scattered
light

(a)

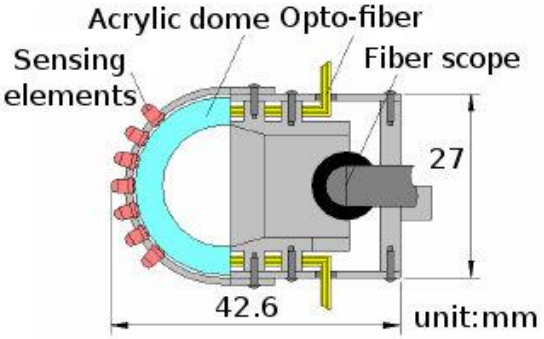
Acrylic dome
Opto-fiber
Sensing
elements
Fiber scope
27
42.6
unit:mm

(b)

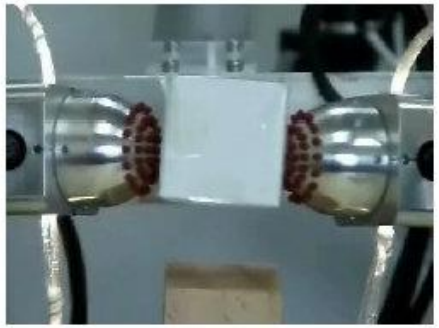

(c)

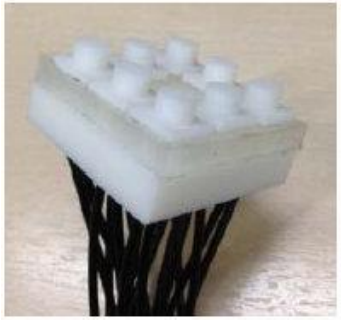

(d)

(e)

(f)

- Optical Tactile Sensors: (a) an optical tactile transducer based on the principle of frustrated total internal reflection [45], (b) a structure of optical three-axis tactile sensor: a displacement of a sensing element fixed on flexible finger surface causes changes in light propagation in opto-fibers [37], (c) fingers with the sensitive optical sensors manipulating a light paper box [37], (d) photo of an optical 3 x 3 tactile array with magnetic field compatibility [77], (e) "GelSight" optical sensor consisting of a piece of clear elastomer coated with a reflective membrane senses the shape of the cookie surface [79], (f) finger configurations of the "GelSight" sensor [79].

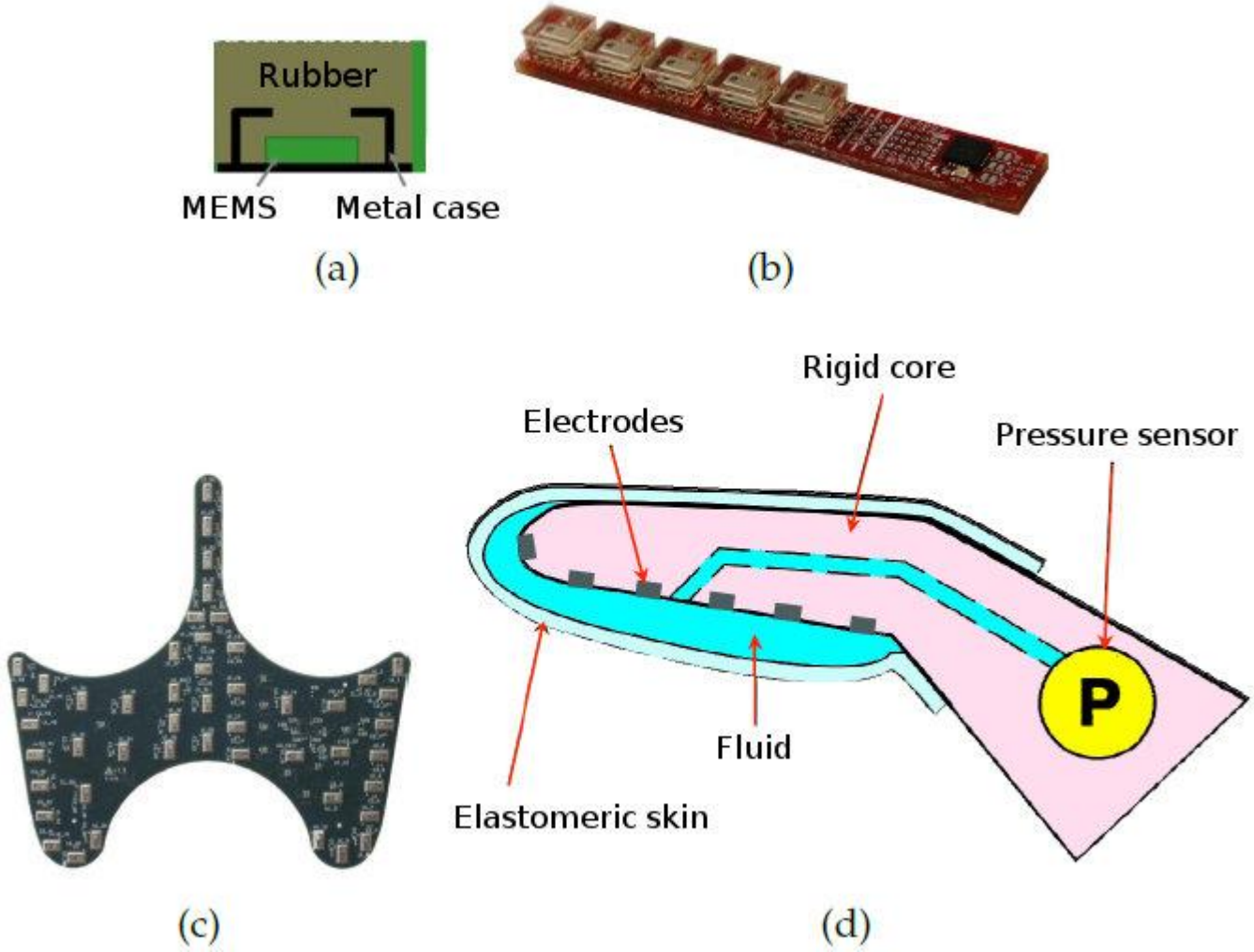

- Sensors based on barometric measurements: (a) the structure of a tactile sensing cell with a barometer and silicon rubber (b), the TakkStrip tactile array of these cells [87], (c) custom shaped array of the pressure sensing barometers of the iHY hand [42], (d) micro-vibration sensing system based on a fluid pressure sensor of the BioTac tactile sensor [83].

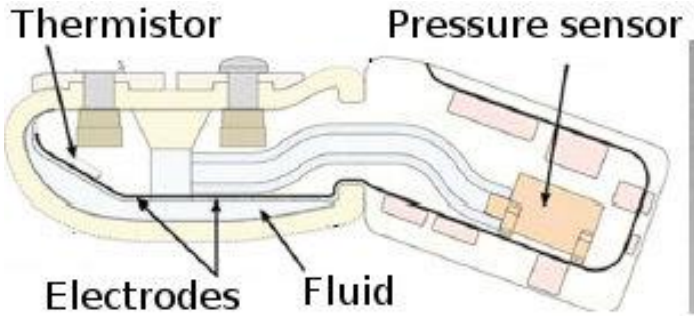
Thermistor
Pressure sensor
Electrodes
Fluid

(a)

(b)

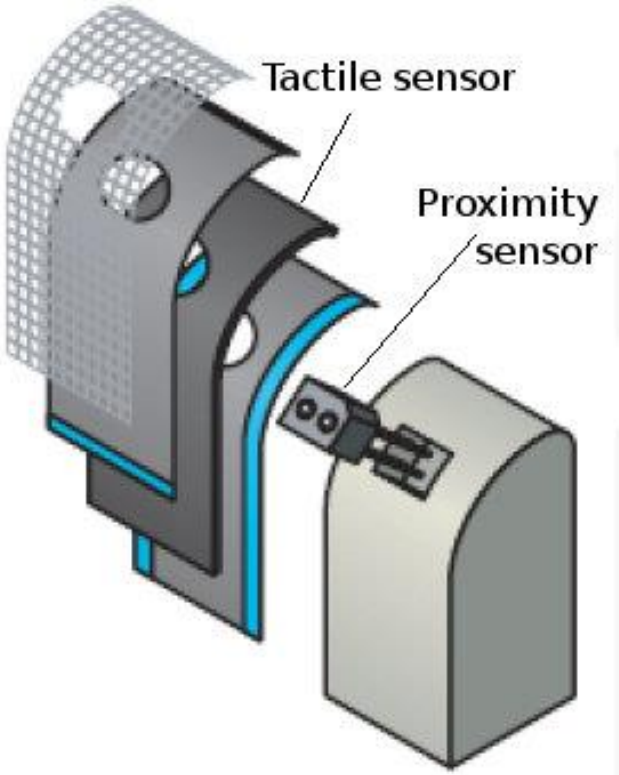
Tactile sensor
Proximity sensor

(c)

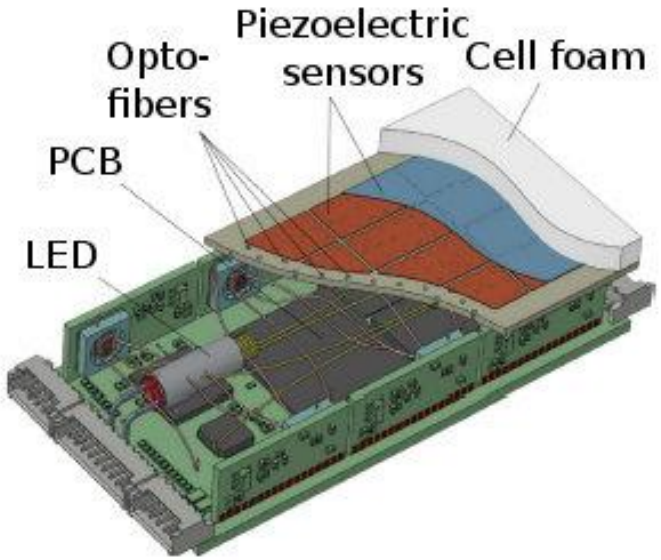
Piezoelectric sensors
Opto-fibers
Cell foam
PCB
LED

(d)

- Multimodal Tactile Sensors: (a) schematic of the biomimetic BioTac tactile sensor with 19 electrodes, fluid pressure sensor and thermometer [84], (b) photo of the multimodal BioTac tactile sensor, (c) combined tactile-proximity sensor that can measure both the distance to an object and the contact pressure [90], (d) drawing of a multi-modal tactile sensing module consisting of optical and piezoresistive sensors [76].


a


b

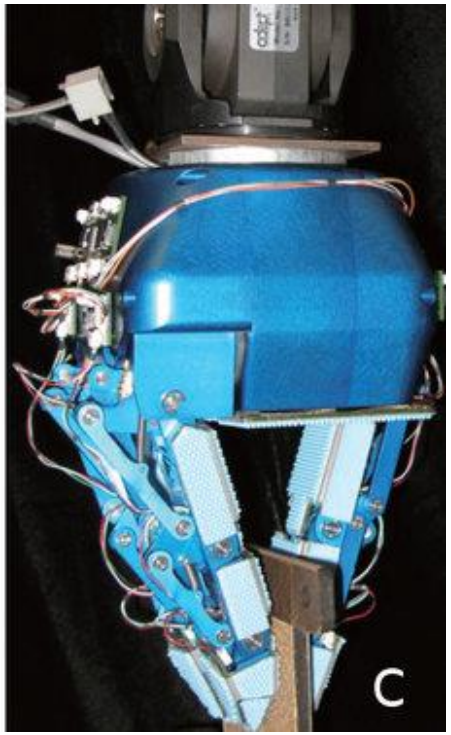
c


a

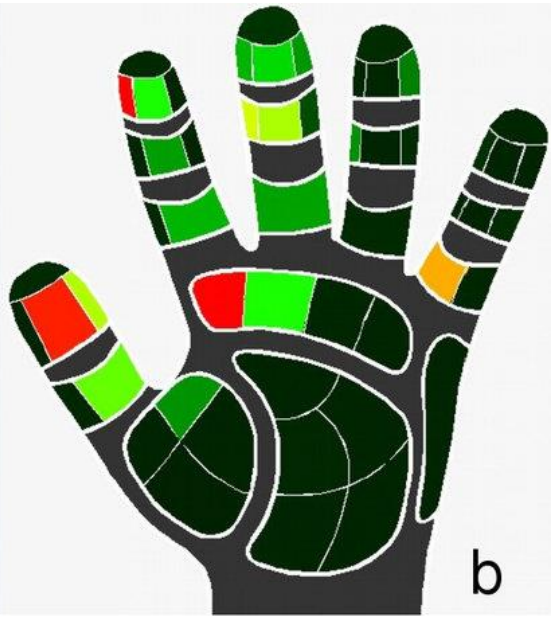
b


CoP tactile sensors

(a)

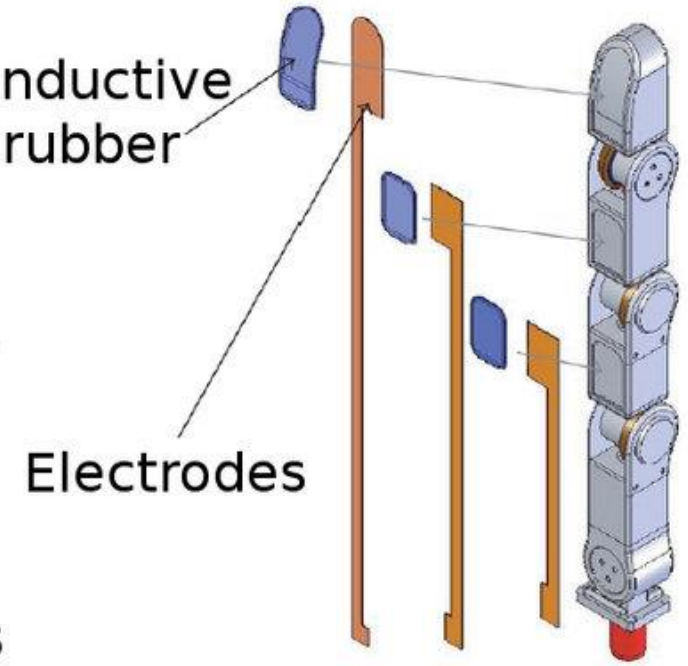
Conductive rubber
Electrodes

(b)

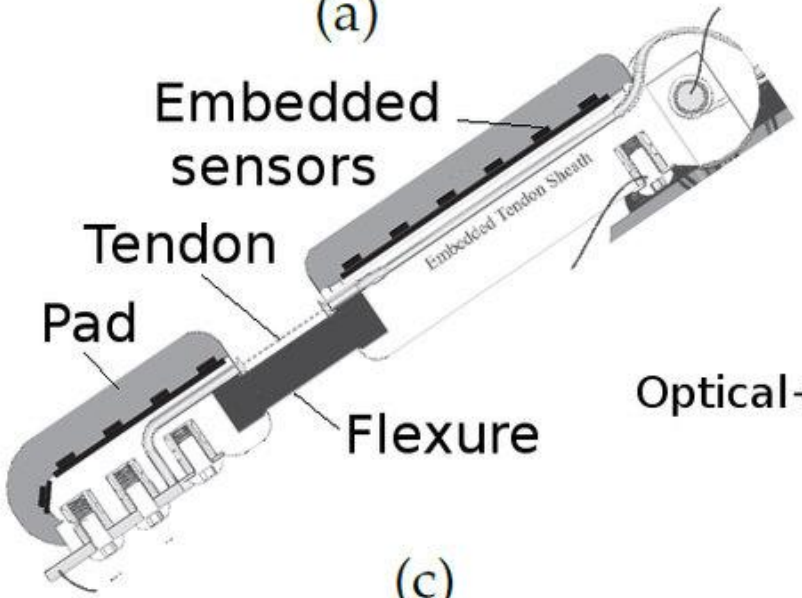
Embedded sensors
Tendon
Pad
Flexure
Embedded Tendon Sheath

(c)

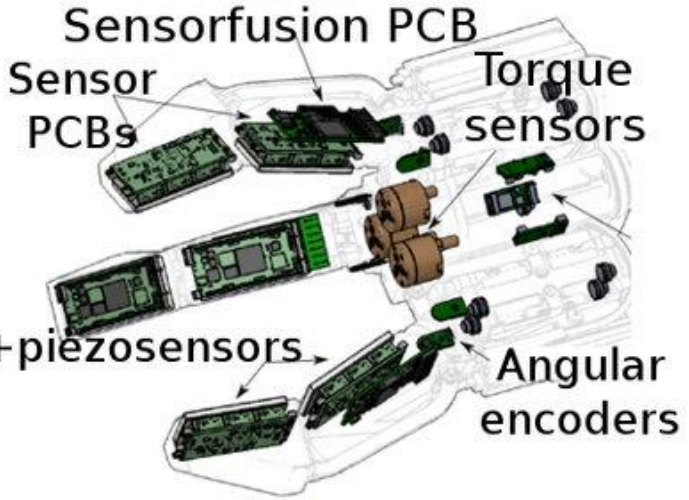
Sensorfusion PCB
Sensor PCBs
Torque sensors
Optical+piezosensors
Angular encoders

(d)

- Three-fingered robot hands with tactile sensors: (a) a finger with tactile sensor of the 3-fingered high-speed robot hand [101], (b) assembly of tactile sensing arrays with a robot finger of the Universal robot hand with 3 movable and 2 immovable fingers [35], (c) schematic illustration of a finger of the iHY robot hand with embedded array of pressure sensors based on digital barometers placed inside the soft paddings of the fingers [42]; (d) schematic illustration of the integration of a multimodal sensing system with a three-fingered robot hand [76]

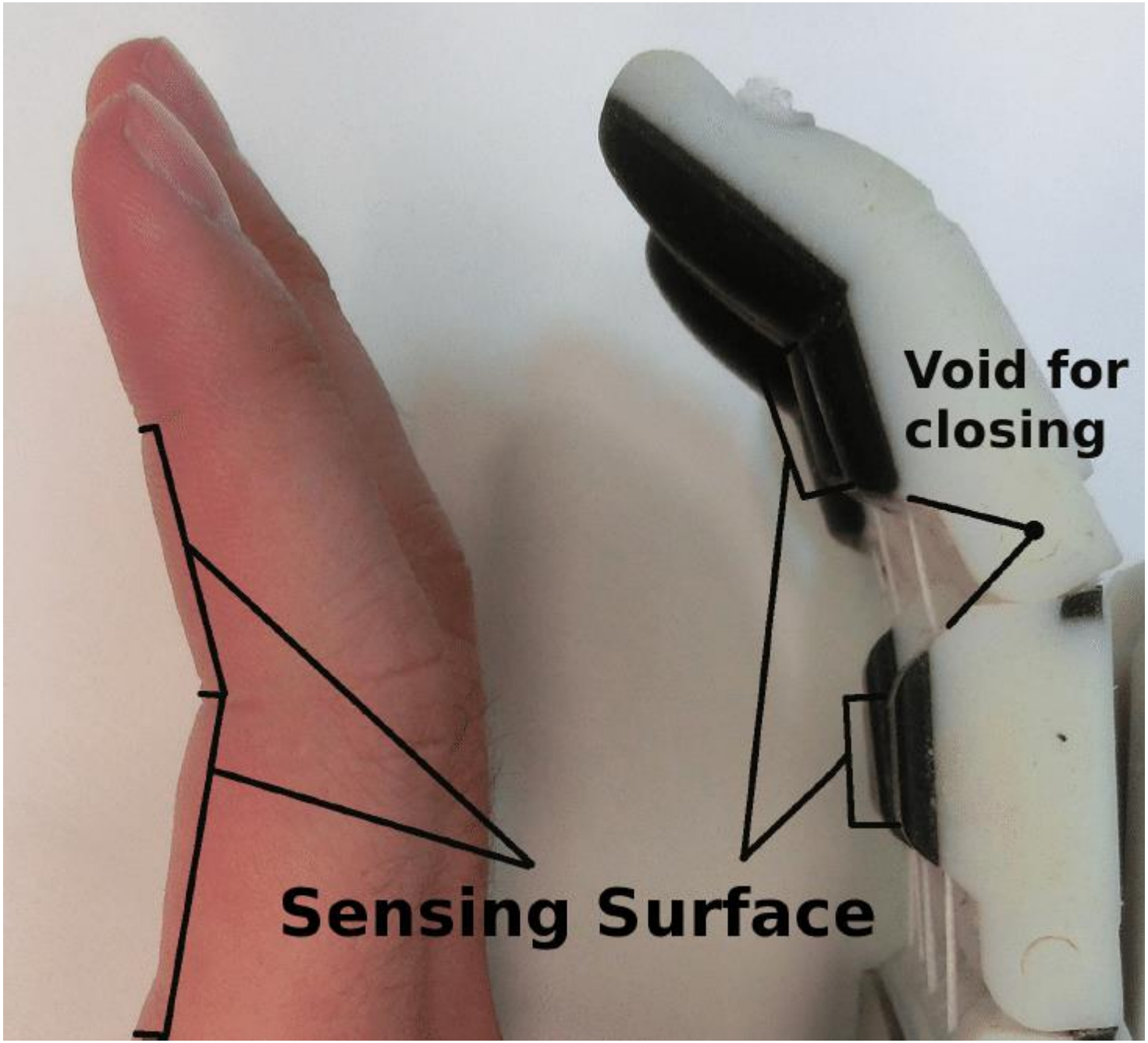
Void for
closing
Sensing Surface

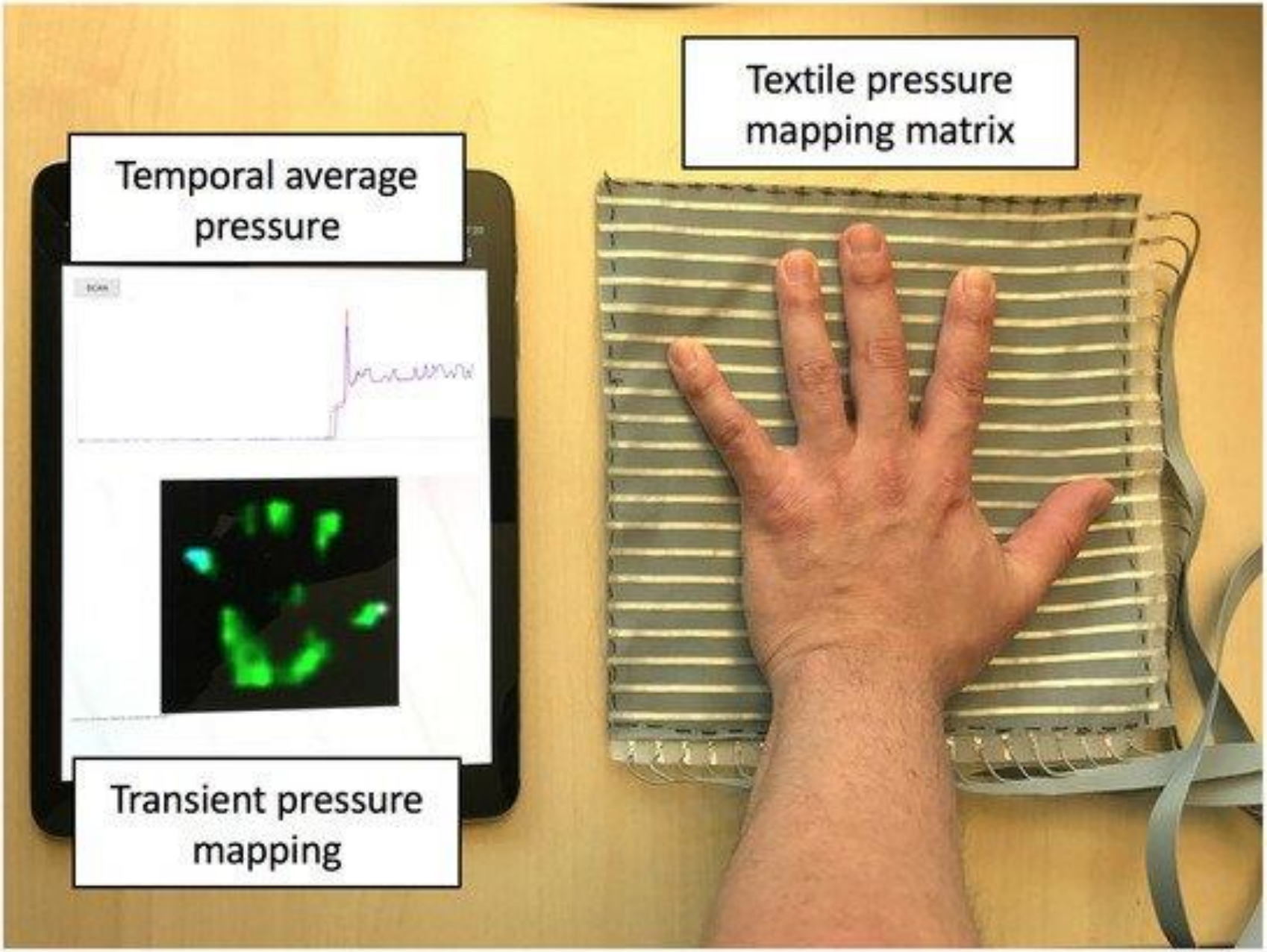
Temporal average pressure
Transient pressure mapping
Textile pressure mapping matrix

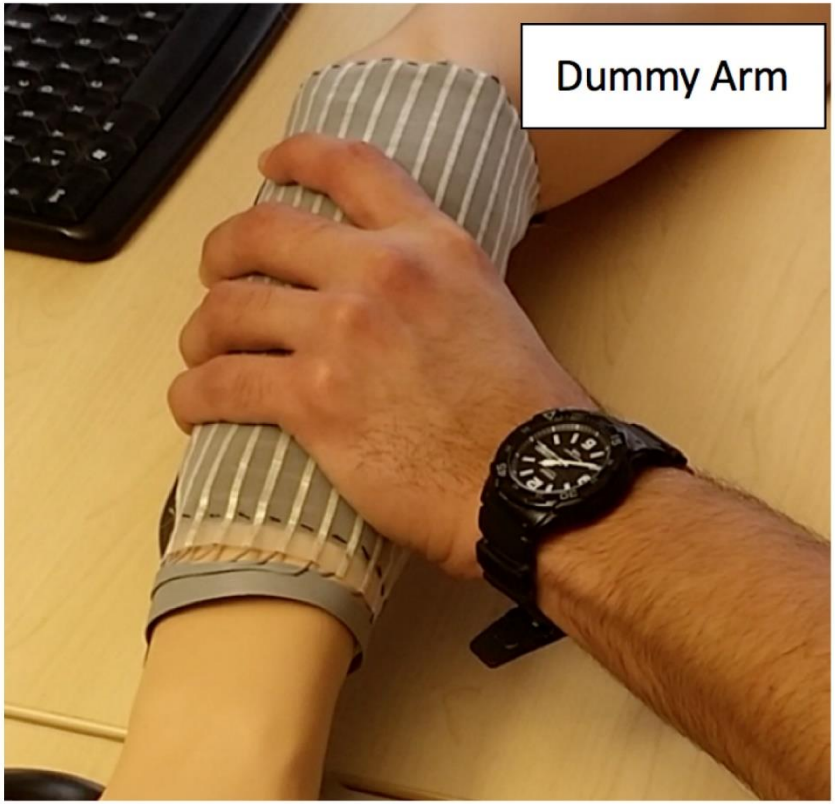

(a) P1 Grab

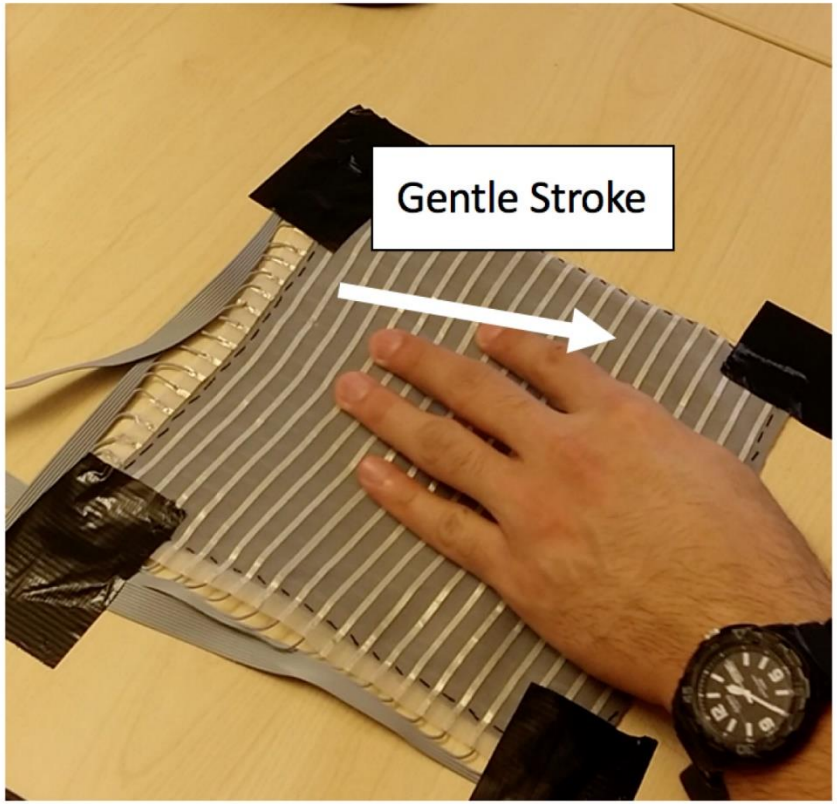

(b) P7 Stroke

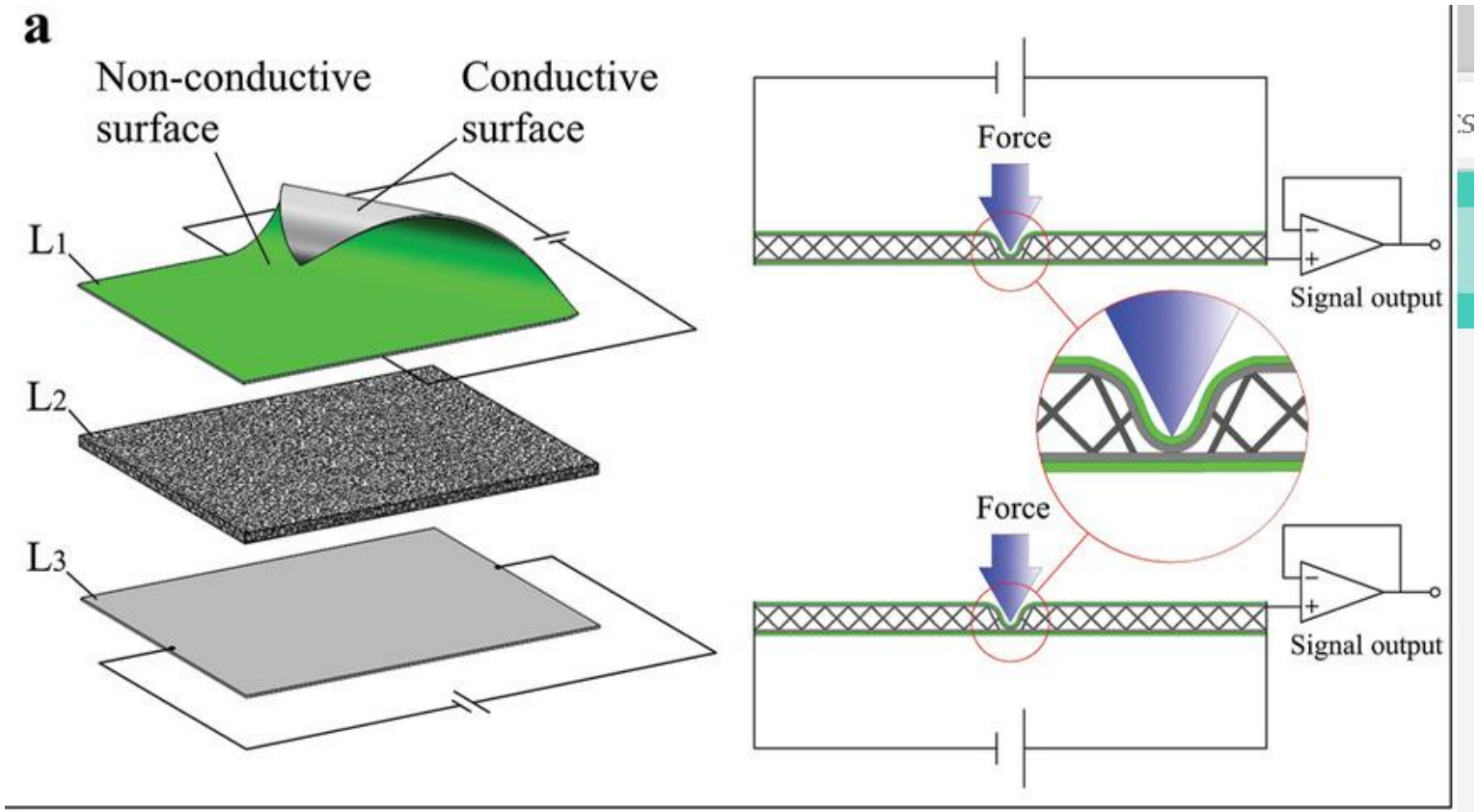
a
Non-conductive surface
Conductive surface
L1
L2
L3
Force
Signal output
Force
Signal output

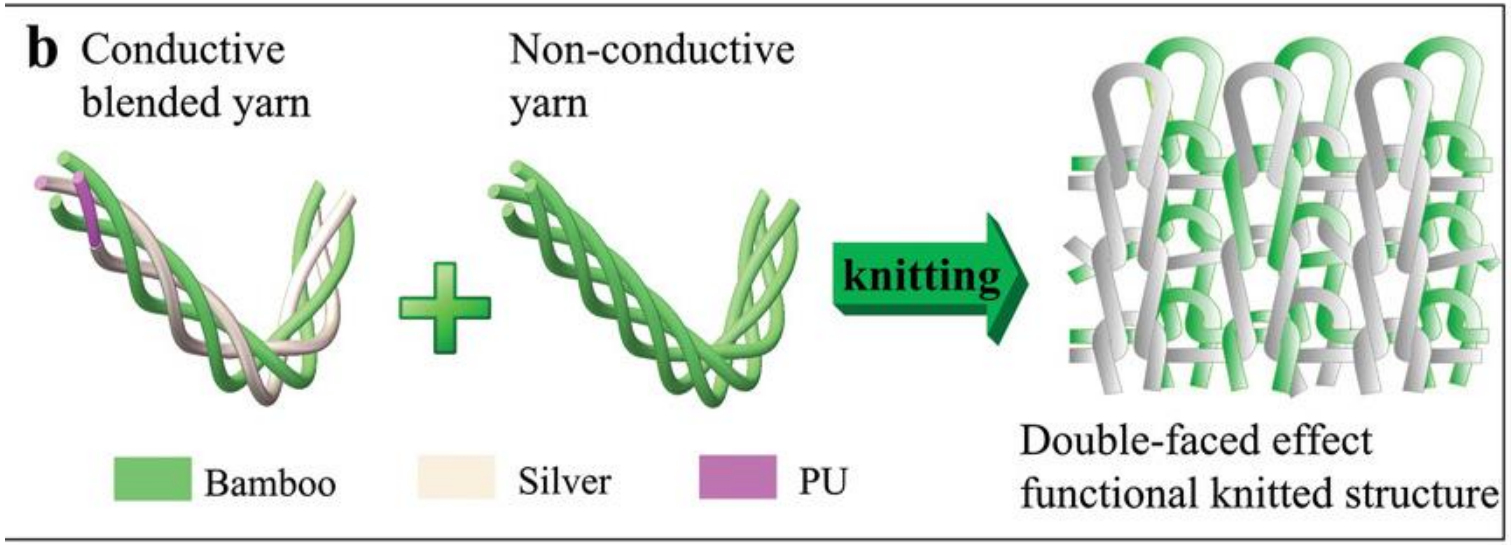
b
Conductive blended yarn
Non-conductive yarn
knitting
Bamboo
Silver
PU
Double-faced effect functional knitted structure

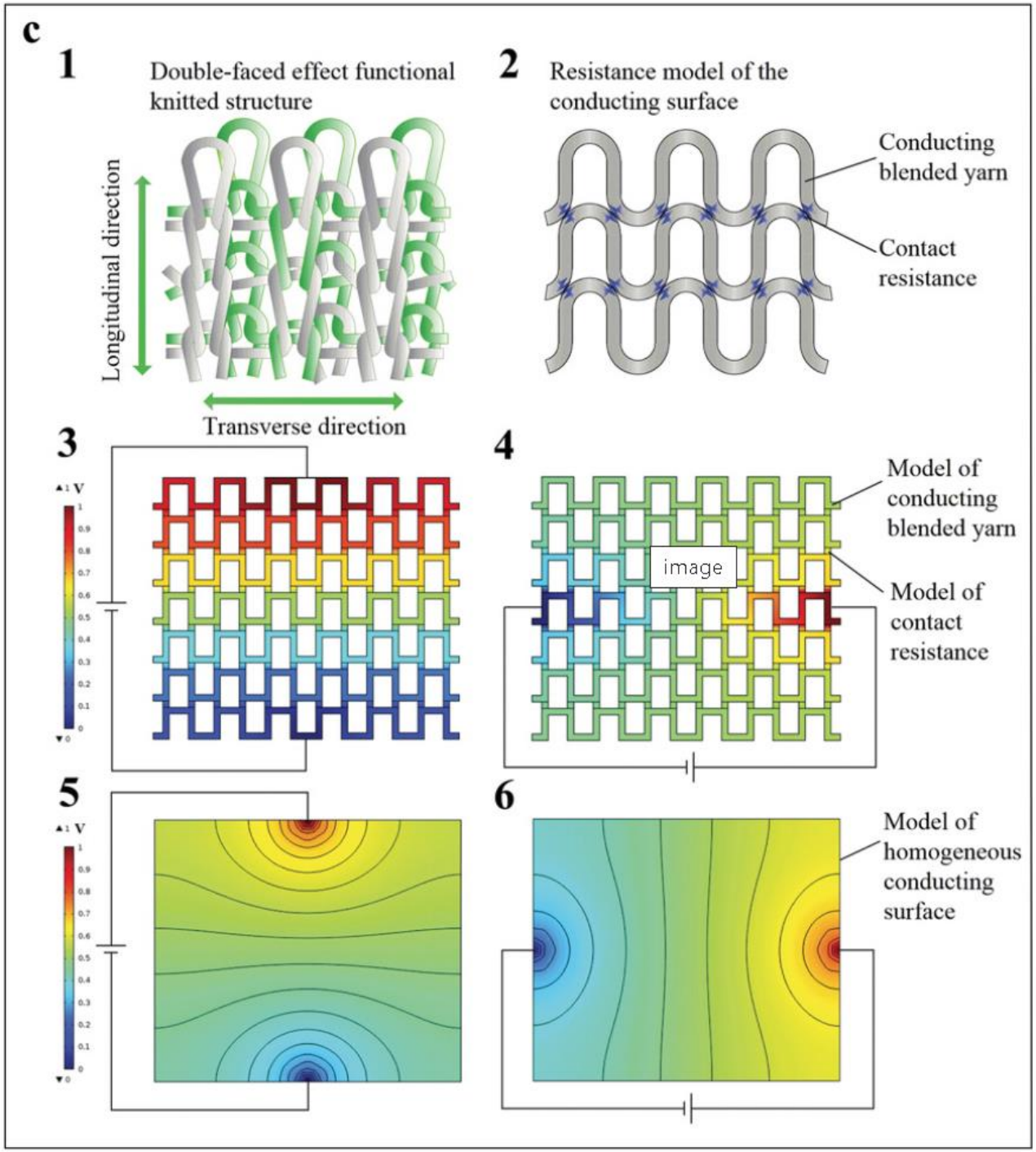
c
1
Double-faced effect functional knitted structure
Longitudinal direction
Transverse direction
2
Resistance model of the conducting surface
Conducting blended yarn
Contact resistance
3
4
Model of conducting blended yarn
image
Model of contact resistance
5
6
Model of homogeneous conducting surface

- a) Structure model and sensing mechanism of the tactile sensor.
- b) Model of the knitted textile.
- c) Structure and resistance model of the knitted textile and simulation of surface potential distribution.

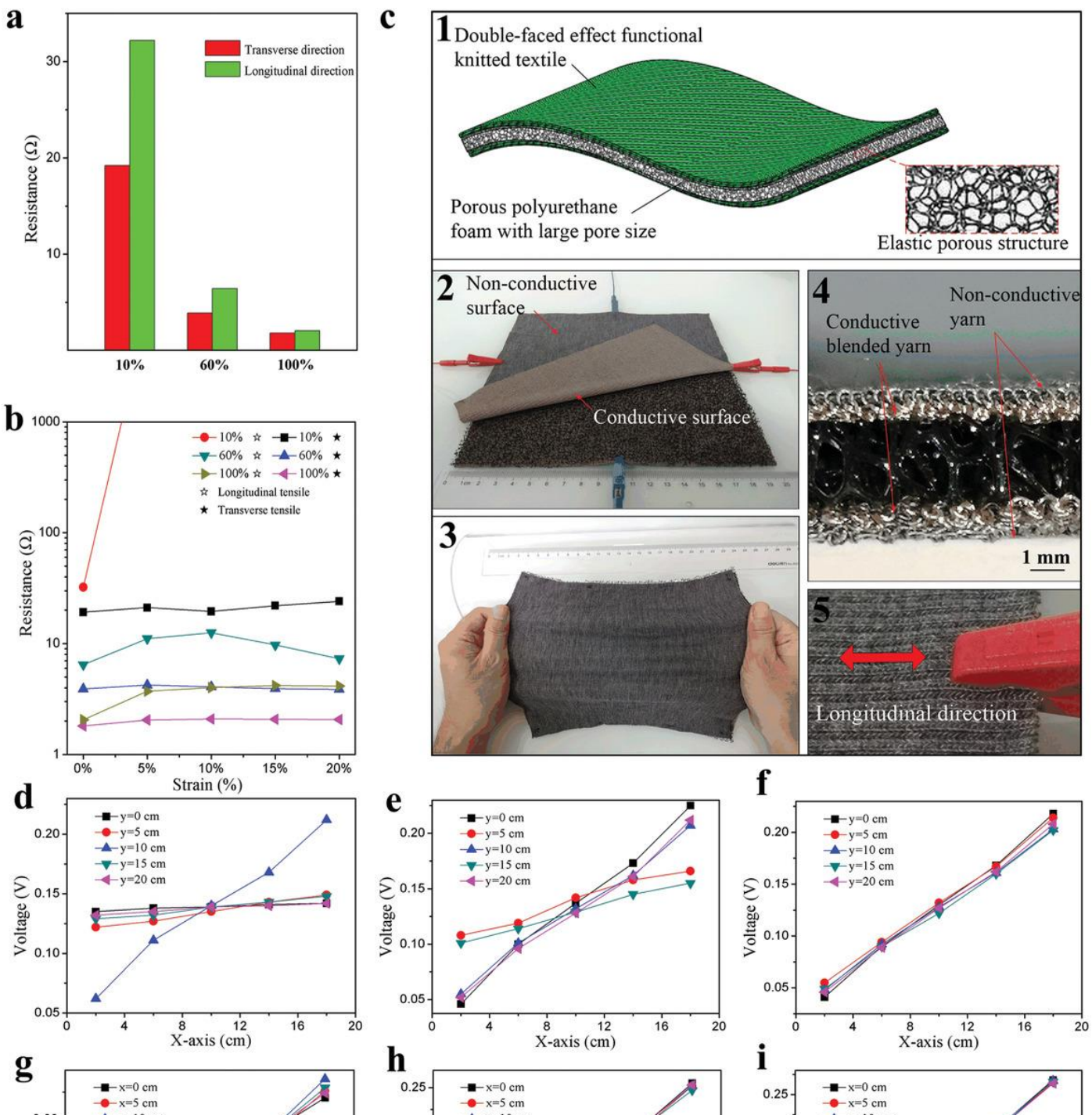
a
Transverse direction
Longitudinal direction
Resistance (Ω)
30
20
10
10%
60%
100%
b
Resistance (Ω)
1000
100
10
1
10% ☆
10% ★
60% ☆
60% ★
100% ☆
100% ★
☆ Longitudinal tensile
★ Transverse tensile
0%
5%
10%
15%
20%
Strain (%)
c
1 Double-faced effect functional knitted textile
Porous polyurethane foam with large pore size
Elastic porous structure
2 Non-conductive surface
Conductive surface
3
4
Conductive blended yarn
Non-conductive yarn
1 mm
5
Longitudinal direction
d
Voltage (V)
y=0 cm
y=5 cm
y=10 cm
y=15 cm
y=20 cm
X-axis (cm)
e
Voltage (V)
X-axis (cm)
f
Voltage (V)
X-axis (cm)
g
x=0 cm
x=5 cm
h
x=0 cm
x=5 cm
i
x=0 cm
x=5 cm

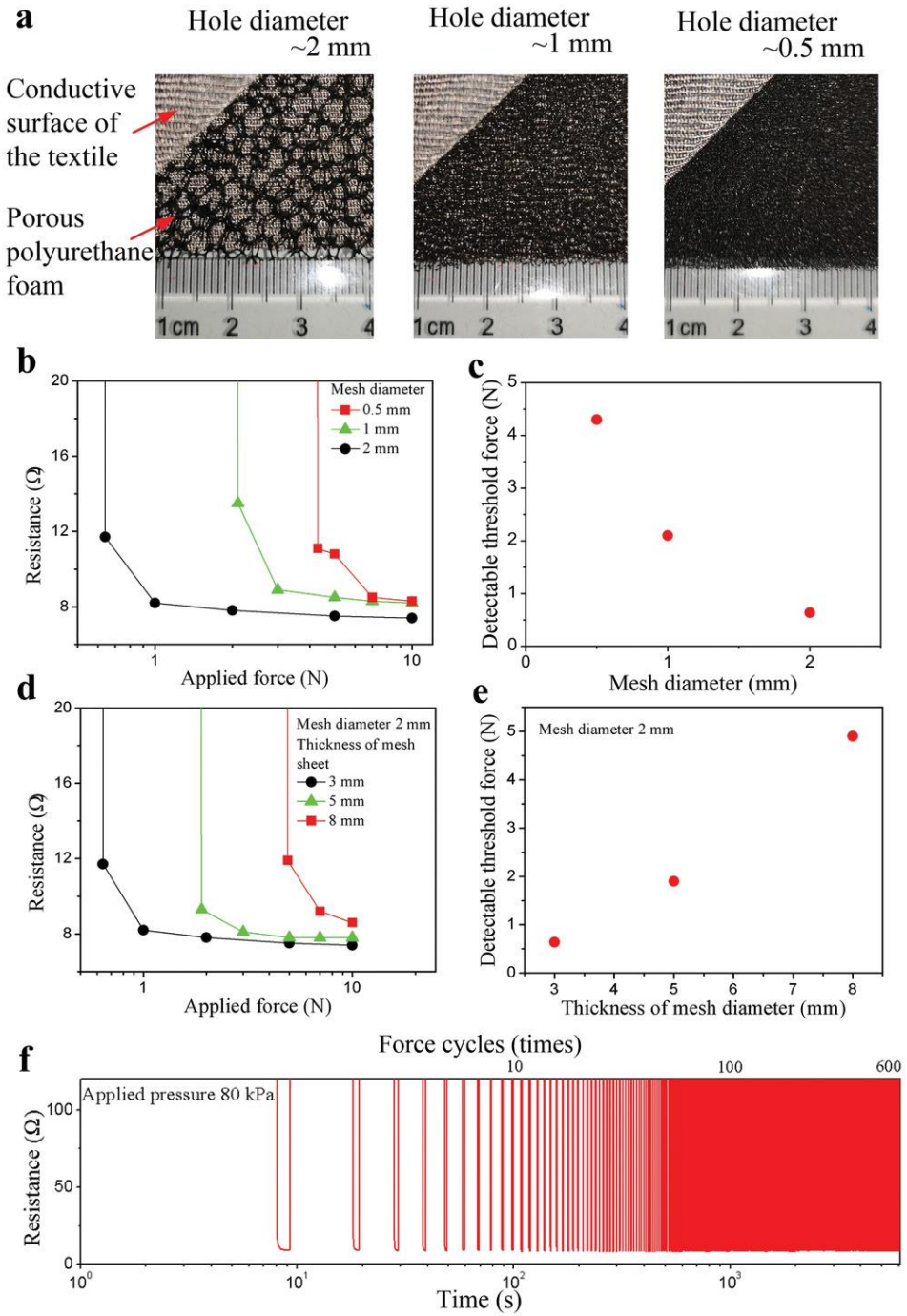
a
Hole diameter ~2 mm
Hole diameter ~1 mm
Hole diameter ~0.5 mm
Conductive surface of the textile
Porous polyurethane foam
1cm 2 3 4
b
Resistance (Ω)
Applied force (N)
Mesh diameter
0.5 mm
1 mm
2 mm
c
Detectable threshold force (N)
Mesh diameter (mm)
d
Resistance (Ω)
Applied force (N)
Mesh diameter 2 mm
Thickness of mesh sheet
3 mm
5 mm
8 mm
e
Detectable threshold force (N)
Mesh diameter 2 mm
Thickness of mesh diameter (mm)
f
Force cycles (times)
10
100
600
Applied pressure 80 kPa
Resistance (Ω)
Time (s)

- a) Photos of the sensor with different pore diameters of the polyurethane foam from ≈0.5 to ≈2 mm. b) Resistance changes as a function of the applied force. c) Compiled detectable threshold force extracted from panel (b). d) Resistance changes as a function of the applied force. e) Compiled detectable threshold force extracted from panel (d) with 2 mm pore diameter. f) Cycle tests as 80 kPa applied force.

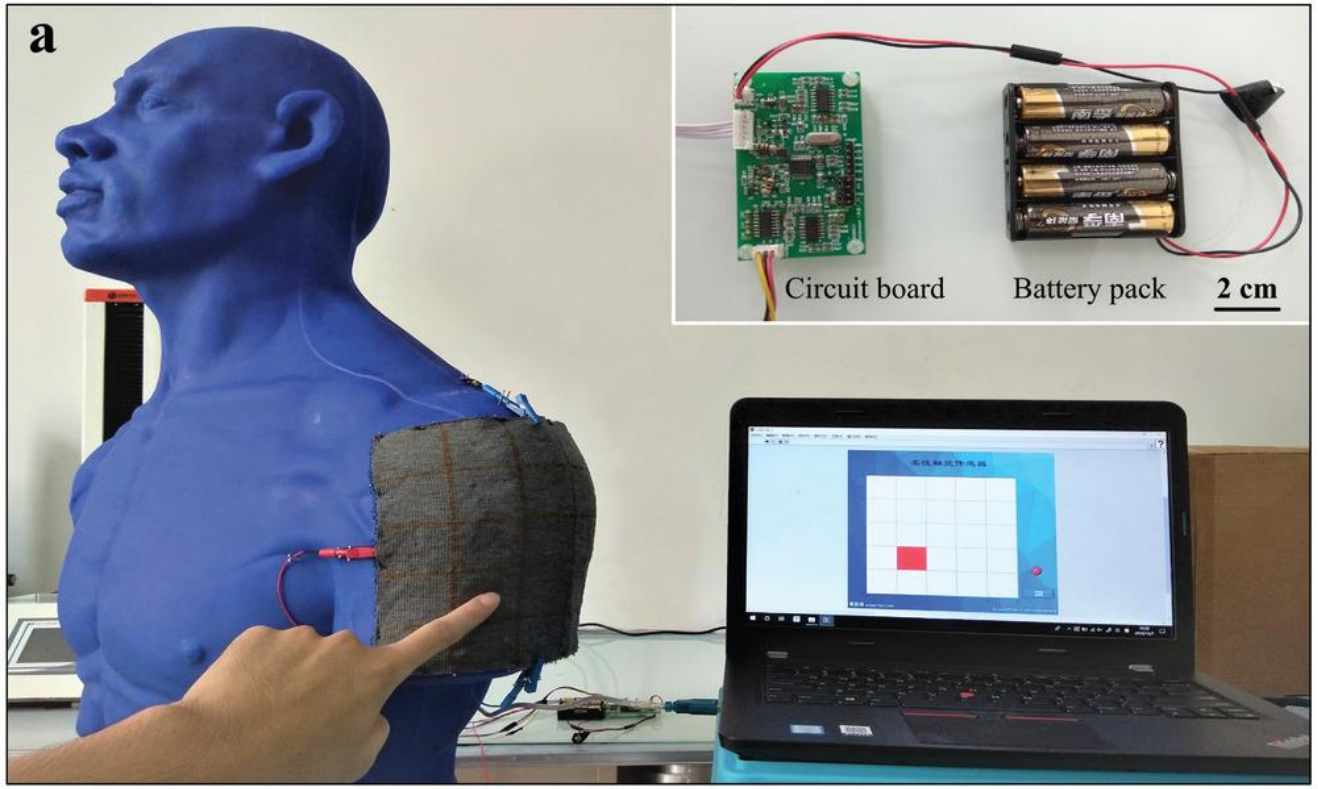
a
Circuit board
Battery pack
2 cm

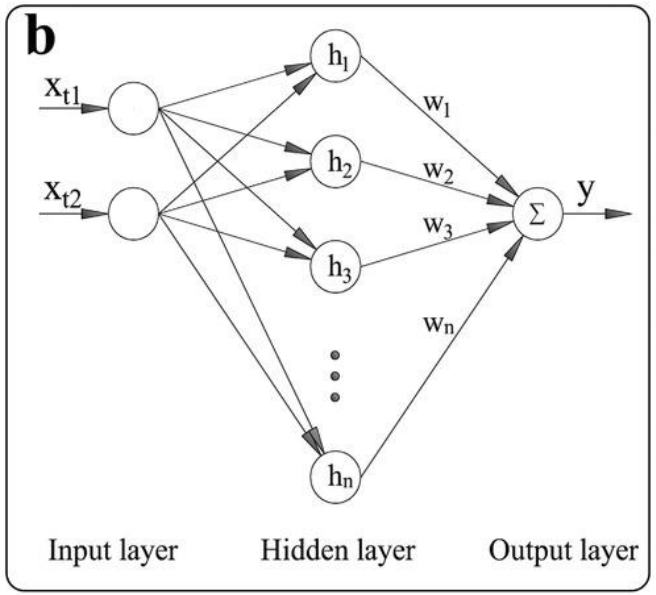
b
x_{t1}
x_{t2}
h_1
h_2
h_3
h_n
w_1
w_2
w_3
w_n
Σ
y
Input layer
Hidden layer
Output layer

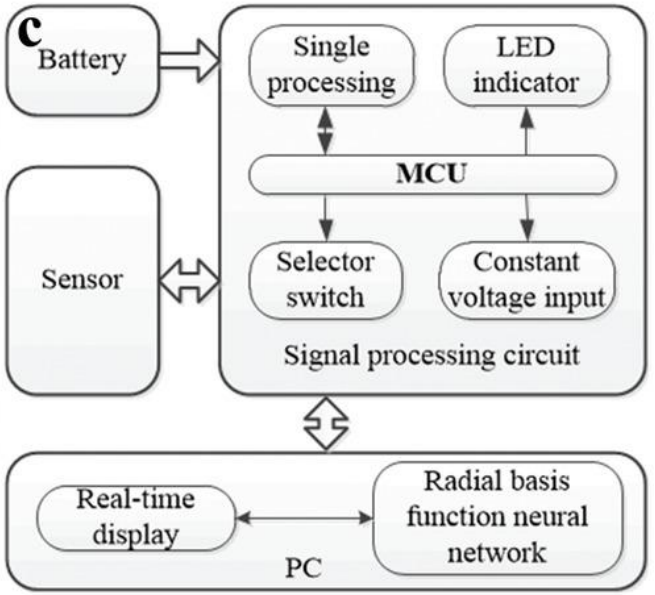
c
Battery
Single processing
LED indicator
MCU
Sensor
Selector switch
Constant voltage input
Signal processing circuit
Real-time display
Radial basis function neural network
PC

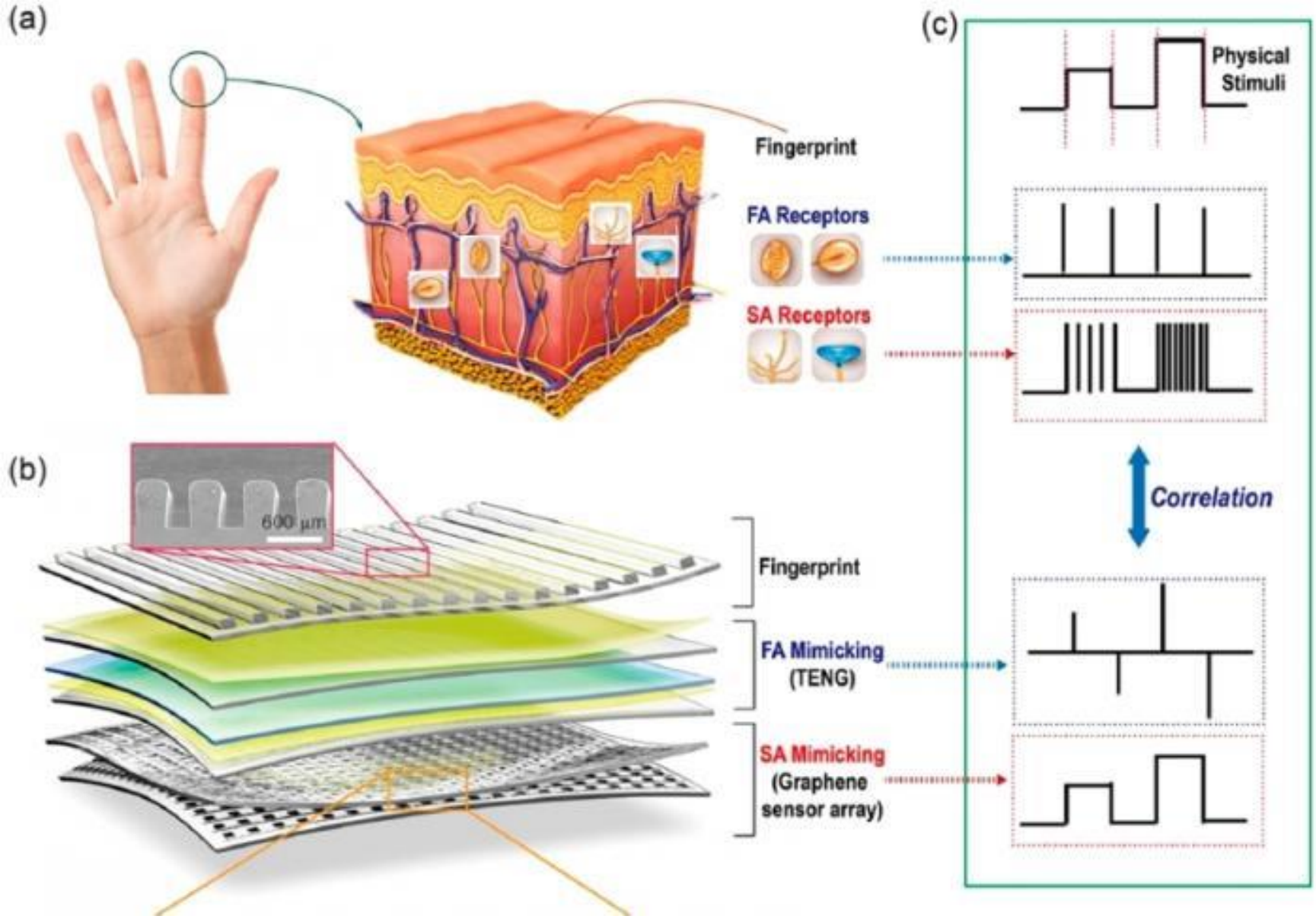

- DOI 10.1021/acs.nanolett.9b00922

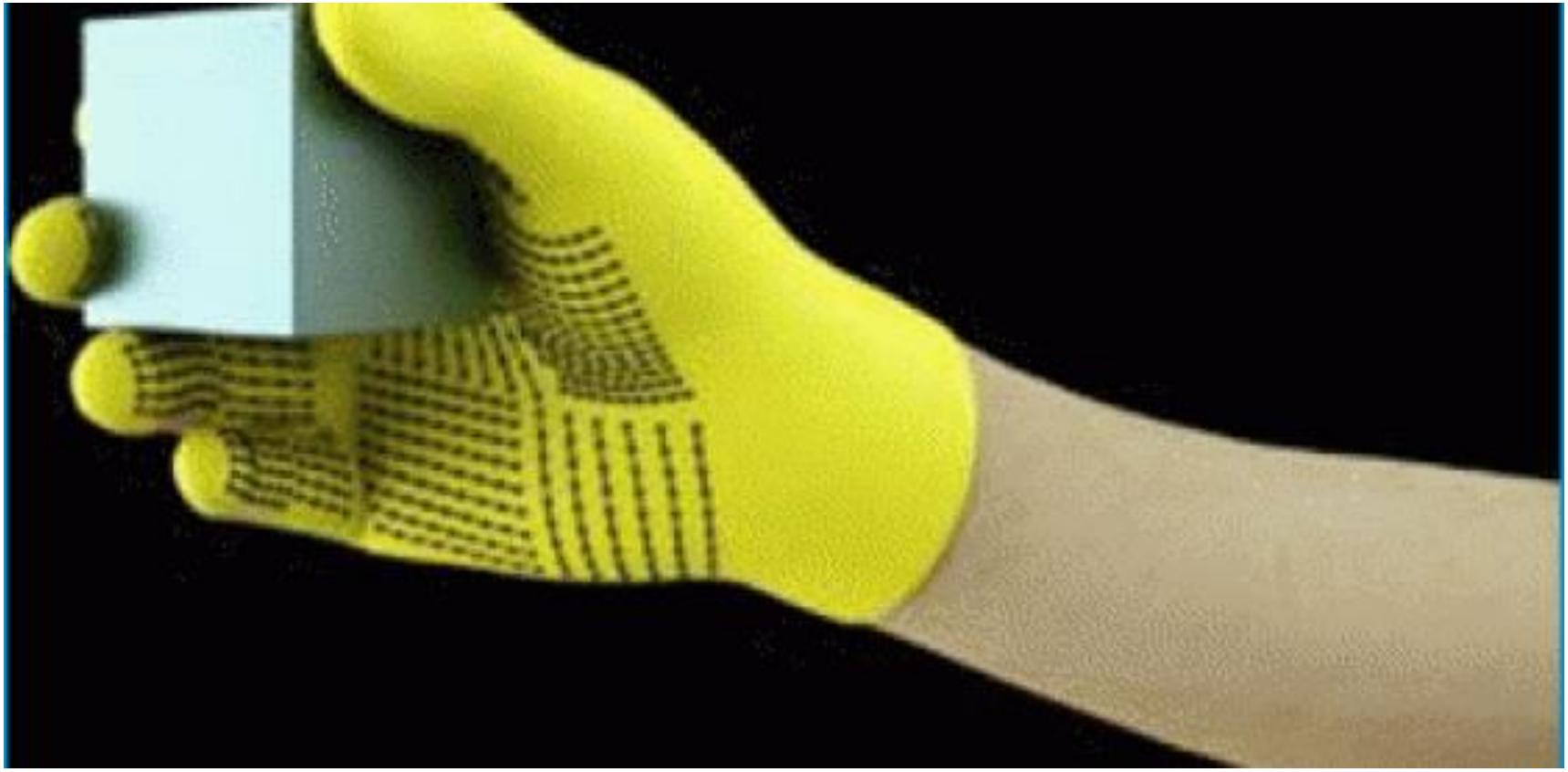

Schematics of TRACE sensor and applications in health monitoring and robotics tactile perception.

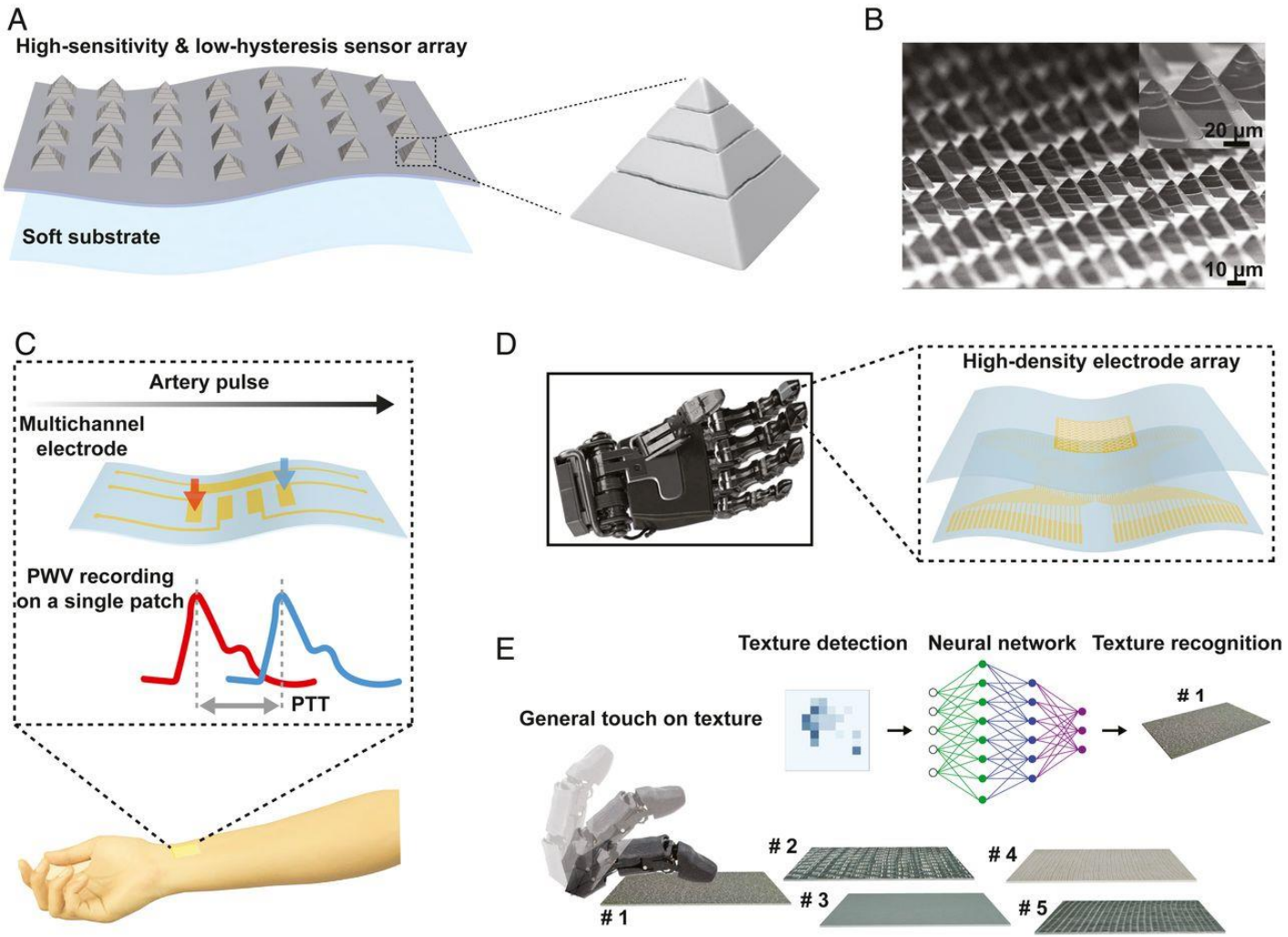

Haicheng Yao et al. PNAS 2020;117:41:25352-25359

- Schematics of TRACE sensor and applications in health monitoring and robotics tactile perception. (*A*) Illustration of TRACE piezoresistive tactile sensing elements with 3D and regularly cracked bilayer micropyramids made of metal film and elastomer microstructure. (*B*) Scanning electron microscope (SEM) image of Pt-coated micropyramid array with controlled annular cracks. (*C*) Demonstration of local PWV measurement on a single-patch healthcare wearable by assembling TRACE on multichannel electrodes. (*D*) Illustration of TRACE sensor matrix on a prosthetic hand with a flexible sensor array. (*E*) Schematic of one-touch surface texture classifications.

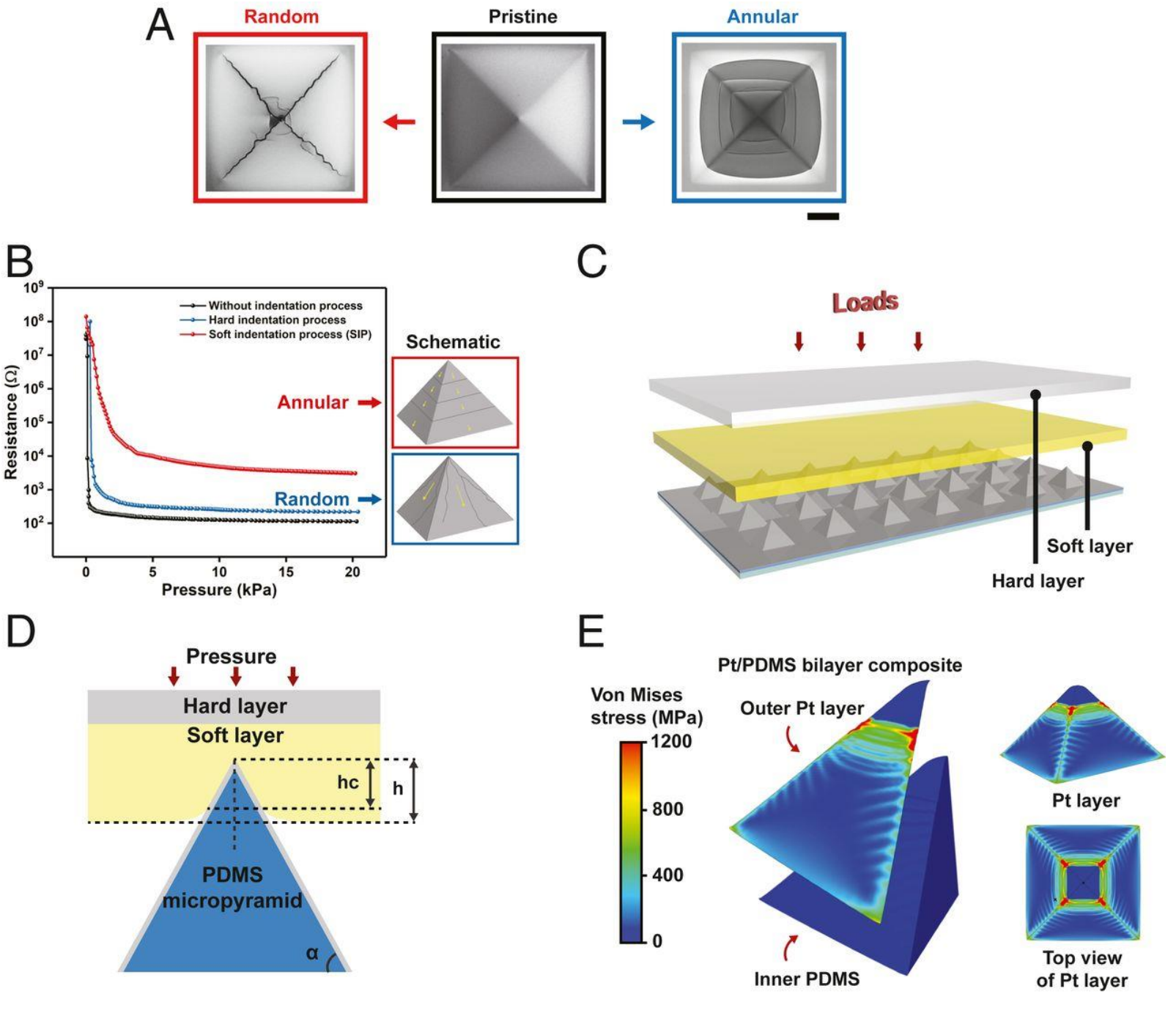
A
Random
Pristine
Annular
B
Without indentation process
Hard indentation process
Soft indentation process (SIP)
Resistance (Ω)
Pressure (kPa)
Annular
Random
Schematic
C
Loads
Soft layer
Hard layer
D
Pressure
Hard layer
Soft layer
hc
h
PDMS
micropyramid
α
E
Pt/PDMS bilayer composite
Von Mises
stress (MPa)
1200
800
400
0
Outer Pt layer
Inner PDMS
Pt layer
Top view
of Pt layer

- Mechanism of SIP method for regular annular cracks. (*A*) Comparison of random and controllable annular cracks of Pt film on micropyramid (*Top* view). The pristine Pt-film coating on micropyramid elastomer leads to the onset crack on the tips due to intensive stress concentration, propagating into uncontrollable random cracks with the increase of pressure. The proposed SIP method can generate regular and annular morphology cracks by rearranging stress distribution on bilayer micropyramid. (*B*) The optimized electromechanical property of the SIP method with annular cracks compared to random cracks. The annular cracks-induced gradual trend of piezoresistance is more suitable for a tactile sensor for a wide range of pressure, in comparison with sharp drops of resistance based on random cracks. (*C*) Schematic of SIP method for generating annular cracks of Pt film on micropyramid. (*D*) Theoretical model of SIP method for the design of stiff Pt film/PDMS bilayer micropyramid structure when applied compression force, where α, *h,* and h_c are the sidewall angle of the pyramid, indentation depth, and the depth of the contact region, respectively. (*E*) FE simulation of stress-field distribution of bilayer microstructure by SIP method. The maximum stress occurs in annular fashion in a one-quarter model of bilayer structure (*Left*), and the stress distribution of Pt film on the surface (*Right*).

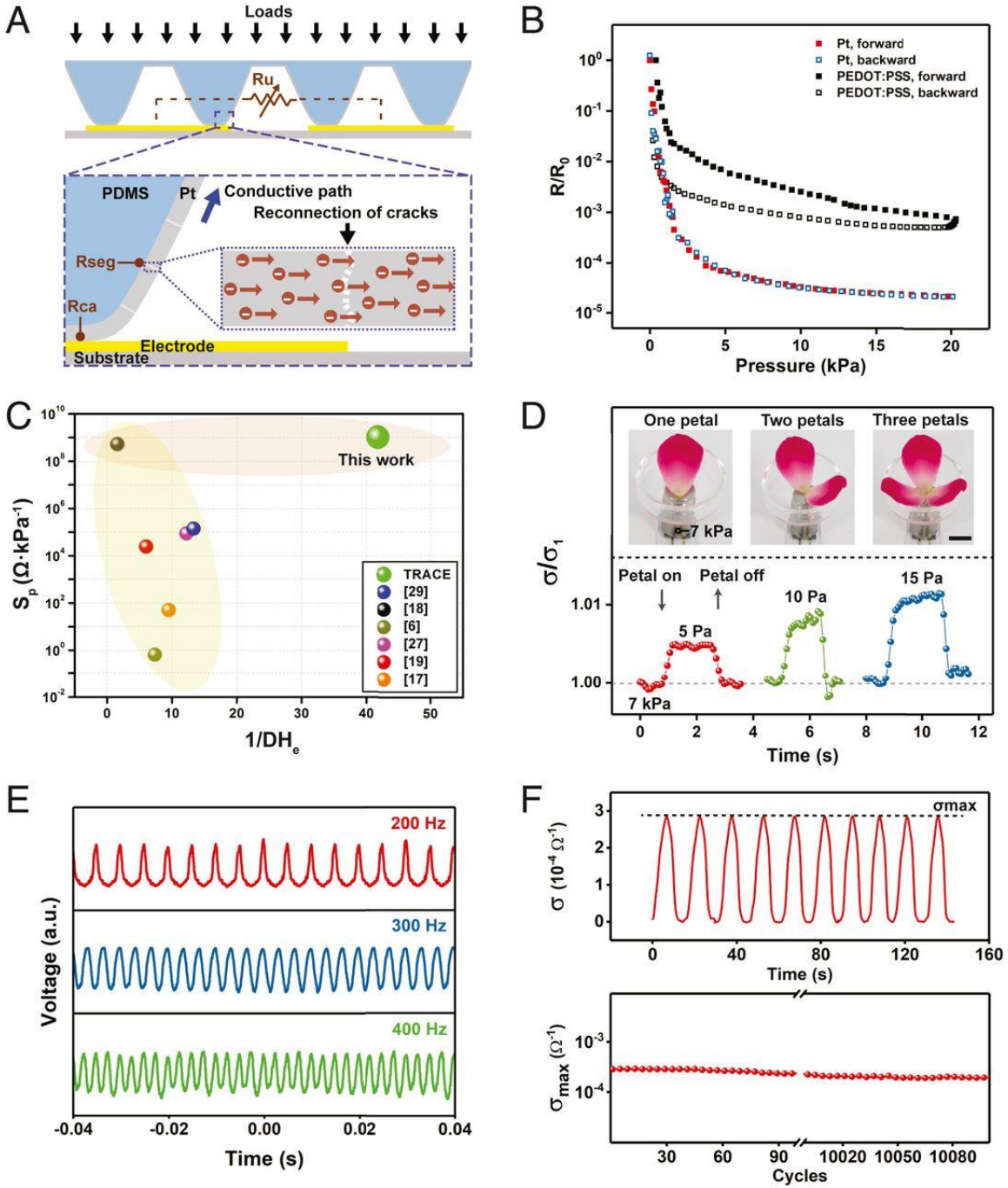
A
Loads
Ru
PDMS
Pt
Conductive path
Reconnection of cracks
Rseg
Rca
Electrode
Substrate
B
Pt, forward
Pt, backward
PEDOT:PSS, forward
PEDOT:PSS, backward
R/R0
Pressure (kPa)
C
This work
TRACE
[29]
[18]
[6]
[27]
[19]
[17]
Sp (Ω·kPa-1)
1/DHe
D
One petal
Two petals
Three petals
7 kPa
Petal on
Petal off
5 Pa
10 Pa
15 Pa
σ/σ1
Time (s)
E
200 Hz
300 Hz
400 Hz
Voltage (a.u.)
Time (s)
F
σmax
σ (10-4 Ω-1)
Time (s)
σmax (Ω-1)
Cycles

- Piezoresistive response of TRACE sensor. (*A*) The schematic model of the conductive pathways of TRACE sensor under compressing loads. (*B*) The pressure-induced electrical performance of TRACE sensor, compared with the PEDOT:PSS-coated micropyramid sensor. (*C*) Benchmark of TRACE sensor with both sensitivity and hysteresis being considered. We used S_p/DH_e as an indicator to simultaneously evaluate sensitivity and hysteresis of resistive-type sensors, where S_p represents the peak sensitivity, and DH_e is the degree of hysteresis, respectively. The smaller DH_e (or namely, larger $1/DH_e$) means a lower hysteresis observed for the piezoresistive sensor, indicating more accurate and repeatable sensing performance of TRACE sensor. Yellow region: low hysteresis; orange region: high sensitivity. (*D*) The ability of TRACE sensor to detect a small pressure of a *floribunda* petal under the preload of 7 kPa, where $_{\sigma 1}$ is the conductance of the preload pressure of 7 kPa, respectively, where the black scale bar is 10 mm. (*E*) The output voltage of TRACE sensor under different frequencies when applied pressure. (*F*) Cyclic testing of TRACE sensor: time-resolved performance of successive 10 cycles (*Top*) and maximum conductivity change over 10,000 cycles (*Bottom*).

Životní funkce

Financováno Evropskou unií NextGenerationEU
Národní plán obnovy
MINISTERSTVO ŠKOLSTVÍ, MLÁDEŽE A TĚLOVÝCHOVY
NPO_TUL_MSMT-16598/2022

Měření tepu

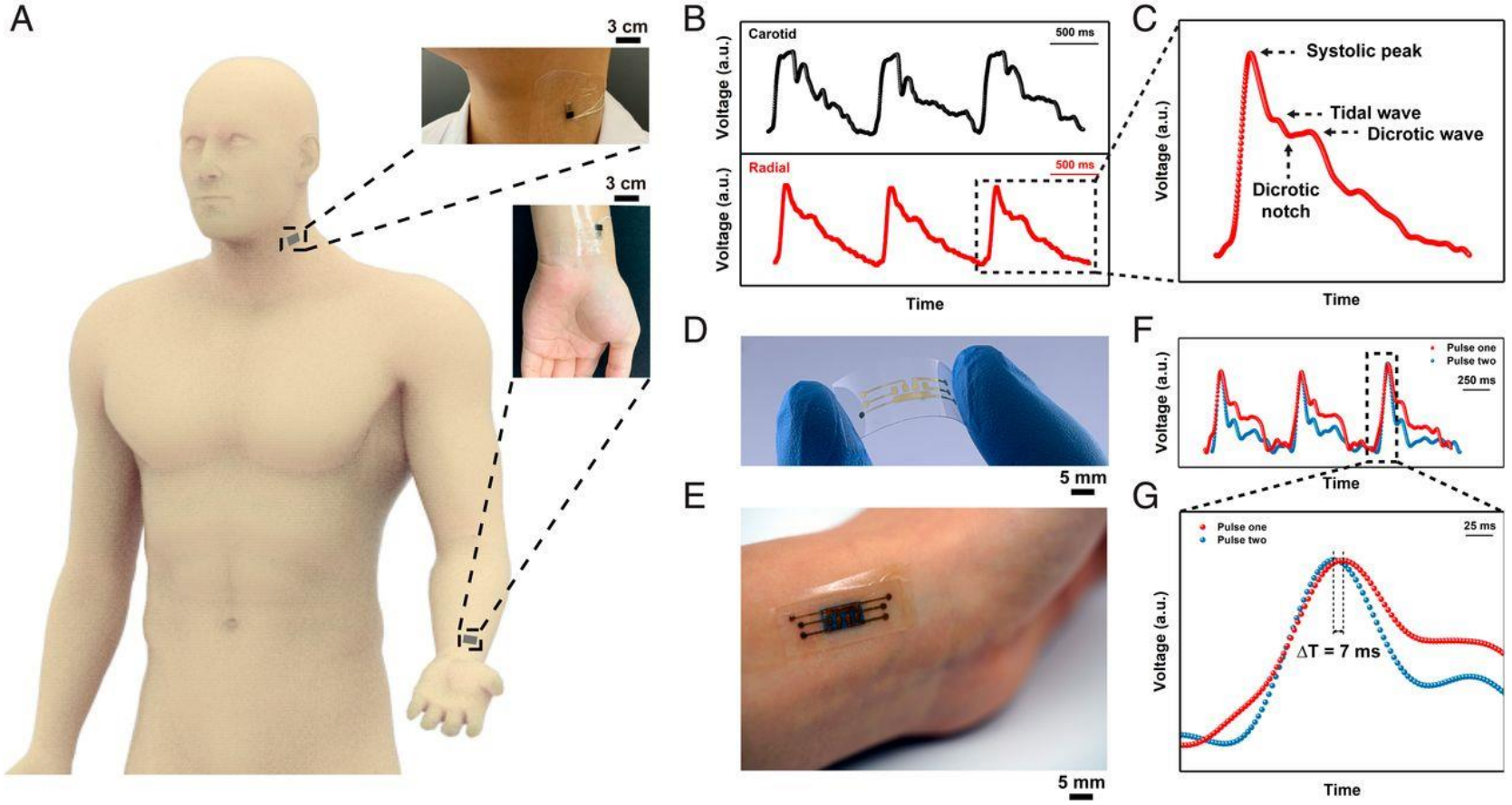
A
3 cm
3 cm
B
Carotid
500 ms
Radial
500 ms
Voltage (a.u.)
Voltage (a.u.)
Time
C
Systolic peak
Tidal wave
Dicrotic wave
Dicrotic notch
Voltage (a.u.)
Time
D
5 mm
E
5 mm
F
Pulse one
Pulse two
250 ms
Voltage (a.u.)
Time
G
Pulse one
Pulse two
25 ms
ΔT = 7 ms
Voltage (a.u.)
Time

Superficial pulse measurement and pulse tracing. (*A*) The illustration of superficial pulse measurement located on the human neck and wrist. The zoom-in images show the photographs of the pulse measurement on a volunteer. (*B*) The graphs show results of the simultaneous pulse measurement at the carotid artery and radial artery, and (*C*) a zoom-in image showing the measurement result of one radial pulse. The specific peak and wave information are indicated. (*D*) The optical image of flexible electrodes with multiple channels. (*E*) The photograph showing localized pulse tracing by integrating TRACE sensor with multichannel electrodes. (*F* and *G*) The graphs showing the results of localized pulse measurement at the radial artery and pulse tracing.

High-Density Pressure Mapping and Tactile Detection

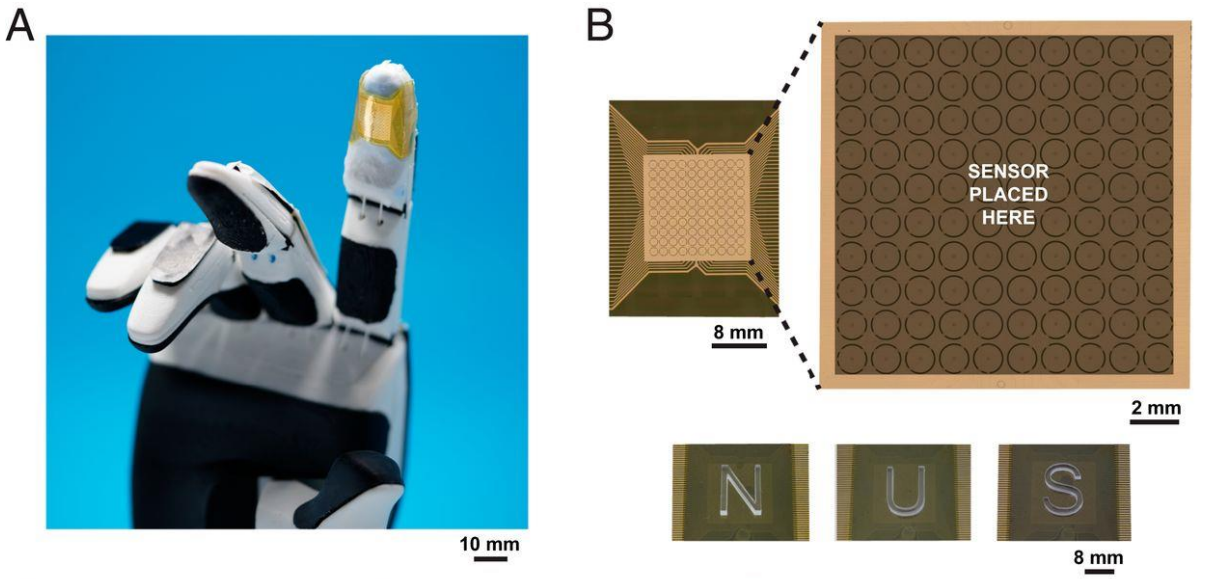

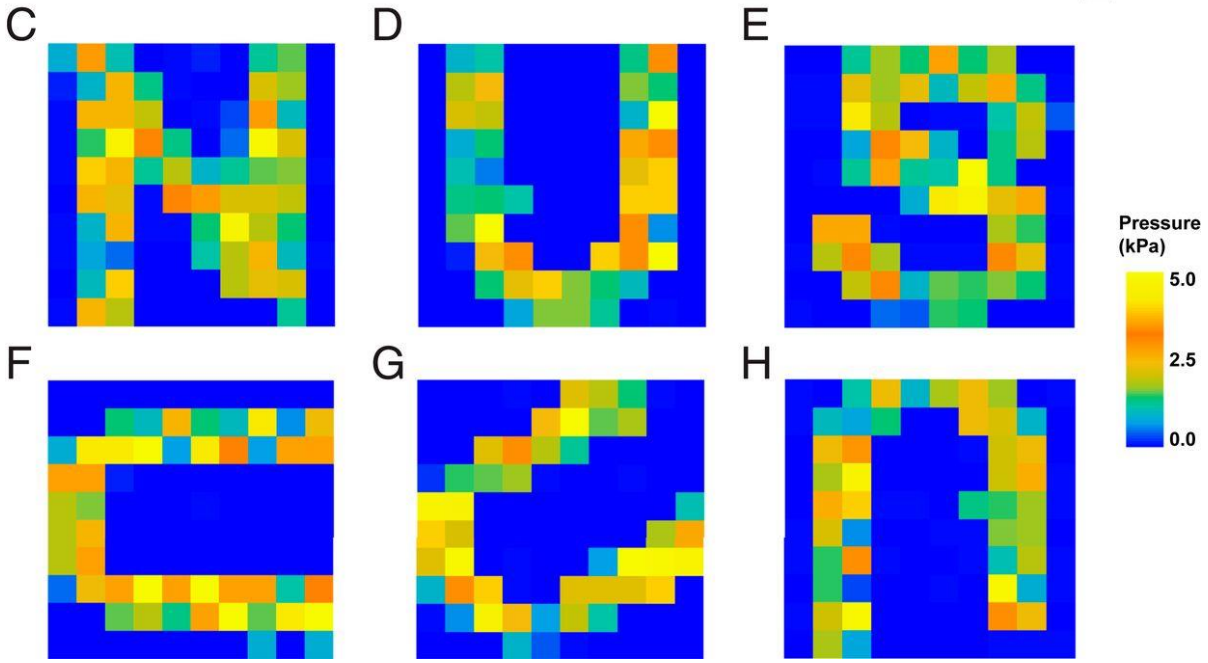

- High-density pressure distribution mapping on a robotic hand. (*A*) Images of conformable electrodes of TRACE-SA/FA sensor matrix attached to the index fingertip of a robot hand. (*B*) Design of electrodes (10 × 10) of sensor matrix, and laser-cut N, U, and S letters were touching TRACE-SA sensor matrix. (*C*–*H*) The pressure distribution map of TRACE-SA sensor matrix touching N, U, and S letters at different rotate angles


Robotic fingertip embodiment of TRACE sensor
for pulse sensing

Elektromechanické senzory

- **Electromechanical sensor** transforms mechanical stimulus into electrical signals. The main electromechanical sensors we focus on are strain and pressure sensors, which correspond to two main mechanical stimuli.
- According to their mechanisms, resistive and capacitive sensor attracts more attention due to their simple structures, mechanisms, preparation method, and low cost. Various kinds of nanomaterials have been developed to fabricate them, including carbon nanomaterials, metallic, and conductive polymers. They have great potentials for health monitoring, human motion monitoring, speech recognition, and related human-machine interface applications.

What are electromechanical sensors? - Quora

Princip

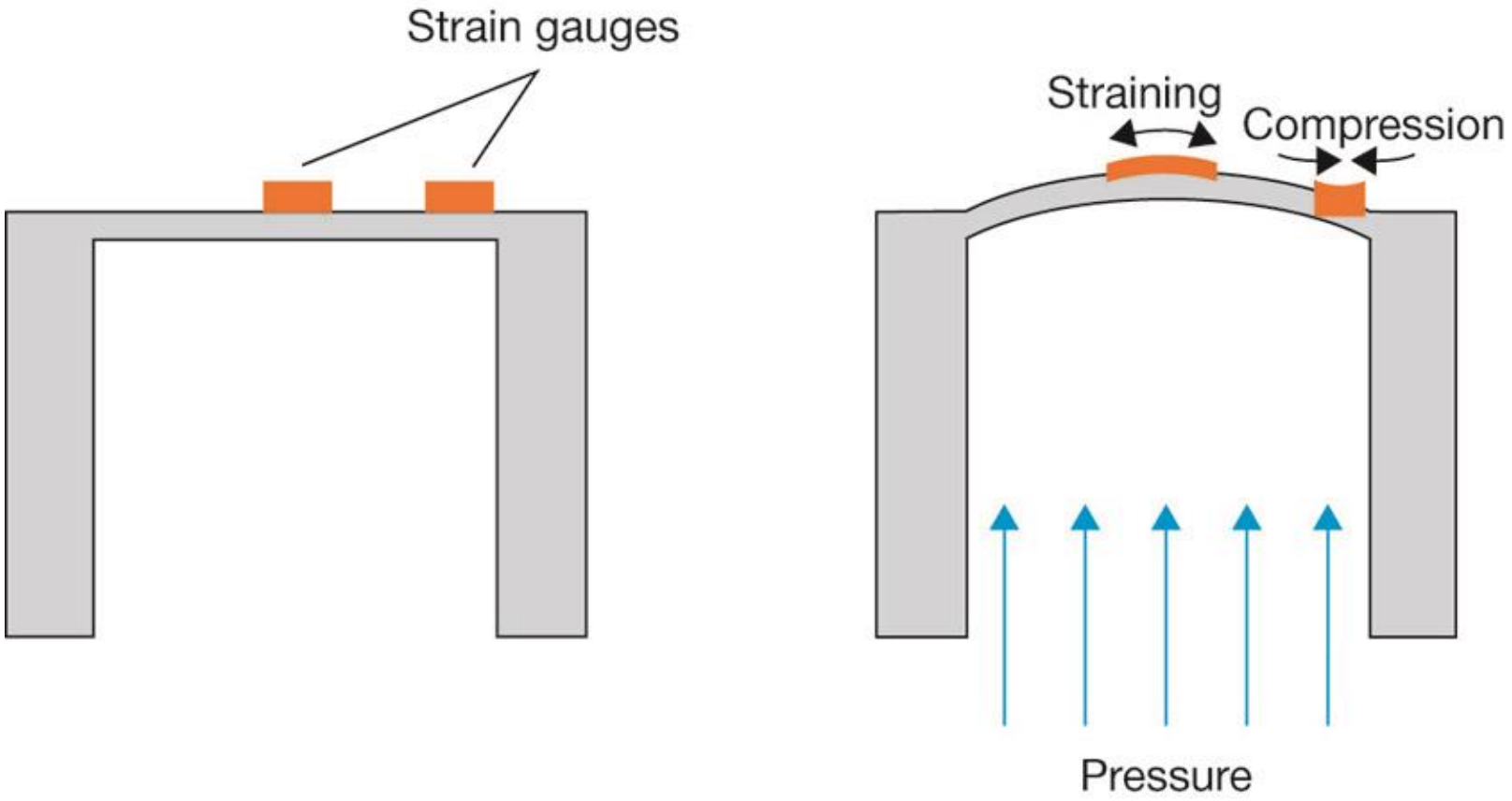

What is the functional principle of a resistive pressure transmitter? - WIKA blog

Elektromechanické senzory

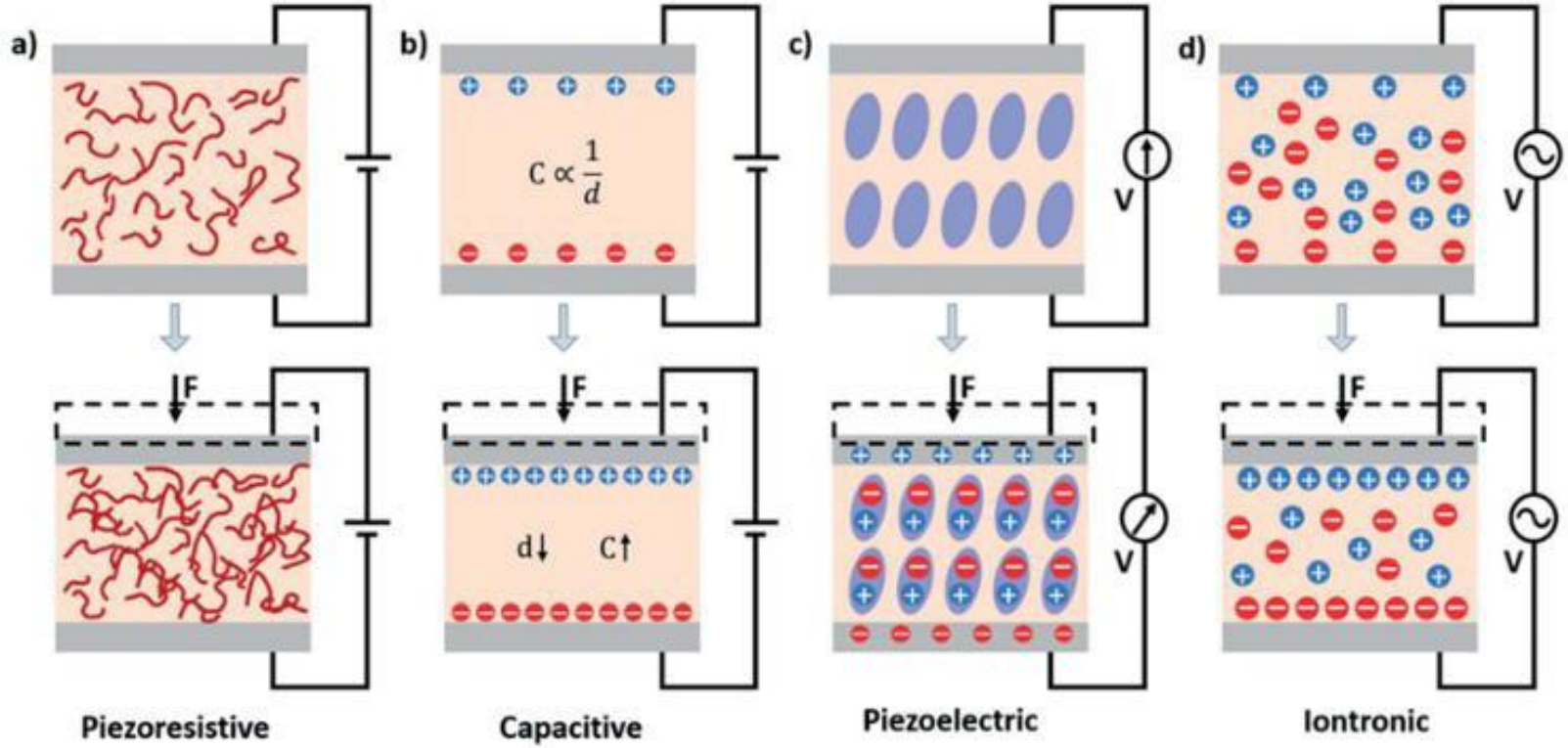

What are electromechanical sensors? - Quora

Elektromechanické senzory

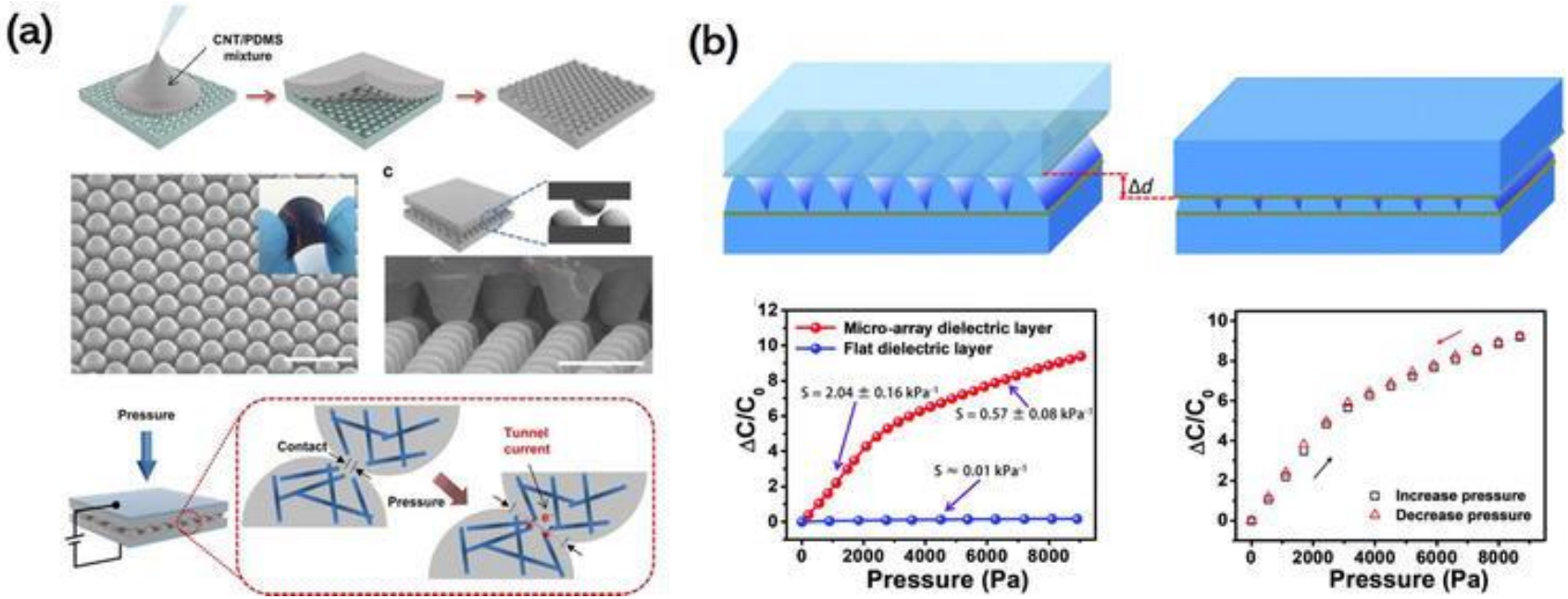

What are electromechanical sensors? - Quora

Elektromechanické senzory

- **Wearable pressure sensor**
- A wearable pressure sensor converts pressure into an electrical signal. The pressure sensor can be fabricated with interlocked structures, percolative networks of nanomaterials, microfabricated structures (e.g., micro pyramids, micropillars), porous structures (e.g., sponges, foams, porous rubbers), and so forth. The image2 presents a pressure sensor fabricated with an interlocked micro dome array. The contact between the micro dome increases when pressure is applied, thus decreasing the tunneling resistance.

What are electromechanical sensors? - Quora

Elektromechanické senzory

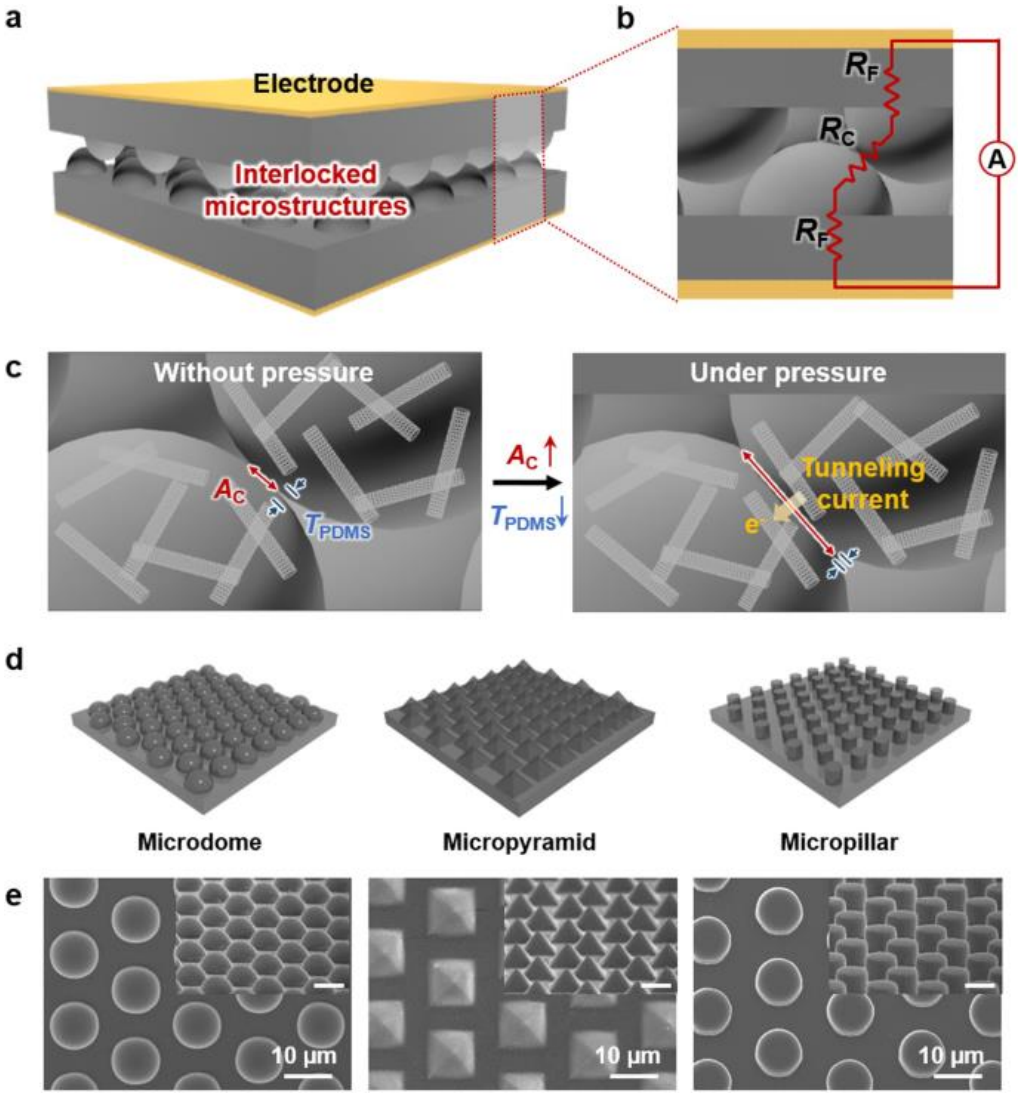

Tailoring force sensitivity and selectivity by microstructure engineering of multidirectional electronic skins | NPG Asia Materials (nature.com)

Elektromechanické senzory

- **a** Schematic illustration of the main structure of the e-skins with interlocked microstructures.
- **b** Schematic showing the bulk film resistance (R_F) and the contact resistance (R_C) between the two neighboring microstructured films.
- **c** Pressure-sensing mechanism of piezoresistive e-skins having interlocked microstructures.
- **d** Schematic illustration of conductive composites with different microstructured arrays.
- **e** Top and tilted (inset) SEM images of the microstructured composites with different surface morphologies (microdome, micropyramid, and micropillar)

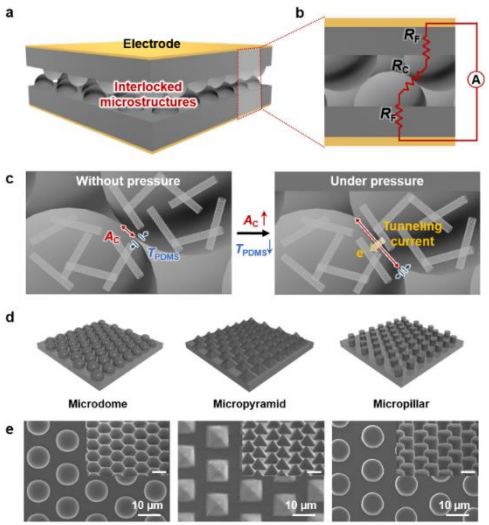

Tailoring force sensitivity and selectivity by microstructure engineering of multidirectional electronic skins | NPG Asia Materials (nature.com)

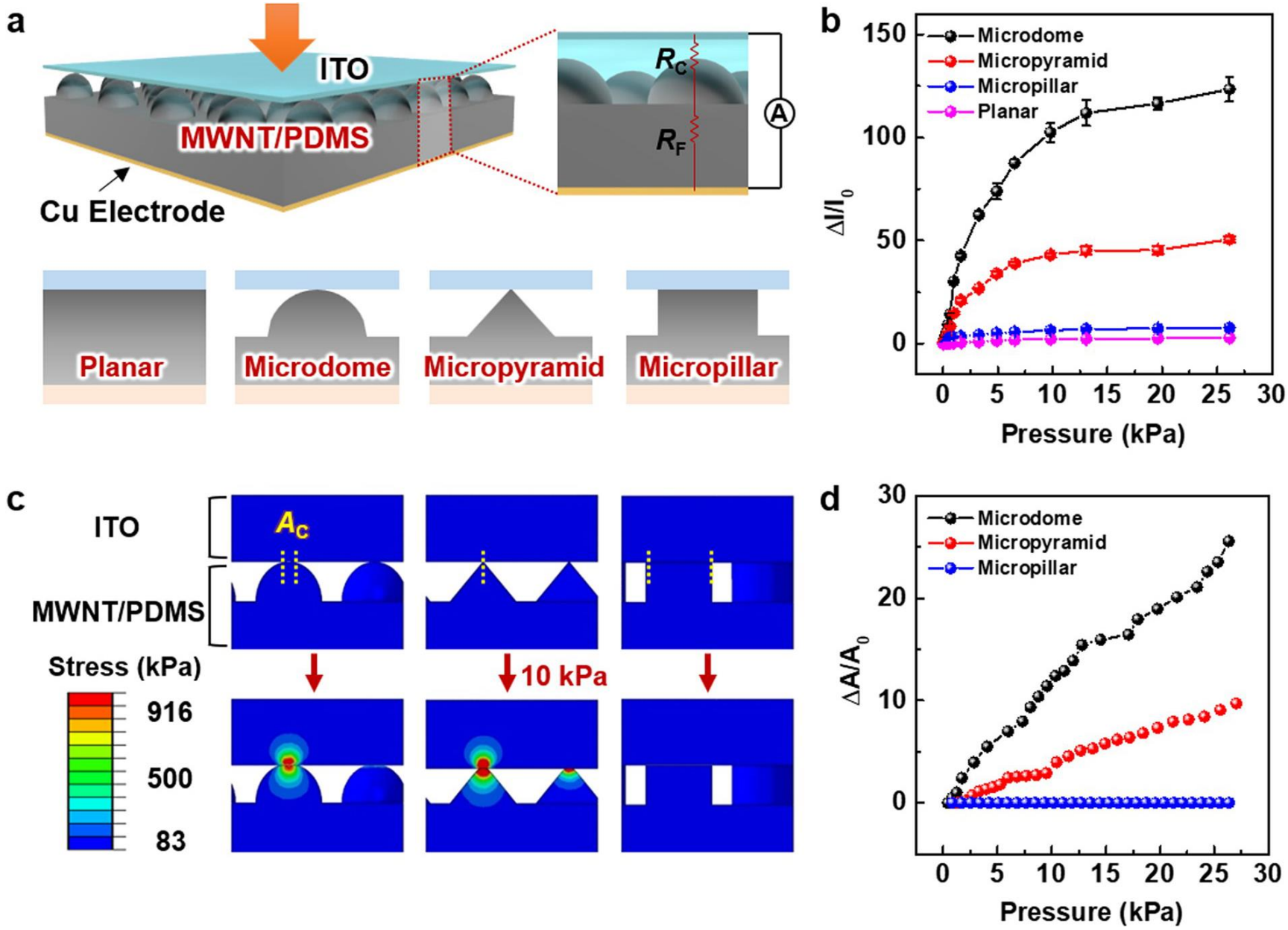

Tailoring force sensitivity and selectivity by microstructure engineering of multidirectional electronic skins | NPG Asia Materials (nature.com)

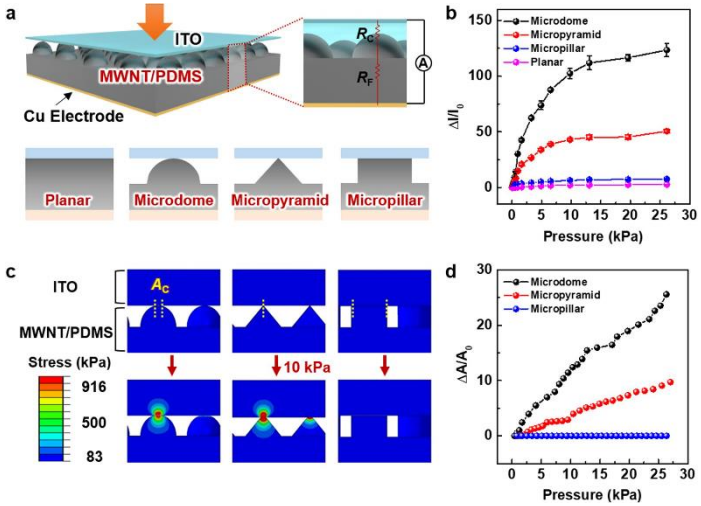

- **a** Schematic illustration of the pressure-sensing principle of single microstructured e-skins with different surface morphologies.
- **b** Relative current changes in response to normal pressure.
- **c** Finite-element analysis (FEA) of localized stress distributions in response to pressure for different surface microstructure arrays (top layer: ITO, bottom layer: MWNT/PDMS composite).
- **d** Calculated relative contact-area changes in response to normal pressure

Tailoring force sensitivity and selectivity by microstructure engineering of multidirectional electronic skins | NPG Asia Materials (nature.com)

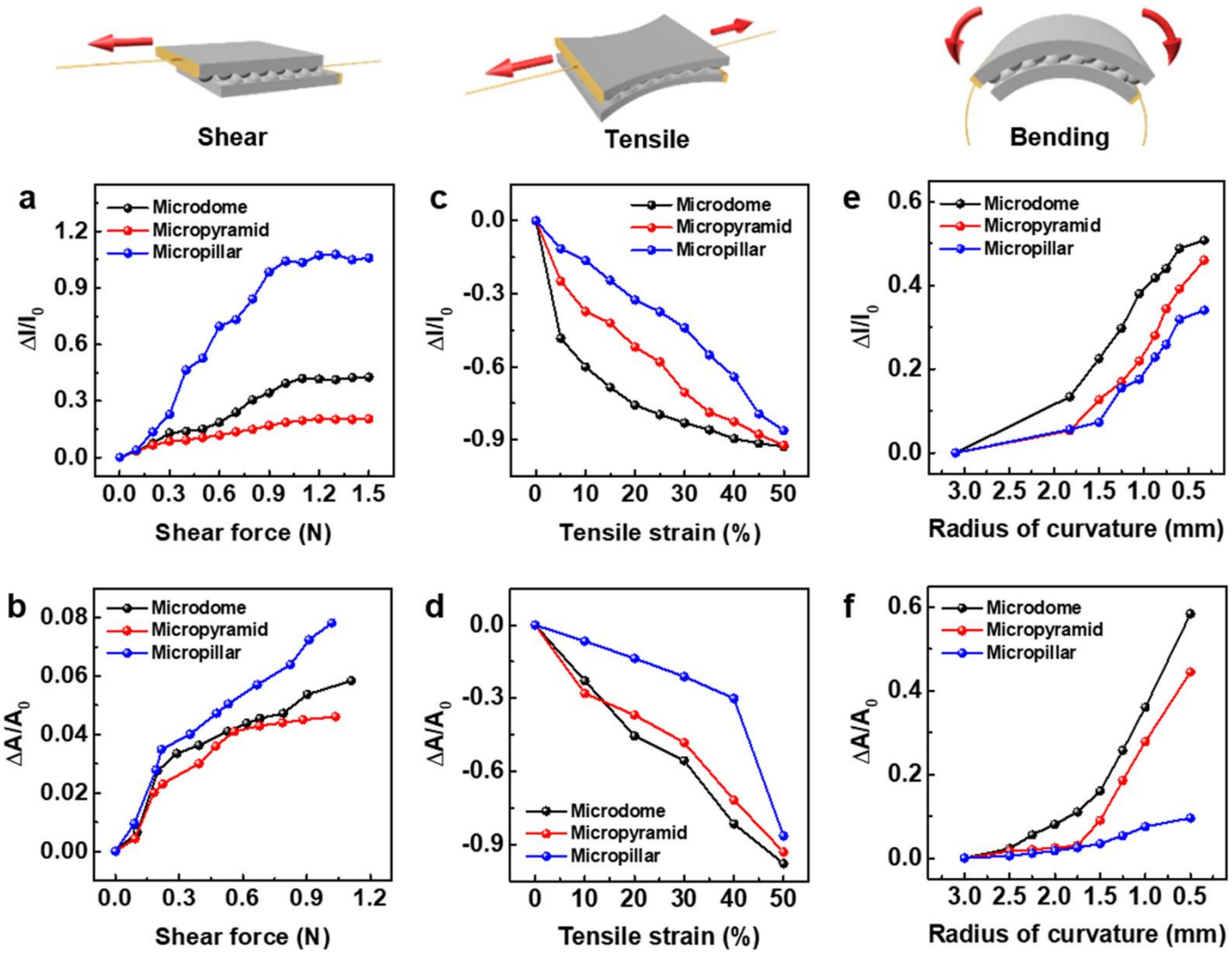

Tailoring force sensitivity and selectivity by microstructure engineering of multidirectional electronic skins | NPG Asia Materials (nature.com)

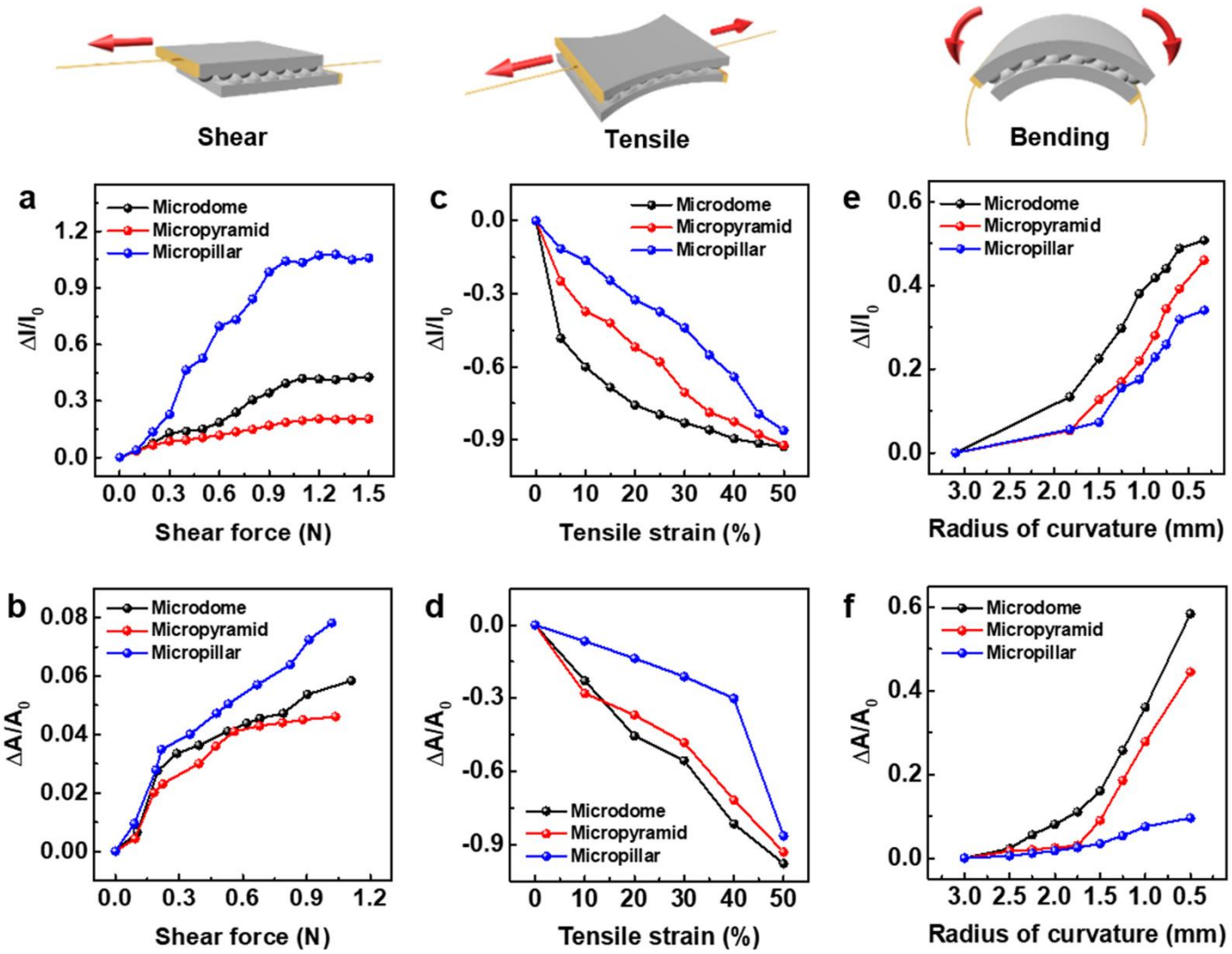

Tailoring force sensitivity and selectivity by microstructure engineering of multidirectional electronic skins | NPG Asia Materials (nature.com)

- Pressure sensors are categorized into
  - resistive,
  - Capacitive
  - piezoelectric types
- based on the pressure transduction mechanism

Applied Sciences | Free Full-Text | Recent Progress in Pressure Sensors for Wearable Electronics: From Design to Applications | HTML (mdpi.com)

Picture and schematic diagrams of the pressure transduction mechanism.

(a) Resistive type.

(b) Capacitive type.

(c) Piezoelectric type.

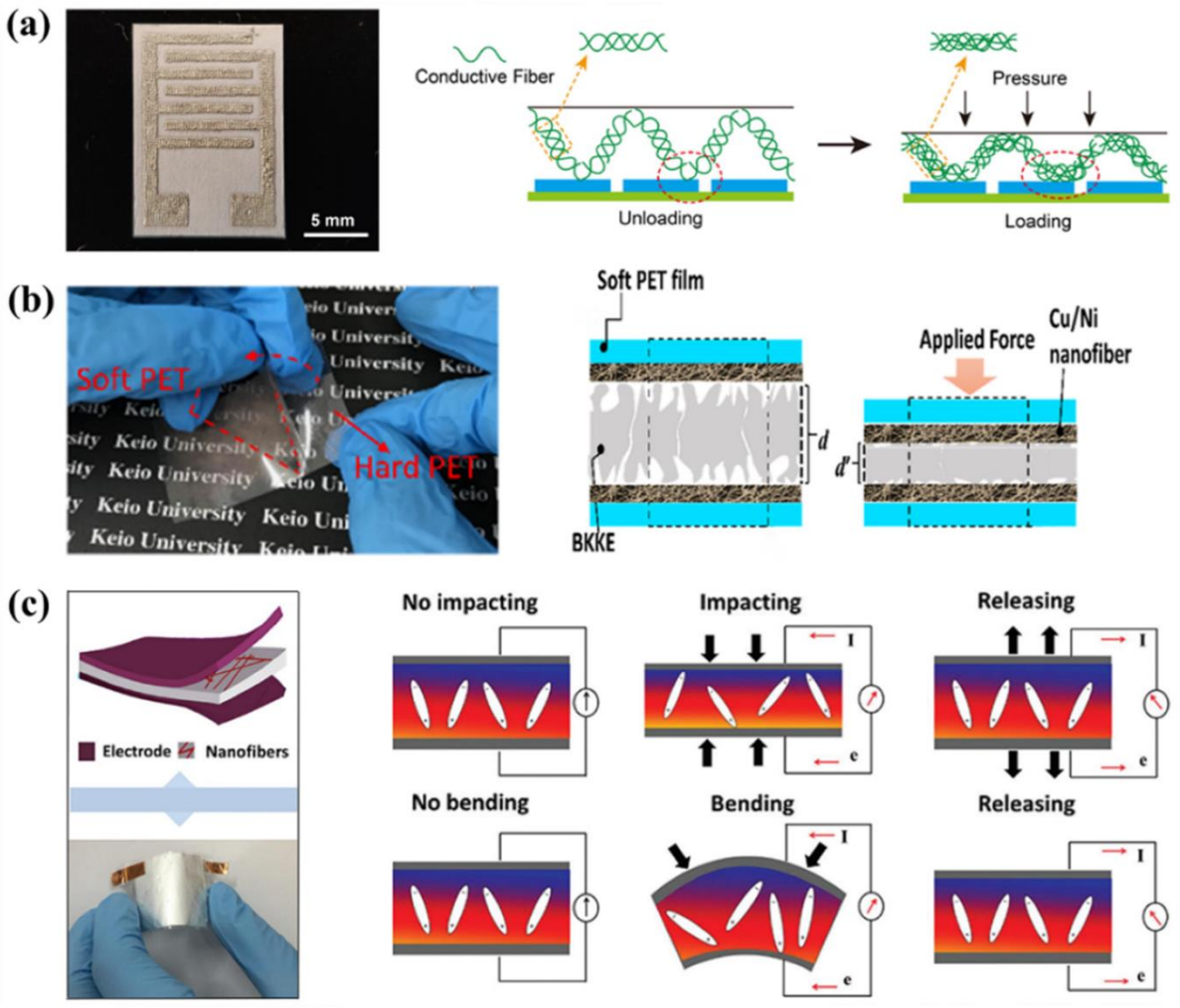

Applied Sciences | Free Full-Text | Recent Progress in Pressure Sensors for Wearable Electronics: From Design to Applications | HTML (mdpi.com), Copyright (2018), American Chemical Society.

Schematic of electrospinning technique and SEM images of electrospun NFs.

(a) Electrospun PVDF-TrFE NFs at different solution concentrations of 14, 18, and 22 *w/v*% from the top to bottom of images.

(b) Electrospun NFs of PVDF and PVP.

(c) Schematic diagram of core-shell electrospinning technique and SEM

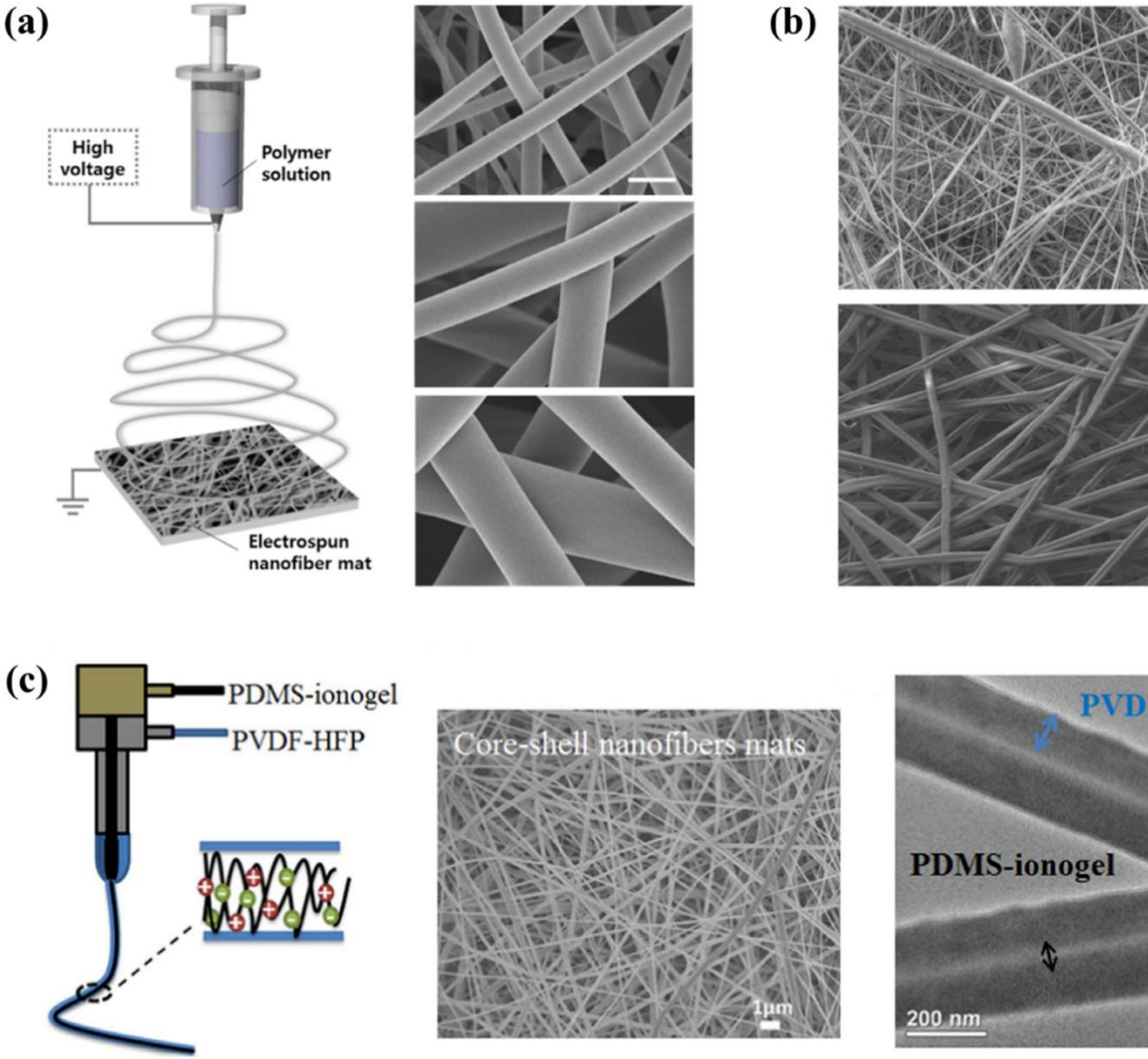

Applied Sciences | Free Full-Text | Recent Progress in Pressure Sensors for Wearable Electronics: From Design to Applications | HTML (mdpi.com), Copyright (2018), American Chemical Society.

Nanohair

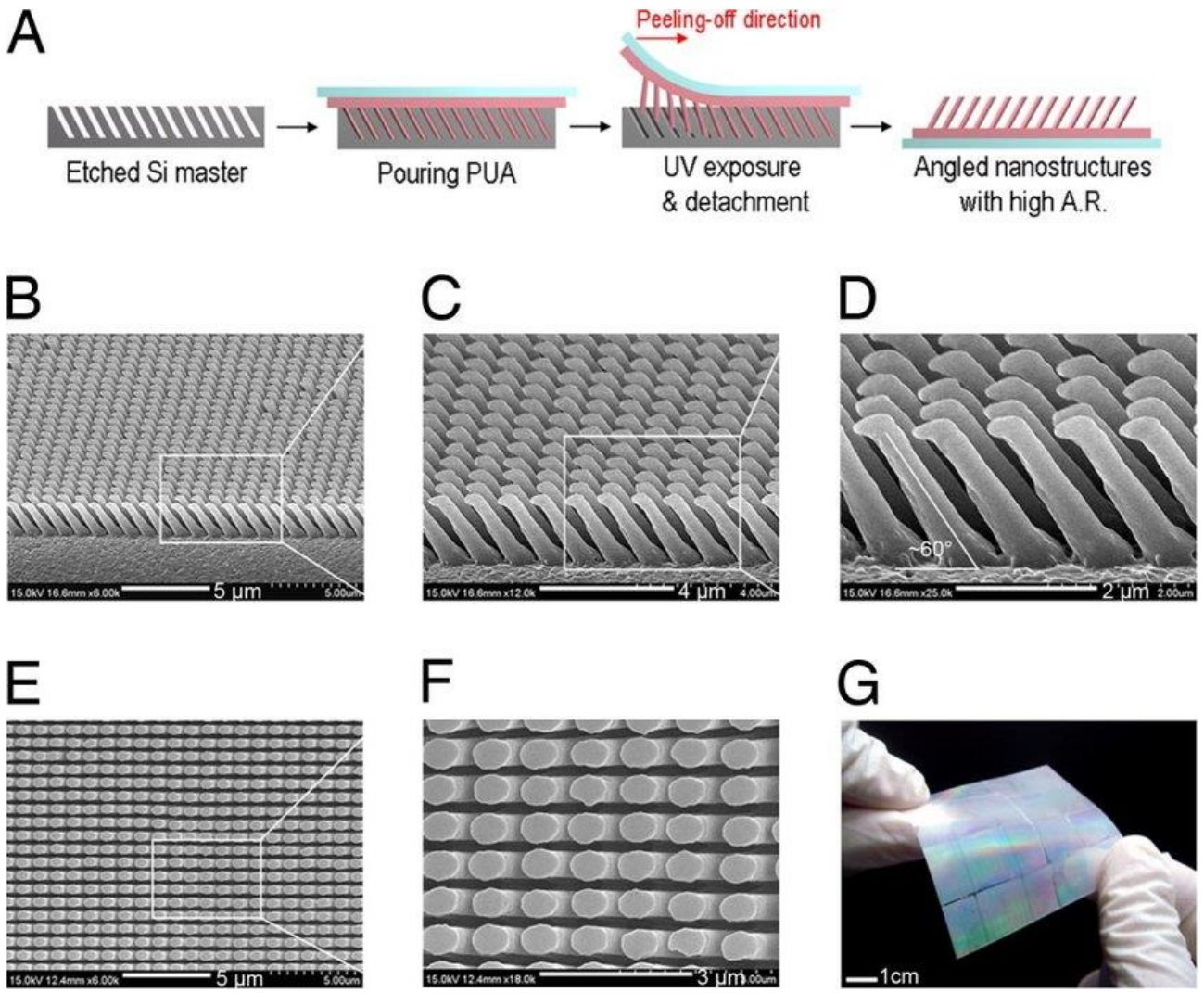

Fabrication of slanted nanohairs with UV-curable PUA resin. (A)... | Download Scientific Diagram (researchgate.net)

Možnosti využití v biomechanice

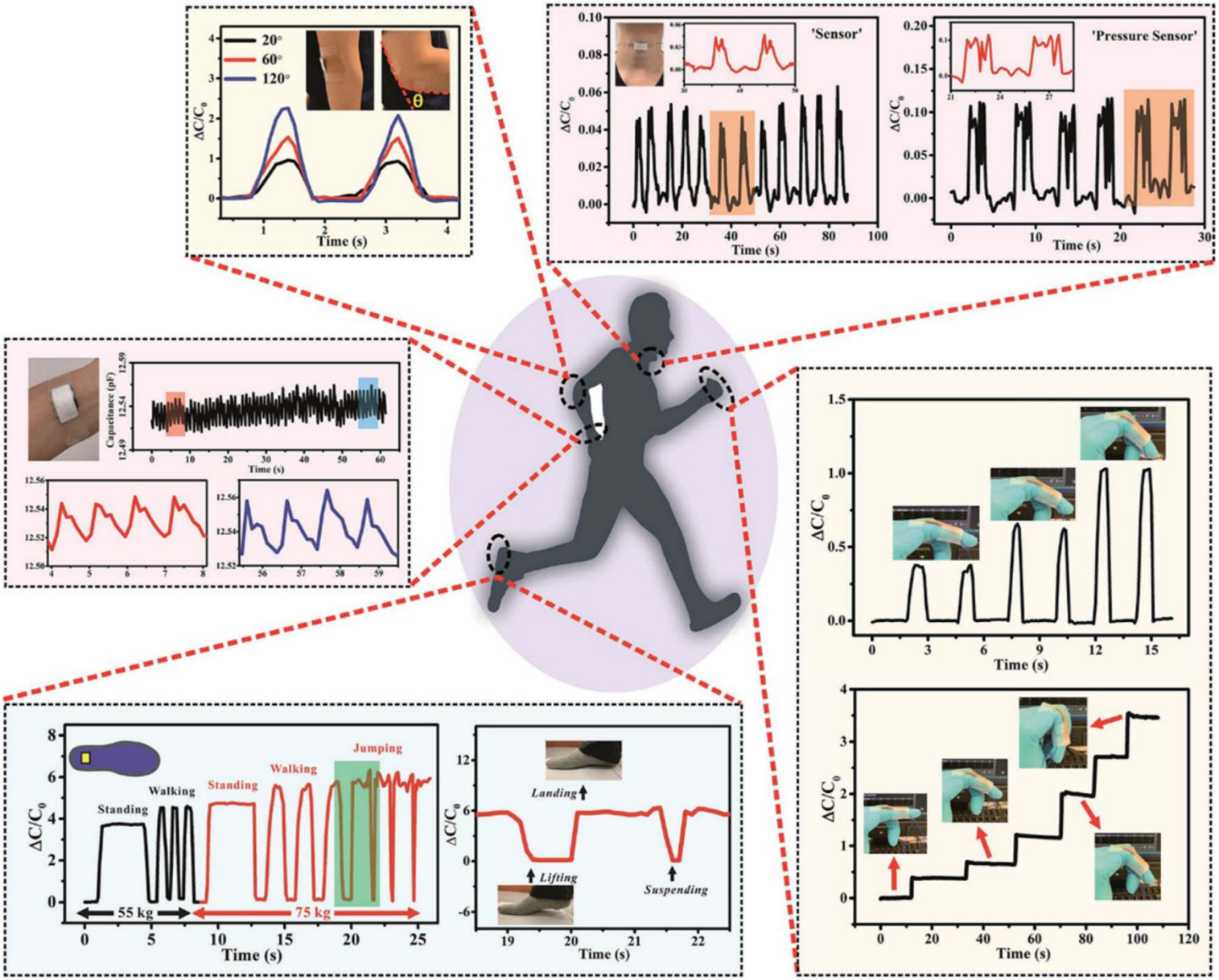

Teplota, teplo

Financováno Evropskou unií NextGenerationEU
Národní plán obnovy
MINISTERSTVO ŠKOLSTVÍ, MLÁDEŽE A TĚLOVÝCHOVY
NPO_TUL_MSMT-16598/2022

Tepelný tok

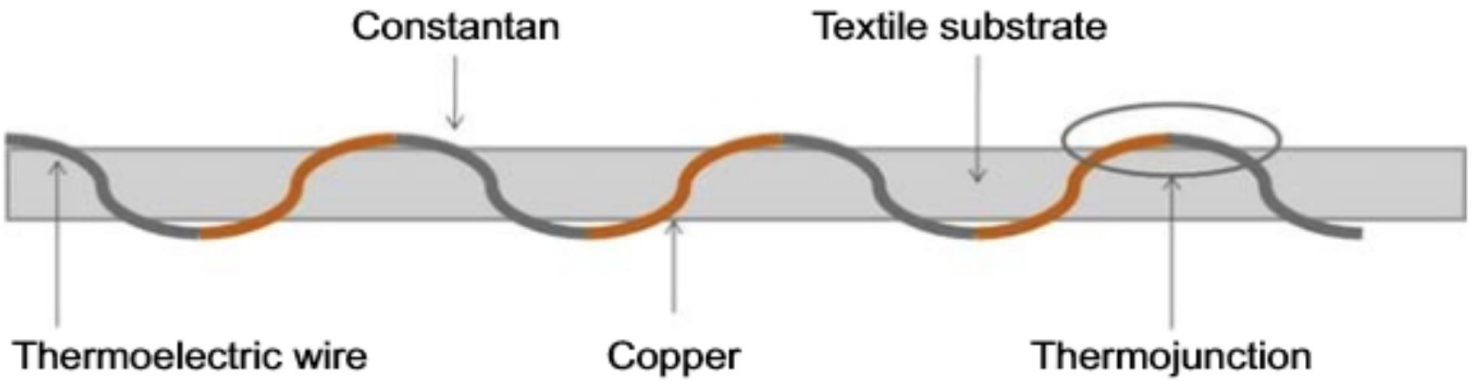

Figure 2.6 A textile-based heat flux sensor comprising a thermoelectric wire woven into a textile substrate.

Jak vyrobit ?

Aplikace vyšívání

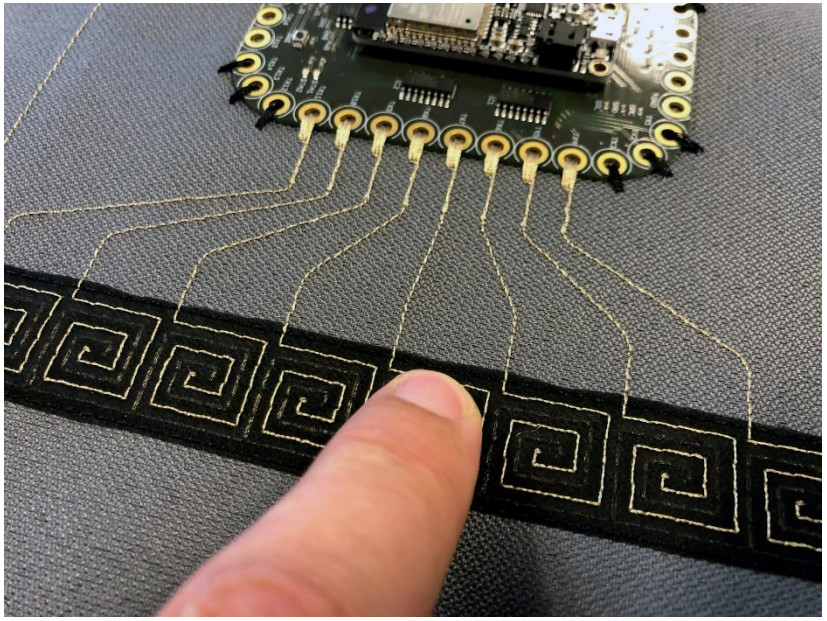

https://youtu.be/eXAlntc2y4s

Embroidered Textile FSR Sensors – Media Interaction Lab (mi-lab.org)

Aplikace vyšívání

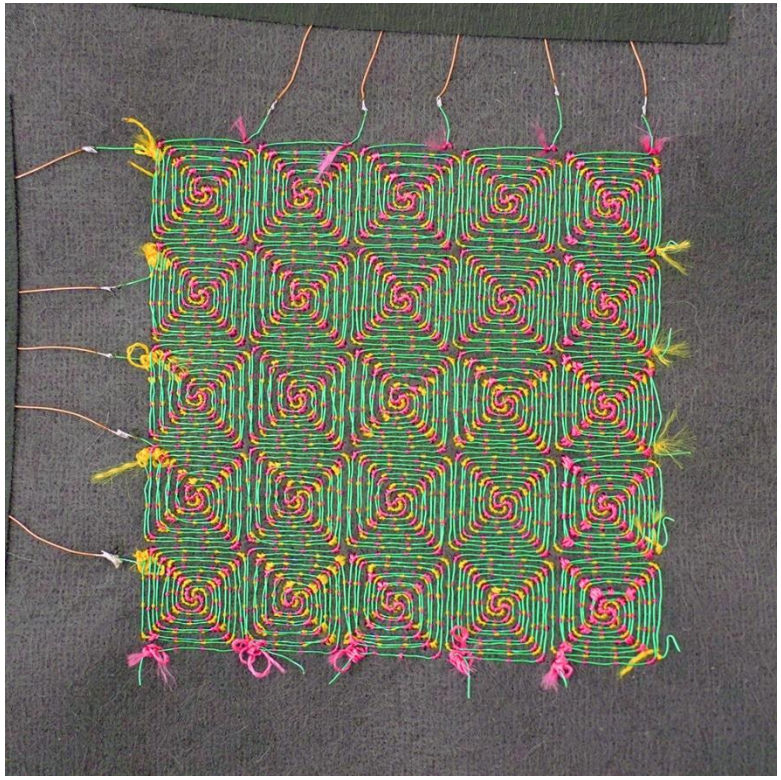

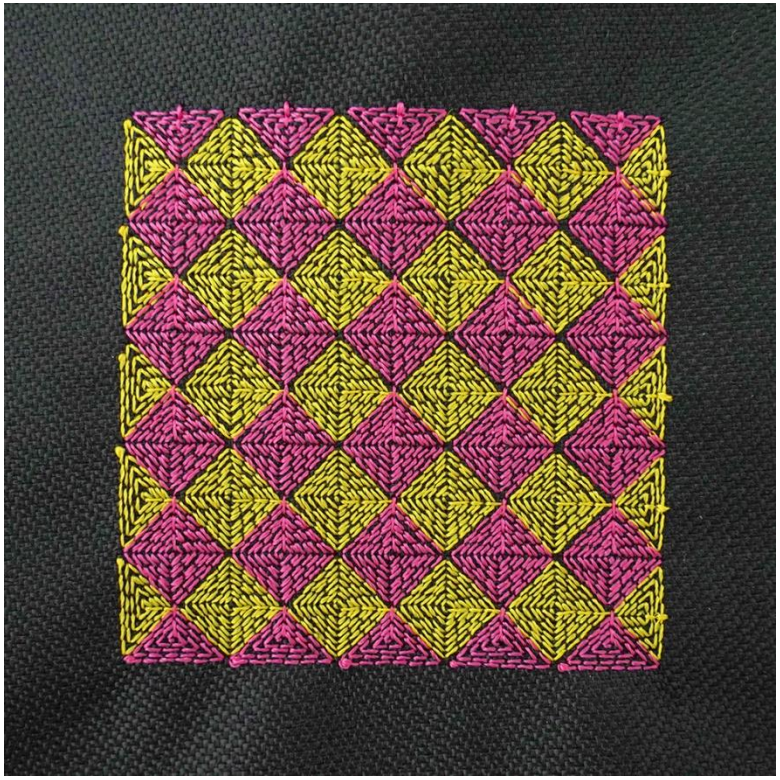

https://youtu.be/oNCTTPauwmc

Embroidered Textile FSR Sensors – Media Interaction Lab (mi-lab.org)

Aplikace vyšívání

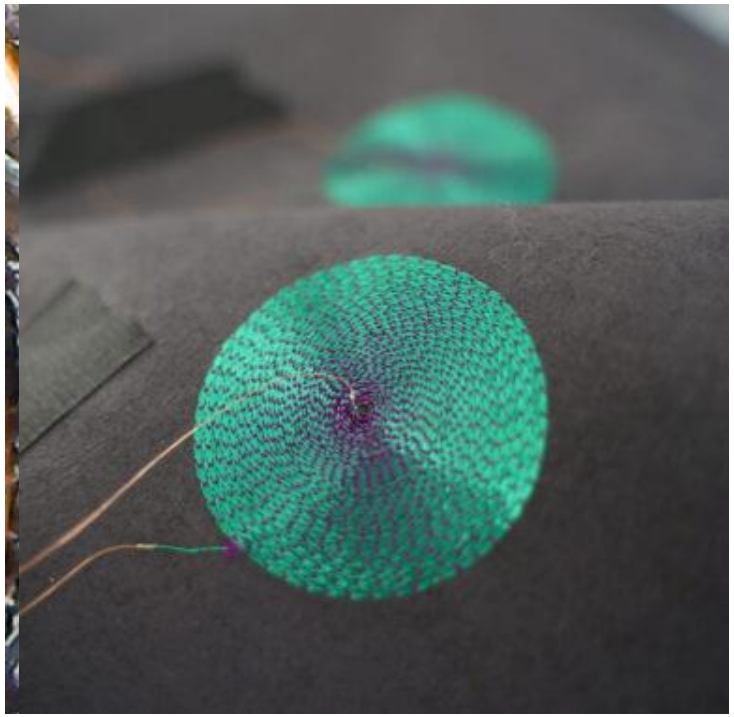

https://youtu.be/JDuBuy0HntA

Embroidered Textile FSR Sensors – Media Interaction Lab (mi-lab.org)

Aplikace vyšívání

https://youtu.be/JDuBuy0HntA

Embroidered Textile FSR Sensors – Media Interaction Lab (mi-lab.org)

Aplikace vyšívání

https://youtu.be/JDuBuy0HntA

Embroidered Textile FSR Sensors – Media Interaction Lab (mi-lab.org)

Aplikace vyšívání

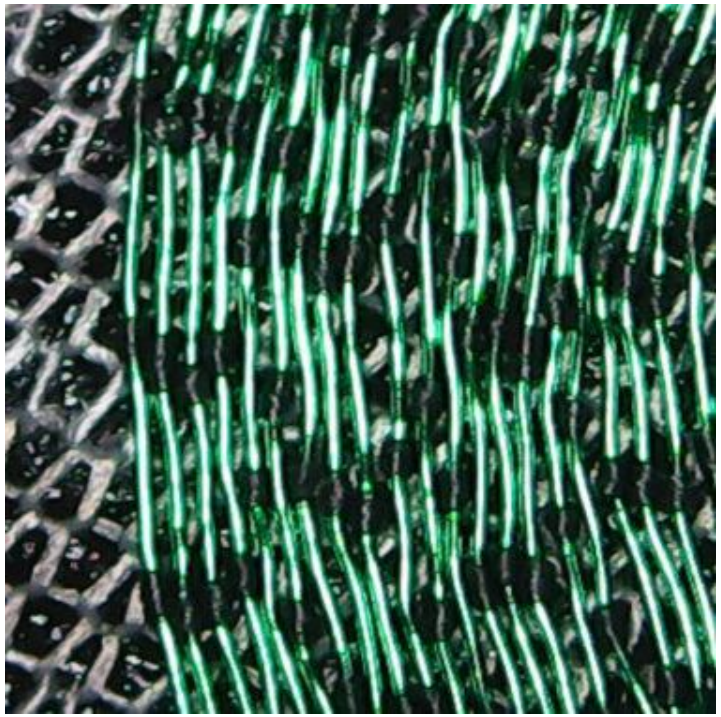

https://youtu.be/JDuBuy0HntA

Embroidered Textile FSR Sensors – Media Interaction Lab (mi-lab.org)

Aplikace vyšívání

https://youtu.be/JDuBuy0HntA

Embroidered Textile FSR Sensors – Media Interaction Lab (mi-lab.org)

Aplikace vyšívání

https://youtu.be/JDuBuy0HntA

Embroidered Textile FSR Sensors – Media Interaction Lab (mi-lab.org)

Aplikace vyšívání

https://youtu.be/JDuBuy0HntA

Embroidered Textile FSR Sensors – Media Interaction Lab (mi-lab.org)

Aplikace vyšívání

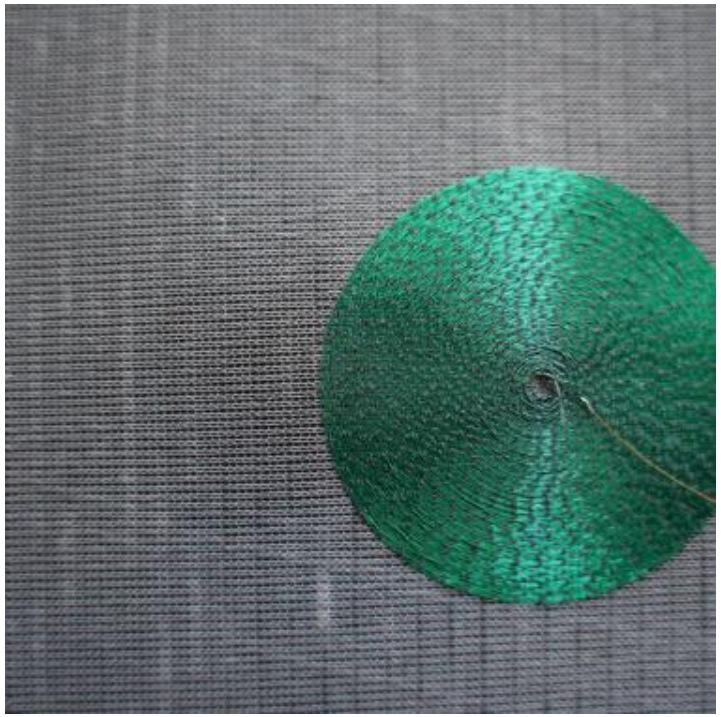

https://youtu.be/JDuBuy0HntA

Embroidered Textile FSR Sensors – Media Interaction Lab (mi-lab.org)

Konec

Financováno Evropskou unií NextGenerationEU
Národní plán obnovy
MINISTERSTVO ŠKOLSTVÍ, MLÁDEŽE A TĚLOVÝCHOVY
NPO_TUL_MSMT-16598/2022